The University of
Nottingham

UNITED KINGDOM · CHINA · MALAYSIA

THE STUDY AND FABRICATION OF A NOVEL THERMALLY RESPONSIVE MICROCARRIER FOR CELL CULTURE APPLICATION

By

CHOU PUI MAY

A thesis submitted to the University of Nottingham
for the degree of Doctor of Philosophy

MAY 2016

ABSTRACT

During conventional microcarrier cell culturing, the use of harmful trypsin or a mechanical scrapper during cell harvesting can damage the cell membranes and reduce cell yield. The development of a non-invasive harvestment process for cells is essential, for preserving cell functions and improving cell yield. The ultimate objective of the present study was to synthesize a novel polyNIPAm thermoresponsive microcarrier, to eliminate the use of trypsin or scrapper approaches for cell harvestment. Comprehensive investigation of processing parameters, of initiator type, surfactant composition, comonomer ratio, stirring rate and cross-linker content were performed, to gain improved understanding of the process-structure-property relationship, and thereby identify optimum processing conditions. PolyNIPAm microspheres possessing different size ranges and surface properties were synthesised successfully via suspension polymerisation. The use of different initiator types affected the polymerisation temperature, size and surface charge of the polyNIPAm product. The surface charge of the polyNIPAm microspheres was controlled by adjusting the surfactant composition. Copolymerisation with butyl methacrylate (BMA) improved the surface hydrophobicity of the microspheres for enhanced protein adsorption. Relatively small microspheres of diameters ~ 30 μm were formed when a high stirring rate of 400 rpm was used. It was found that the compressive modulus of the microspheres increased with increasing cross-linker content. *In vitro* cell trials were performed to appraise the cellular response to the polyNIPAm microspheres. The polyNIPAm microspheres were found to be biocompatible with human embryonic kidney (HEK) cells. Spontaneous cell detachment from the microspheres occurred upon lowering the incubation temperature of the culture media. The incorporation of 10 wt% of cetrylmethylammonium bromide (CTAB) surfactant and 30 wt% of BMA comonomer to the polyNIPAm exhibited a cell yield of ~ 1.7×10^6 cells/ml, which is comparable to commercial microcarriers (1.0×10^6 cells/ml).

ACKNOWLEDGEMENTS

TABLE OF CONTENTS

CHAPTER 3   MATERIALS AND METHODOLOGY

CHAPTER 7   OPTIMISATION OF PROCESSING PARAMETERS FOR THE SYNTHESIS OF POLYNIPAM MICROSPHERES

CHAPTER 8   OVERVIEW DISCUSSION

CHAPTER 9   CONCLUSIONS

REFERENCES   171

LIST OF FIGURES

LIST OF TABLES

LIST OF ABBREVIATIONS

AIBN	2,2-azobis(iso-butyronitrile)
APS	Ammonium persulfate
BHK	Baby hamster kidney
BSE	Backscattered electrons
BMA	Butyl methacrylate
C	Carbon
CHO	Chinese hamster ovary
CL	Cathodoluminescence
CPC	Cetylpyridinium chloride
CTAB	Cetrylmethylammonium bromide
DEAE	N,N-diethylaminoethyl
DMEM	Dulbecco's modified Eagle medium
DSC	Differential scanning calorimetry
DSD	Drop size distribution
ECM	Extracellular matrix
EDX	Energy dispersive X-ray spectroscopy
EPA	Environmental Protection Agency
FDA	Food and Drug Administration
FTIR	Fourier transform infra-red
FBS	Fetal bovine serum
GRGDS	Gly-Arg-Gly-Asp-Ser peptides
HEK	Human embryonic kidney
HLB	Hydrophile–lipophile balance
KBr	Potassium bromide
LCST	Lower critical solution temperature
MAA	Methacrylic acid
MBAm	N,N'-methylenebisacrylamide

MC	Methylcellulose
MDCK	Madin-Darby Canine Kidney
MHS	Milan hypertension rat strain
MTAC	[2-(methacryloyloxy)ethyl]-trimethylammonium chloride
NaCl	Sodium chloride
NaOH	Sodium hydroxide
N	Nitrogen
NP-15	Pentadecylethoxylated-nonyl-phenol
NSO	Mouse myeloma
O	Oxygen
ODN	Oligodeoxynucleotide
PBS	Phosphate-buffered saline
PEG	Poly(ethylene glycol)
PEGDA	Polyethylene glycol diacrylate
PEO	Poly(ethylene oxide)
PET	Poly(ethylene terephthalate)
PPO	Poly(propylene oxide)
RGD	Arg-Gly-Asp tripeptide
PVA	Poly(vinyl alcohol)
SEM	Scanning electron microscopy
TCPS	Tissue culture polystyrene
TEMED	N,N,N',N'-tetramethylethylene-diamine
TGA	Thermogravimetric analysis
TTAC	Tetradecyl-trimethyl-ammonium chloride
UCST	Upper critical solution temperature

CHAPTER 1

INTRODUCTION

1.0 Introduction

In vitro cell culturing is a process of growing mammalian tissues under controlled conditions [1]. It is vital for studying the physiology and biochemistry of cells, mutagenesis and carcinogenesis. Cell culturing is a major tool used in the development of vaccines and therapeutic proteins. It can be used also for replacement tissues or organs [2]. All these applications are beneficial for improving human health.

Most of the mammalian cell lines are anchorage-dependent, *i.e.* the cells are not adapted to live in suspension, and can only survive upon adhering to a solid substrate [1]. The first generation of cell cultures used petri dishes. However, this method requires a large amount of labour and space, limiting the production of cells. Hence, microcarrier was introduced by van Wezel in 1967 [3] to replace the role of the petri dish. Microcarrier cell cultures offer numerous advantages over conventional culturing methods using petri dish or roller bottle approaches. One advantage is the capability of producing high yields of cells, owing to the large culture surface area to volume ratio of microcarriers. Fewer culture vessels are required, due to the ability of microcarriers to culture large numbers of cells in small volumes, which leads to a decrease in production costs [4]. However, there is a significant drawback of using commercial microcarriers for cell culturing. Proteolytic enzymes such as trypsin, are required to detach the cells from the microcarriers during cell harvesting. The use of trypsin damages the cell membrane-associated matrix proteins, leading to a loss of cell function or cell death [5].

In this context, thermally responsive polymers have attracted significant attention, as one of the most promising materials for use as a substitute for commercial microcarriers. Amongst the thermally responsive polymers, poly(*N*-isopropylacrylamide) (polyNIPAm) has been studied extensively for biomedical applications, such as drug delivery systems and the tissue engineering of cell sheets, owing to its sharp phase transition at temperatures close to the physiological body temperature [6]. It has been

established that polyNIPAm in aqueous solution exhibits a reversible hydrophilic-hydrophobic change, in response to temperature changes around its lower critical solution temperature (LCST) at 32°C [7]. It undergoes a sharp transition from coil to globule form as the temperature is raised above 32°C. During the cell culturing process, performed at 37°C, the polyNIPAm chains became strongly hydrophobic and suitable for cell adhesion and growth [8]. In a recent study by Nakayama *et al.* (2010) [8], a polyNIPAm-coated petri dish was used to culture endothelial cells. Spontaneous detachment of cells was observed by simply reducing the culture temperature to 20°C. A similar finding was documented by Schmidt *et al.* (2010), whereby a polyNIPAm microgel film allowed complete detachment of mouse fibroblasts when the culture temperature was lowered from 37 to 20°C [9]. Additionally, Cooperstein and Canavan (2013) reported that polyNIPAm films are biocompatible and non-cytotoxic to fibroblasts, epithelials and smooth muscle cells, making polyNIPAm a promising candidate material for microcarrier cell culturing [10].

1.1 Research Significance

Many studies highlighted the grafting of polyNIPAm onto tissue culture polystyrene (TCPS) petri dishes to promote thermally-induced cell detachment [8,9,11]. However, these studies involved culture substrates in thin film form, which did not offer high enough surface area to volume ratios for the production of high cell yields at low cost [4]. To the best of our knowledge, no study has reported on the synthesis of polyNIPAm microspheres for non-invasive cell culture. Hence, a comprehensive study was performed to optimise the polymerisation process to obtain microcarriers that exhibit maximal cell attachment and cell growth.

Microcarrier size has a great influence on the attachment and growth of anchorage-dependent cells. In general, a larger number of cells can be loaded on to microcarriers of larger size. However, increased numbers of large microcarriers may not be appropriate for suspension during the cultivation of cells. On the other hand, smaller microcarriers offer higher surface area, leading to higher cell densities. However, most anchorage-dependent cells do not multiply well on small microcarriers, due to their excessively high curvatures. Hence, the ideal size of a microcarrier is between 100 and 300 µm [12].

The size of polyNIPAm particles depends on the type of polymerisation technique employed. It has been reported that the size of polymer particles produced using emulsion polymerisation and precipitation polymerisation is < 10 µm [13]. On the other hand, suspension polymerisation is particularly suitable for the production of large polymer particles, ranging from 5 to 1000 µm. Hence, suspension polymerisation is utilised in the present work to produce polyNIPAm microspheres of diameter 100 - 300 µm [14]. Although polyNIPAm is a promising candidate material for cell culturing, its poor mechanical properties constitute a significant challenge for use as microcarrier in cell culture application. One effective approach to improve the mechanical properties of polyNIPAm is the crosslinking method, although the addition of a crosslinker reduces the flexibility of the polymer. Hence, there is a need for compromise between the rigidity and flexibility of the polymer.

Initiator type, surfactant and comonomer composition all influence the surface chemistry, and physical and thermal properties of polyNIPAm microspheres [15]. Further, stirring rate and cross-linker content used in the polymer synthesis also affect the size and mechanical properties of the microspheres, respectively. All these properties have a significant effect on cellular response to the microspheres. The key challenge is to identify and optimize both formulation and process, to obtain the desired microcarriers for the non-invasive culturing of human embryonic kidney (HEK) cells. The novelty of this research work is the production of an alternative microcarrier that facilitates cell attachment and growth, and induces cell detachment without the use of proteolytic trypsin or scrapper.

In order to be used as a microcarrier for anchorage-dependent cell culturing, the polyNIPAm must meet the following basic criteria [12]:

Size:
i. The microcarrier must be larger than the cell size in order to allow cell proliferation and growth.

LCST:
ii. The microcarrier LCST must not be higher than 37°C, the standard incubation temperature for cell cultures. If the LCST of the microcarrier is > 37°C, no cells will attach to the polyNIPAm as it will still exhibit a hydrophilic state which inhibits cell attachment.

Rigidity:

iii. The microcarrier must be sufficiently rigid for cell support, and retain its shape throughout the culturing process.

1.2 Aim and Objectives

The aims and objectives of the present study are:

i. To synthesise polyNIPAm microspheres satisfying the basic criteria for microcarrier cell culturing.

ii. To study the effect of initiator type on the synthesis of polyNIPAm microspheres via the suspension polymerisation technique.

iii. To study the effect of surfactant composition on the surface charge of polyNIPAm microspheres.

iv. To study the effect of comonomers on the surface hydrophobicity of polyNIPAm microspheres.

v. To study the effect of stirring rate and cross-linker content on the physical and mechanical properties of polyNIPAm microspheres.

vi. To study the effect of physical, mechanical and surface properties on the cellular response to polyNIPAm microspheres.

vii. To study cell detachment from polyNIPAm microspheres without the use of harmful trypsin or scrapper.

1.3 Thesis Outline

The thesis consists of nine chapters. The research significance, aims and objectives are outlined in Chapter 1. Chapter 2 provides an overview of the characteristics and synthesis of thermoresponsive polymers, along with surfactant types and applications. Additionally, a literature review for polyNIPAm-related studies is presented. Chapter 3 describes the specifications of the raw materials, experimental procedures, and characterisation techniques used in the present study. Chapter 4 demonstrates the synthesis of polyNIPAm microspheres using two different types of initiator. Modification of the surface charge of polyNIPAm microspheres, and its effect on cellular response, are studied in Chapter 5. The incorporation of a butyl methacrylate (BMA) comonomer to improve cell attachment is demonstrated in Chapter 6. Chapter 7 presents the effect of stirring rate and cross-linker content on the physical and mechanical properties of microspheres, and shows a correlation with cell proliferation and growth. An overview discussion is presented in Chapter 8. Chapter 9 concludes the present research work and makes suggestions for the future development of polyNIPAm microcarrier.

CHAPTER 2

LITERATURE REVIEW

2.0 Introduction

This Chapter presents an overview of cell culture development, followed by an overview of thermoresponsive polymers, the mechanisms of free radical polymerisation, polymerisation techniques used to prepare polymer microspheres, the classification of surfactants, and the mechanisms of protein adsorption on culture substrates. Additionally, a literature review on surface modification for improving cell attachment is presented.

2.1 Microcarrier Developments

Cell culturing is vital for the study of animal cell structure, function and differentiation, and for the production of many important biological materials such as vaccines, enzymes, hormones, and antibodies. Most mammalian cell culture products are manufactured using cells grown in suspension. The cells can be cultivated in fermenters like microorganisms. However, the majority of cells used in the manufacture of viral vaccines for human and veterinary use are anchorage-dependent, which means that the cells need to attach to a compatible surface in order to survive and multiply rather than stay in suspension. On the laboratory-scale, anchorage-dependent cells are grown as monolayers on petri dishes, flasks or roller bottles, as shown in Figure 2.1. Conventionally, roller bottles are used in the production of biologics, such as cytokines and viruses derived from those cells. In a typical production plant for those biologics, a large amount of labour is required for roller bottle handling, as thousands of roller bottles are employed in cell cultivation [4].
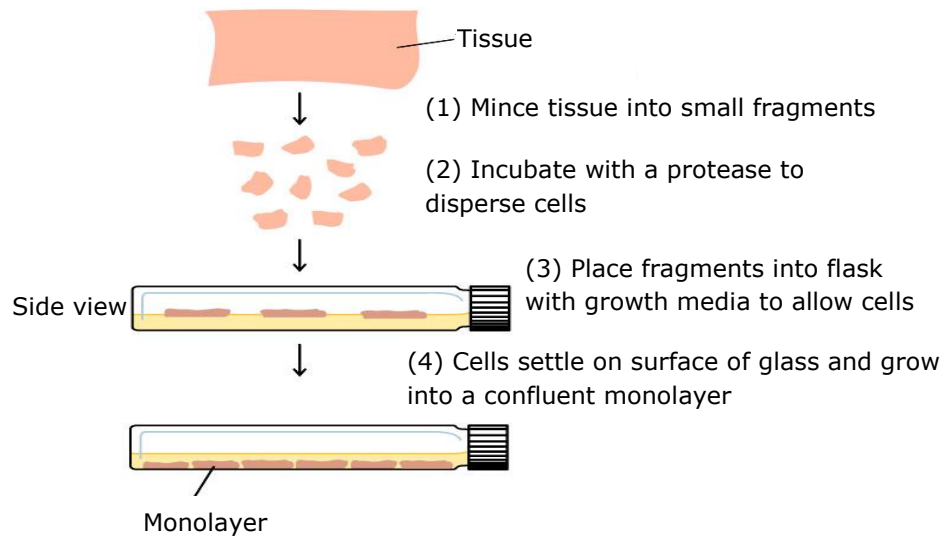
Figure 2.1 *Schematic diagram of the conventional cell culture method using a culture flask*

In this context, microcarrier cultures constitute an alternative method for culturing anchorage-dependent cells on the large-scale. A microcarrier is a support matrix, allowing for the growth of adherent cells in bioreactors. Figure 2.2 depicts a microcarrier fully attached with cells. The microcarrier culture introduces new possibilities and makes possible the practical, high-yield culturing of anchorage-dependent cells. In microcarrier culture, cells grow as monolayers on the surfaces of small spheres, or as multilayers in the pores of macroporous structures suspended in culture medium with gentle stirring. By using microcarriers within simple suspension cultures, *i.e.* fluidized or packed bed systems, it becomes possible to obtain high-yields of up to 200 million cells per milliliter. The first microcarrier culture was demonstrated by van Wezel in 1967 [3] using diethylaminoethyl (DEAE) Sephadex A50 particles. In 1972, the first industrial-scale product (Inactivated Polio Vaccine) manufactured in microcarrier culture was developed [16]. Since then, a variety of microcarriers have been introduced and much research has provided insight into the optimization of culture conditions.
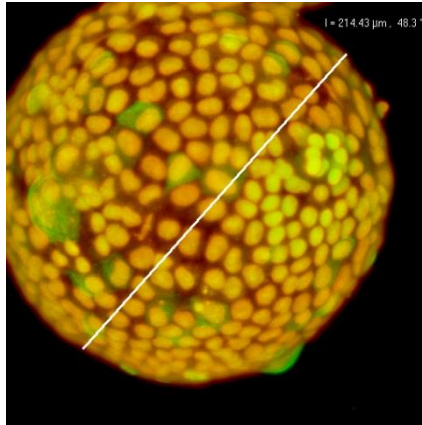
Figure 2.2 *Phase contrast micrograph of a Cytodex microcarrier attached with Vero cells [17]*

2.1.1 Advantages of Microcarriers

There are numerous advantages of microcarrier culture over conventional monolayer culture methods, as follows [18]:

(i) New applications for animal cell culture

Microcarriers offer convenient surfaces for the growth of animal cells, or increasing the yield of cells from standard monolayer culture vessels and perfusion chambers. Studies on differentiation and cell function, the isolation of cells, and the storage and transportation of cells can be performed using microcarriers.

(ii) Increased production capacity

The very large culture surface area to volume ratios offered by microcarrier systems provides for the high yield of cells without the use of bulky equipment and time consuming methodology. Owing to their large surface area to volume ratios, microcarriers occupy less space in storage, production and waste-handling, compared to conventional culture method.

(iii) Improved control

The monitoring and sampling of microcarrier cultures become easier for the production of large numbers of anchorage-dependent cells. Microcarrier systems provide for excellent control of culture parameters,

such as pH and gas tension. Improved control allows for homogeneous culture systems with a wide variety of process designs.

(iv) Reduced requirements for culture medium

Stirred microcarrier cultures yield up to 100-fold as many cells, for a given volume of medium, as compared to other monolayer techniques. Superior yields have been reported for a wide variety of systems including human fibroblasts [19], and transformed mouse fibroblasts [20]. Thus, microcarrier cultures reduce the requirements for culture medium, and subsequently reduce the cell culture costs, particularly when expensive serum supplements like fetal calf serum is required.

(v) Reduced requirements for labour

Fewer culture vessels are required with microcarrier cultures, due to the ability of microcarriers to culture large numbers of cells in small volumes (more than 1000 cells/L). Moreover, the separation of cells from culture medium is simple and no centrifugation steps are required. As a result, less labour is required for routine production.

(vi) Lower risk of contamination

In cell culture, the risk of contamination is related to the number of handling steps (*e.g.* the opening and closing of culture vessels), as required to produce a given quantity of cells or products. Microcarrier cultures reduce the number of handling steps. Hence, the risk of contamination is lowered when producing a large quantity of cells in a single microcarrier culture in comparison with several hundred roller bottles.

2.1.2 Mechanisms of Cell Attachment to Microcarriers

The attachment of anchorage-dependent cells to microcarriers can be divided into four stages (Figure 2.3). The first phase comprises slight attachment to the surface. The second phase is characterised by flattened but still spheroidal cells, where the cells are significantly more adherent due to increased contact area and bond density. Cells in the third attachment phase are significantly more adhesive than cells in phase two

because of the increased number of bonds. Cells in the fourth spreading phase are fully attached and extremely flat [21]. Figure 2.3 depicts the adhesion of cells in culture, involving: (a) the adsorption of attachment factors to the culture surface; (b) contact between the cells and the surface; (c) attachment of the cells to the coated surface; and (d) spreading of the attached cells.
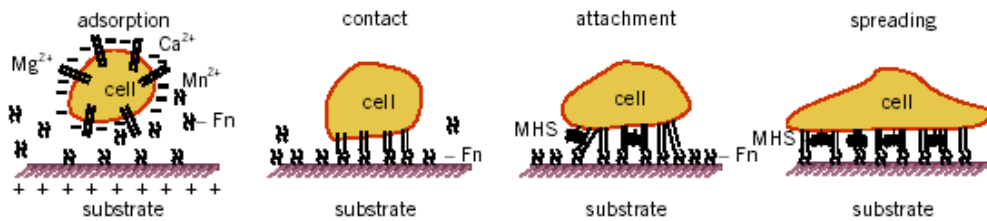
Figure 2.3 *Depiction of the four phases of the adhesion process [21]*

Two factors in culture medium that are essential for cells to adhere to culture surfaces are: divalent cations and glycoproteins in the medium or adsorbed to the culture surface. Many established and transformed cell types secrete only very small amounts of fibronectin and thus require a fibronectin or serum supplement in the culture medium before adhesion can occur [22]. Certain types of cells, such as diploid fibroblasts, can secrete more significant quantities of fibronectin and hence do not require an exogenous source for attachment [23]. When initiating a culture, it is usual practice to let the culture surface come into contact with medium containing serum before cells are added to the culture. Culture medium supplemented with 10% (v/v) fetal calf serum contains ~ 2–3 µg fibronectin/mL, and a large proportion of the fibronectin adsorbs to culture surfaces within a few minutes. Serum-free media often require the addition of fibronectin (1–50 µg/mL) before many cells can attach to the culture surfaces. Further, culture procedures affect the rate at which cells attach to surfaces. For the case of microcarrier cultures, the microcarriers and cells are often in a stirred suspension. Under such conditions, the attachment of cells to Cytodex usually occurs to the same extent as with static culture systems. However, with some cell types, an initial static culture period is required so that all steps of adhesion are fully completed.

2.1.3 Requirements of Microcarriers for Cell Culture

(i) Size, shape and diffusion limits

The diameter of different microcarriers varies from ~ 10 µm up to ~ 5 mm. The smaller microcarriers are best suited for use within stirred tanks, whilst the higher sedimentation rates of larger microcarriers make them more suitable for use within fluidised and packed beds. The smaller the microcarriers, the larger the surface area in settled bed volumes because of the smaller void volumes between them. However, the microcarrier size must be larger than the cell size for stable support. The optimum size for smooth microcarriers is ~ 100–300 µm as larger microcarriers limit the oxygen penetration into cell layers [24]. A very narrow size distribution is important for ensuring good mixing in the reactor and uniform sedimentation of the microcarrier beads, which allows for scale-up to large-scale processing.

Mass transfer in cell aggregates is a significant problem in immobilized cultures. The poor solubility of oxygen in medium at 37°C and the high consumption rate of cells make it a marker for cell aggregate limitations. For example, it has been reported that in high-density cell cultures (up to $2 \times 10^{14}/m^3$ in the cell layer), with an oxygen consumption rate of 5×10^{-17} mol/cell and a medium volume that is 10-fold the cell mass, the oxygen is consumed within three minutes [25].

A single oxygen molecule has to overcome three barriers before it reaches a cell in the middle of the carrier: firstly transport from the gas phase into the medium; then transfer from the medium to the cell mass; and then diffusion through the cell layers and consumption. The oxygen transfer rate (OTR) can be increased by increasing the volume-specific surface, or by using pure oxygen instead of air. The cells themselves should not be exposed directly to oxygen because of its toxic effect. Depending on the size of the carrier, the oxygen concentration on its outside must be increased [26].

(ii) Rigidity and shear force

The microcarrier rigidity is important for long-term cultures. The materials used should withstand the organic acids and proteases found in culture supernatants. Abrasive carriers made of brittle materials such as glass or

ceramics could harm the cells, and cause problems when filtering the culture supernatants.

In turbulent fluids, the collisions between particles and the stirrer are very energetic. In contrast to stirred tanks, the shear forces in fluidized beds are distributed homogeneously and impeller/carrier collisions are not possible. Shear forces in fluidised beds correlate with the particle sedimentation velocity and reactor type. The linear velocity should not be more than 0.3 km/h during attachment of anchorage-dependent cells, whilst a velocity of 95 km/h is necessary for cell detachment [27].

(iii) Transparency

Microcarrier transparency is important for cell observation using light microscopy. In vaccine production especially, it is important to see the morphology of cells directly on the carrier to identify the right moment to infect cells or harvest viruses. Unfortunately, due to the size, three-dimensional structure and the material of certain microcarriers, the cells cannot be observed clearly under light microscope. Furthermore, conventional scanning electron microscopy (SEM) is not suitable because of the long preparation time and effect of dehydration on cell shape and morphology [3].

2.1.4 Commercial Microcarriers

Microcarriers can be produced from various materials including DEAE-dextran, glass, collagen, polystyrene plastic, and acrylamide. Different materials possess different surface chemistries, which will influence cellular morphology and proliferation. The properties of these commercial microcarriers are outlined in the following sections:

(i) Cytodex 1

Cytodex 1 microcarriers are composed of a cross-linked dextran matrix substituted with positively charged *N*,*N*-diethylaminoethyl (DEAE) groups to a degree that is optimal for cell growth. The charged groups are located throughout the microcarrier matrix, as shown in Figure 2.4.
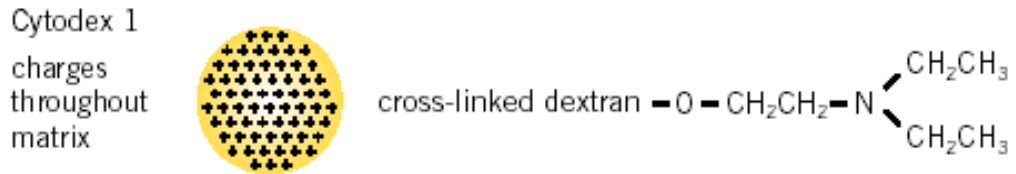
Figure 2.4 *Schematic diagram of the Cytodex 1 microcarrier [18]*

The chemical reaction conditions used to produce Cytodex 1 microcarriers ensure that the number of tandem groups is minimized (only ~ 15% of groups [28,29]. The stability and homogeneity of the charged groups is thus maintained and their possible leakage minimized. Pyrolysis mass spectroscopy has been used to test for the presence of leaked DEAE dextran in concentrated polio vaccines prepared from microcarrier cultures using Cytodex 1, and was found to be below the limits of detection, *i.e.* less than 20 ppm [30].

(ii) Cytodex 3

Cytodex 3 microcarriers work on an entirely different principle. Whilst most surfaces used in cell culture (*e.g.* glass, plastic, Cytodex 1) possess a specific proportion of small charged molecules to promote cell attachment and growth, certain proteins can also provide a surface suitable for cell growth. The connective tissue protein collagen has proved to be a valuable cell culture substrate. Cytodex 3 microcarriers feature a surface layer of denatured collagen bound covalently to the matrix of cross-linked dextran (Figure 2.5). The amount of denatured collagen bound to the microcarrier matrix is ~ 60 $\mu g/cm^2$, which results in maximum cell yields [32]. The denatured collagen is derived from pig skin type I collagen, extracted and denatured by acid treatment, concentrated and purified by an ion exchange, and steam sterilized before being coupled to the matrix.
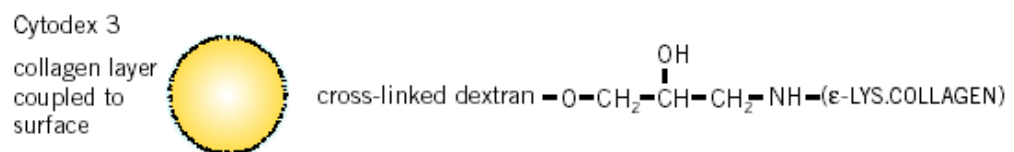
Figure 2.5 *Schematic diagram of the Cytodex 3 microcarrier*

The Cytodex 3 microcarrier combines the advantages of collagen-coated culture surfaces with the advantages of microcarrier culture. In addition, it can also be used as a general-purpose collagen-coated cell culture substrate. Most normal epithelial cells will attach more efficiently to collagen than to other surfaces. Consequently, collagen-coated culture surfaces are used frequently for establishing primary cultures and for growing cells that are normally difficult to grow in culture. Collagen-coated surfaces are beneficial because they allow differentiation of cells *in vitro* at either little or colonial culture densities. Such surfaces are also advantageous when culturing for extended periods, since they delay the detachment of the cell sheet that eventually occurs following long-term mass culture on uncoated surfaces [33].

A variety of cell types, including hepatocytes, fibroblasts, chondrocytes, epidermal cells, myoblasts and mammary epithelial cells, are cultured routinely on collagen-coated surfaces. Differentiation of myoblasts at small densities *in vitro* depends on the presence of collagen bound to the culture surface. Myoblasts attach and spread more satisfactorily on collagen than on standard cell culture surfaces [34]. Hepatocytes can be cultured more successfully on collagen surfaces. The collagen permits freshly isolated hepatocytes to attach with maximum efficiency, whilst spreading is more rapid than on any other cell culture surface. Since fibronectin is not required for attachment of hepatocytes to collagen, this surface is most suitable for the culture of hepatocytes in protein-free media.

(iii) Cytopore microcarriers

Cytopore is composed of cross-linked cellulose (Figure 2.6). With a pore size averaging 30 μm, its porosity is > 90%. Similar to Cytodex, this microcarrier is also hydrophilic due to the introduction of DEAE groups on the cellulose.

The major cell culture applications for Cytopore are in the production of recombinant products and monoclonal antibodies from Chinese hamster ovary (CHO), baby hamster kidney (BHK), mouse myeloma (NSO) and hybridoma cells. Apart from anchorage-dependent cells, Cytopore can be used to culture cells in suspension. Hence, Cytopore is used mainly for stirred tank reactors. The physical properties of Cytopore are very similar

to those of Cytodex, and the design of the stirred tank reactor, impeller and retention device can be the same for both microcarriers.
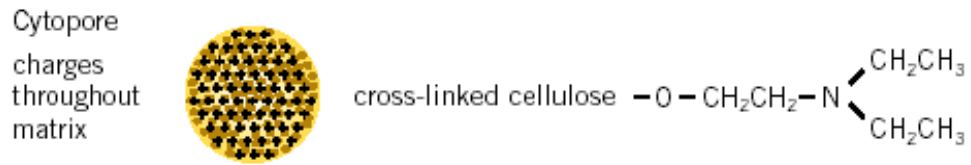
Figure 2.6 *Schematic diagram of the Cytopore macroporous microcarrier*

The main features of Cytopore are:

1. Optimised surface characteristics for the efficient attachment and spreading of cells.

2. Optimised size, density and macroporosity to facilitate suspension or fluidization, providing for healthy growth and high yields for a wide range of cells.

3. A biologically inert matrix providing a strong non-rigid substrate for stirred microcarrier cultures.

4. The macropores protect cells from shear forces and allow cells to create a micro-environment.

Cytopore exhibits high rigidity and stability under both acidic and alkaline environments and can withstand autoclaving at 121°C for 30 minutes without loss of function. It is supplied as a dry granulated powder, can be stored between 8 and 25°C with a shelf-life up to 5 years. The hydrated form of the microcarrier, sterilised and stored at 4°C, is stable for ~ two years.

(iv) Cytoline microcarriers

Cytoline microcarriers are negatively charged macroporous microcarriers, composing high-density polyethylene weighted with silica. Cytoline microcarriers are mainly hydrophobic from the polyethylene with hydrophilic contribution from the silica (Figure 2.7). The major application of Cytoline microcarrier is in the culture of CHO, in the form of adherent and semi-adherent cells for recombinant protein and monoclonal antibody production in fluidised bed perfusion cultures.

Figure 2.7 Schematic diagram of Cytoline microcarriers

Cytoline is the microcarrier of choice for 95% of adherent or semi-adherent cells in fluidized beds. It works well with cells requiring high oxygen transfer rates to reach high final cell densities. However, Cytoline is not suitable for stirred tank reactors due to its high sedimentation rate. However, one of the limitations of Cytoline is that it cannot be autoclaved at high temperatures, although repeated autoclaving at 121°C for 30 minutes is possible. Cytoline is supplied in lentil-shaped macroporous particle form, and the storage temperature and shelf-life for Cytoline are identical to that for Cytopore.

2.1.5 Cell Harvesting Process

Cell harvesting is a process of separating the adherent cells from the culture substrate surface. This process is performed when the cells have reached a population density that suppresses cell growth. Ideally, cells are harvested when they reached semi-confluency, to maximize the efficiency of transformation. In general, cells are harvested using either mechanical scrapper or trypsin. Mechanical scrapper is a rubber spatula that removes the cells from the growing surface physically. This method is used commonly when harvesting many different samples of cells for preparing extracts. On the other hand, trypsin is proteolytic enzyme that cleaves the cell membrane protein, leading to dissociation of the cells from the growing surface [35]. Figure 2.8 illustrates the cell harvesting process using mechanical scrapper and trypsin.
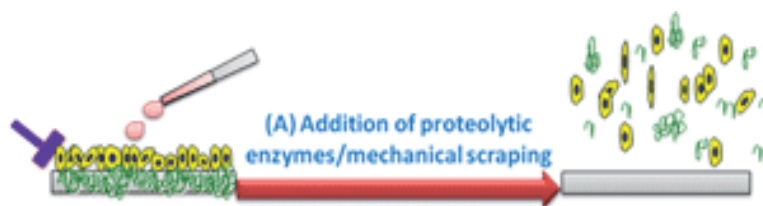
Figure 2.8 Depiction of cell harvesting process using mechanical scrapper and trypsin

Although both of the harvesting methods are fast and easy, these methods may damage the cell membrane and reduce cell yield. In this context, thermoresponsive polymers are identified as a promising candidate material for non-invasive cell culturing without the use of trypsin during harvesting process. The overview of thermoresponsive polymers is presented in the following section.

2.2 Overview of Thermoresponsive Polymers

Thermoresponsive polymers are smart polymers that exhibit a reversible physical change when external thermal stimuli are presented. This type of polymer exhibits a critical solution temperature at which the phases of polymer and solution are changed with response to their composition typically in water. Thermoresponsive polymers are divided into two categories, namely lower critical solution temperature (LCST) and upper critical solution temperature (UCST) systems. LCST systems become soluble below the critical temperature but insoluble above the critical temperature. Conversely, UCST systems exhibit single phase above the critical temperature while showing phase separation below the critical temperature, as depicted by Figure 2.9. Poly(ethylene oxide) and poly(propylene oxide) block copolymers, methylcellulose and poly(N-isopropylacrylamide) are the typical LCST polymers, whilst xyloglucan is a typical UCST polymer [36]. The characteristics of these thermoresponsive polymers are presented in the following section.
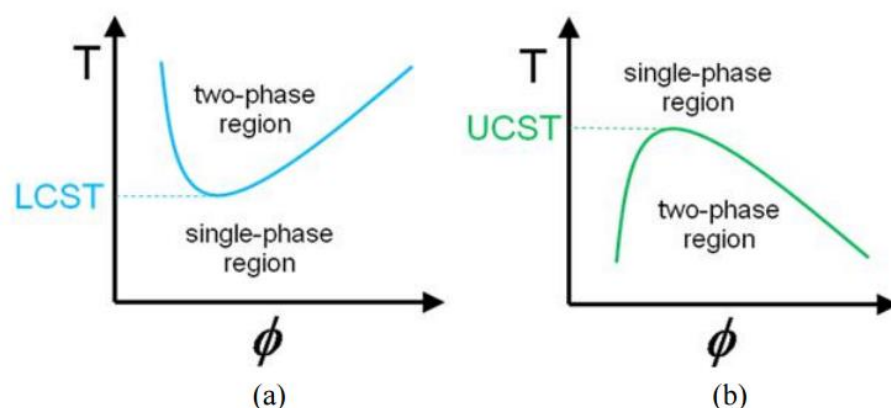
Figure 2.9 *Schematic diagram of phase diagrams for (a) LCST polymers and (b) UCST polymers [36]*

2.2.1 Xyloglucan

Xyloglucan consists of a backbone of glucose residues with side groups of xylose attached through glycosidic linkages. Figure 2.10 depicts the chemical structure of xyloglucan. It is the major hemicellulose found in the primary walls of plants. Xyloglucan exhibits a unique reversible phase transition. Xyloglucan gel is formed by removing > 35% of the galactose residues using fungal β-galactosidase as the galactose moieties facilitate steric hindrance that inhibits gel formation [37]. Gelation occurs in a limited temperature range from 40 - 80ºC. The gel reverts to sol upon cooling to 5ºC or heating to 110ºC. The xyloglucan gel has been utilised as a food additive, thickener and starch modifier [38].

Representative xyloglucan repeat unit
X = Xylose G = Glucose
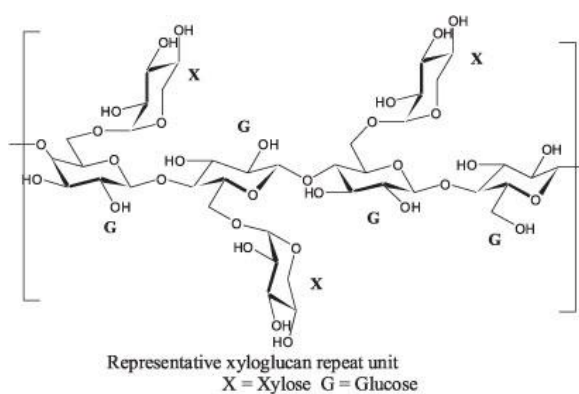
Figure 2.10 *Chemical structure of xyloglucan [39]*

2.2.2 Poly(Ethylene Oxide) and Poly(Propylene Oxide) Block Copolymers

The poly(ethylene oxide) (PEO) polymer is highly soluble in water up to 85°C. The poly(propylene oxide) (PPO) polymer is hydrophobic in nature. However, copolymers of PEO and PPO can be prepared with a wide range of solubilities and phase transition behaviours. PEO–PPO sequences are commercially available as triblock copolymers with the following trade names: Pluronics® and Tetronics® (Figure 2.11).
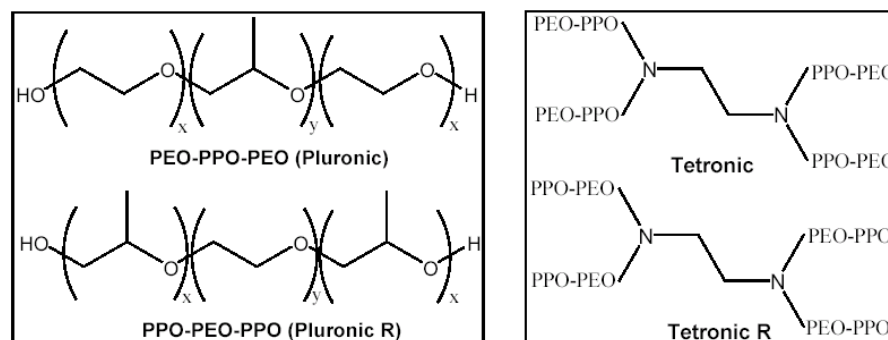
Figure 2.11 *Chemical structures of Pluronics® and Tetronics® [40]*

Pluronics® and Tetronics® may be used as thermoreversible gels and have been approved by the Food and Drug Administration (FDA) and Environmental Protection Agency (EPA) for applications as food additives, pharmaceutical ingredients, drug delivery carriers and injectable systems for tissue engineering [41]. Their gelation temperatures depend on the polymer composition and solution concentration. For example, Pluronic® gels at 37ºC in solutions that contain ~ 20 wt% of polymer. This system has been used in the treatment of burns and other wound healing applications [42]. Further, Pluronic® has been studied as an injectable drug delivery carrier. On the other hand, Tetronics® exhibits a gel-sol transition around 50ºC. Tetronics® in solution with isolated chondrocytes has been used as an injectable cartilage formulation, for testing tissue formation after subcutaneous injections in mice [43]. Furthermore, Tetronics® has been tested for the delivery of proteins and peptides [44].

2.2.3 Methylcellulose

Methylcellulose is a family of insoluble in water polysaccharides [45]. The chemical structure of methylcellulose is shown in Figure 2.12. It is produced when cellulose is exposed to methylchloride and sodium hydroxide (NaOH) solution under agitation, with methylation occurring more rapidly in NaOH-rich and higher temperature environments. Cellulose is hydrophilic but it is insoluble in water as the cellulose fibers contain crystalline regions defined by intra- and intermolecular hydrogen bonds. Methylcellulose forms a gel in aqueous solution at temperatures between 60 and 80ºC, attributed to hydrophobic association caused by

19

dehydration of the methoxyl groups. Conversely, the gel changes to a solution at temperatures below 0ºC [46]. It is used widely as a thickener in food, pharmaceutical and ceramic processing applications.
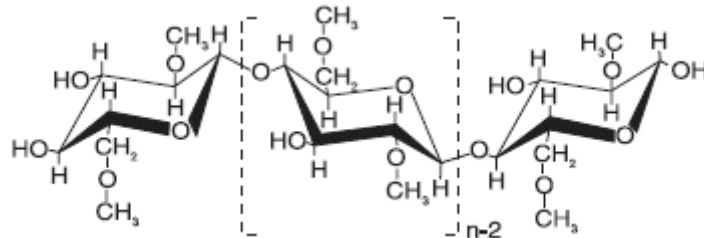
Figure 2.12 *Chemical structure of methylcellulose [45]*

2.2.4 Poly(*N*-isopropylacrylamide)

PolyNIPAm is a thermoresponsive polymer that has been studied extensively for many applications, owing to its thermosensitive properties in water [46]. PolyNIPAm exhibits a LCST at ~ 32°C, in which a reversible conformational transition occurs from expanded coil (soluble) to compact globule (insoluble) in water [47,48]. Figure 2.13 depicts the phase change of polyNIPAm at the LCST.
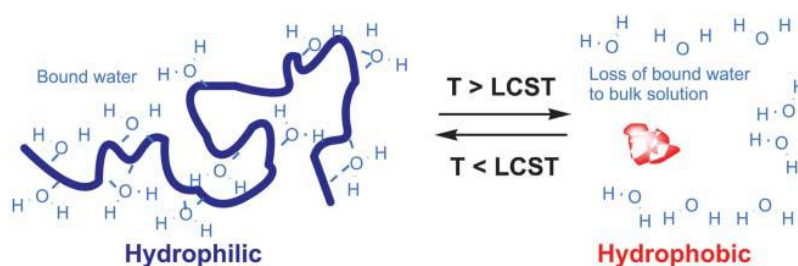
Figure 2.13 *Reversible phase change of polyNIPAm in response to temperature*

The solubility is affected as the amphiphilic polyNIPAAm chains hide the hydrophilic amide groups, whilst exposing the hydrophobic isopropyl groups, in the compact globule conformation at T > LCST. During this transition, the hydrogen bonds formed between water molecules and the

polymeric chains become disrupted, being associated with a thermodynamically favourable rise in entropy, *i.e.* the main driving force for the transition. Further, the transition can be seen as an abrupt shrinkage of the gel above the LCST, being associated with a change in the swelling capability of these crosslinked structures. Since the LCST of polyNIPAm is close to the body physiological temperature, and can be increased above or below 37 °C by the incorporation of comonomer units, it becomes particularly suitable for use as a pharmaceutical or biomedical carrier [49,50]. Based on the *in vivo* toxicity of polyNIPAm, as evaluated by Malonne *et al.* (2005), no significant acute toxic signs in mice, upon oral administration of polyNIPAm, were observed even after a month [51]. The chemical structure of polyNIPAm is depicted by Figure 2.14.
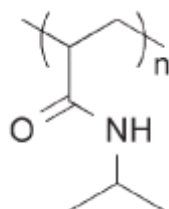
Figure 2.14 *Chemical structure of polyNIPAm*

In the tissue engineering field, temperature sensitive scaffolds and surface modifications have been investigated for the manipulation of cell sheets. For example, poly(NIPAAm-*co*-acrylic acid) (poly(NIPAAm-*co*-AA)) gels have been applied as extracellular matrices for pancreatic islets in biohydrid pancreas [52]. In tissue engineering, it is required to grow cells at a surface and to detach the confluent cells for harvesting, ideally without a biochemical or chemical reagent step. In this context, polyNIPAm grafted surfaces have been shown to support the growth of cells, as diverse as bovine endothelia and rat hepatocytes, when above the LCST, and to allow recovery of the cells when the temperature was reduced below the LCST [53]. This type of application has been tested on biodegradable polymers such as poly(L-lactic acid), showing similar behaviour to that conducted on polystyrene culture plates [54].

An emerging medical field for responsive polymer-biopolymer conjugates is the targeting of gene expression via switchable polymers that display antisense nucleotide binding behaviour [55]. PolyNIPAm conjugated with pendent oligodeoxynucleotides (ODNs) display the expected temperature-induced coil–globule transition at 33°C in physiological-like buffers (pH 7.4, 100 mM NaCl). It has been reported that translation of a plasmid encoding enhanced green fluorescent protein (EGFP) was suppressed in a dose-dependent fashion by the polyNIPAm-antisense ODN conjugate, whilst no translational repression was observed for polyNIPAm alone [55].

The use of polyNIPAm co-polymers as mediators for prokaryotic cell adhesion was first reported by Ista and co-workers [56]. LCST mediated transitions of surface-grafted polyNIPAm homopolymer materials resulted in reversible changes for adsorbed bacteria, *i.e.* staphylococcus epidermidis and Halomonas marina, being dependent on the inherent preferences of these bacterial strains for hydrophilic or hydrophobic substrates.

In general, polyNIPAm can be synthesised via various approaches, including thermal-induced free radical polymerisation, microwave irradiation, ultraviolet light irradiation, and precipitation polymerisation. It has been reported that the form of the final product depends on the synthesis technique used. Table 2.1 lists work regarding polyNIPAm synthesis using different techniques for biomedical applications. It is found that most of the synthesis methods involved functionalisation and grafting of polyNIPAm onto other materials such as gold and glass. These methods are tedious and require a lot of different chemical substances. In particular, for use as cell culture membrane, the tissue culture polystyrene (TCPS) dish was grafted with polyNIPAm to induce cell detachment thermally. However, two-dimensional planar structure of the TCPS dish limits the production of cells. To the best of my knowledge, none of the study reported about polyNIPAm microcarrier synthesis for cell culturing. Hence, the aim of my present study is to develop a thermally responsive polyNIPAm microcarrier for non-invasive harvesting of cells without the use of trypsin. The mechanism of polymerisation technique used in polyNIPAm microcarrier synthesis is presented in the following section.

Table 2.1 *Overview of work on the synthesis of polyNIPAm*

Refer-ence	Material	Form	Synthesis method	Applica-tion
[57]	*N*-isopropylacrylamide (NIPAAm)-vinylpyrrolidone (VP)-acrylamide (AAm)	Nanogel	Free radical polymeri-sation	Drug delivery system
[58]	PolyNIPAm-functionalised Pt/C catalyst	Membrane	EDC-surface functionali-sation	Proton exchange membrane fuel cell
[59]	Dextran-aldehyde/PNIPAm/superparamagnetic iron oxide	Nano-particles	Hydrazide functionali-sation	Drug delivery
[60]	Hybrid polyNIPAm-pentapeptide conjugate	Solution	Atom transfer radical polymerisation	Controlled uptake and release
[61]	PolyNIPAm grafted on graphene	Sheet	Atom transfer radical polymerisation	Controlled release drug delivery
[62]	PolyNIPAm brush grafted PCL substrate	Monolayer	Atom transfer radical polymerisation	Cell sheet engineering
[63]	Hydrazide-functionalised polyNIPAm	Hydrogel	Adipic acid dihydrazide functionalisa-tion	Biomedical applications
[8]	RGDS-immobilized polyNIPAm grafted on TCPS dish	Monolayer	Electron beam irradiation	Cell culture membrane
[64]	PolyNIPAm/methacrylic acid (MAA)	Multisensitive core-shell microgel	Free radical polymerisation	Controlled uptake and release
[65]	Comb-type grafted polyNIPAm on TCPS dish	Monolayer	Electron beam irradiation	Cell sheet engineering
[66]	PAEMA/PolyNIPAm core cross-linked micelles	Micelles	Reversible addition-fragmentation chain transfer	Controlled release drug delivery

Table 2.1 (Continued)

[67]	PolyNIPAm brush on TCPS dish	Brush	Atom transfer radical polymerisation	Cell culture membrane
[68]	Au/PNIPAm nanogel	Nanosphere	Precipitation polymerisation	Drug and gene delivery
[69]	PolyNIPAm brush grafted on Au-coated polycarbonate track-etched membrane	Nanocapillary array membrane (NCAM)	Atom transfer radical polymerisation	Controlled filtration devices
[70]	PolyNIPAm/polyarginine bioconjugate	Nanosphere	Radical polymerisation & EDC-activated coupling	Non-viral transgene vector
[71]	Au-Silica/PolyNIPAm core shell microgel	Microsphere	MPS coupling & emulsion polymerisation	Photonic device
[72]	Gold coated polyNIPAm particles	Particles	UV irradiation	Photonic device
[73]	PolyNIPAm modified glass	Monolayer	Surface initiated radical graft polymerisation	Optical valve underwater engineering
[74]	PolyNIPAm/PEG grafted on PET culture membrane	Porous membrane	Electron beam irradiation	Cell culture membrane
[75]	PolyNIPAm grafted on glass substrate	Monolayer	Free radical polymerisation	Protein adsorption study
[76]	Poly(*N*-isopropylacrylamide)	Porous gel	Free radical polymerisation using benzol-peroxide as initiator	Tunable filters, actuators & sensors

Table 2.1 (Continued)

[77]	Poly(*N*-isopropylacrylamide) thin layer on a gold	Thin layer	Free radical polymerisation using AIBN as initiator	Biomedical applications
[78]	PEG-modified poly(*N*-isopropylacrylamide) Poly(ethylene glycol) (PEG) as the porogen	Macro-porous disc	APS & TEMED redox initiated polymerisation	Controlled release of macro-molecular active agents
[79]	PNIPAm grafted on polystyrene (TCPS) culture membrane	Nonporous membrane	Electron beam irradiation	Cell culture membrane
[80]	Poly(*N*-isopropylacrylamide-co-acrylic acid)	Cylindrical disc	APS & TEMED redox initiated polymerisation	Injectable scaffolds for tissue engineering applications
[81]	Poly(*N*-isopropylacrylamide-co-methacrylic acid)	Cylindrical disc	Free radical polymerisation using AIBN as initiator	Size-selective permeation/ controlled drug delivery
[82]	Poly(*N*-isopropylacrylamide) / Hydroxypropyl cellulose was used as pore-forming agent	Macro-porous disc	APS & TEMED redox initiated polymerisation	Controlled active agent delivery/ microrobotic devices

2.3 The Free Radical Polymerisation of PolyNIPAm

Free radical polymerisation is a type of chain growth polymerisation process by which a polymer is formed through the addition of free radical building blocks. The polymerisation process comprises three stages, namely initiation, propagation and termination. Each stage of the polymerisation reaction will be described in the following sections.

2.3.1 Initiation

In the present study, the polymerisation reaction was initiated by free radicals generated from the 2,2-azobis(iso-butyronitrile) (AIBN) initiator. AIBN is an azo compound, *i.e.* containing an −N=N− group. The decomposition temperature of AIBN is 65°C. Two 2-cyanoprop-2-yl radicals are produced and a molecule of nitrogen gas is eliminated upon thermal decomposition of each AIBN molecule when heated up to 70°C [83]. The formation of free radicals from AIBN decomposition is depicted by Figure 2.15.
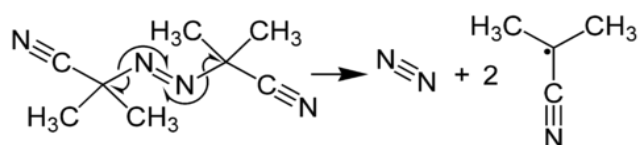
Figure 2.15 *Free radical formation from AIBN decomposition*

The reactive AIBN free radicals add to a monomer molecule by opening the unstable carbon-carbon double bond in the NIPAm monomer to produce secondary free radicals. Figure 2.16 illustrates the mechanism of NIPAm chain initiation by free radical attack.
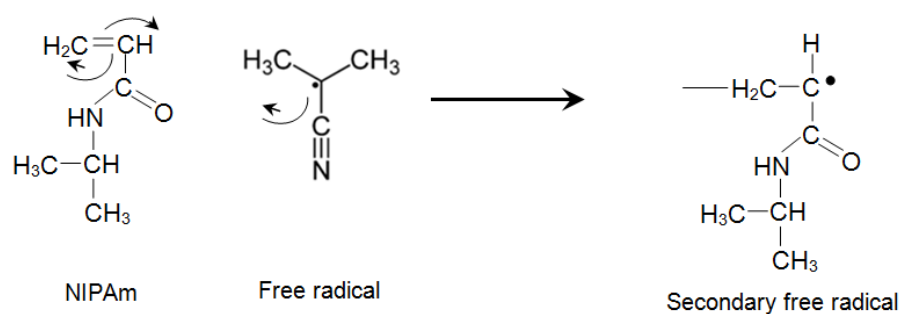
Figure 2.16 *Mechanism of NIPAm chain initiation*

2.3.2 Propagation

Once a polymer chain has been initiated, the chain propagates until all the monomers are used up or until termination occurs. The propagation process usually takes place within a fraction of a second, in which thousands of monomers are added to the chain within this period. Since the O-O bond is weak (with bond dissociation energy of 154 kJ/mol) and non-polar, O_2 can cleave homolytically to produce two oxygen free radicals. In the homolytic cleavage process, a two-electron covalent bond breaks and one electron goes to each of the oxygen atom, as shown in Figure 2.17. Hence, the reaction vessel was purged with inert nitrogen gas to remove all oxygen and prevent any free radicals from reacting with the polymer chain.

Oxygen molecule   Oxygen radicals

Figure 2.17 *Formation of free radicals via homolytic cleavage of oxygen*

2.3.3 Termination

Chain termination can occur by two different mechanisms, *i.e.* by coupling or disproportionation. These mechanisms involve a reaction between two growing chain ends. Some monomers terminate exclusively by either coupling or disproportionation. If longer chains are desired, the initiator concentration should be kept low; otherwise, many shorter chains will result [83].

(i) Coupling

Coupling occurs when two growing radicals at the chain terminals simply join to form a single chain, as depicted by Figure 2.18.

Figure 2.18 *The coupling mechanism for polyNIPAm chain formation*

(ii) Disproportionation

Disproportionation occurs when a free radical at the end of one chain attacks a hydrogen atom attached to the penultimate carbon atom of the second chain, associated with the formation of a carbon-carbon double bond and two inactive polymer chains, as depicted by Figure 2.19.
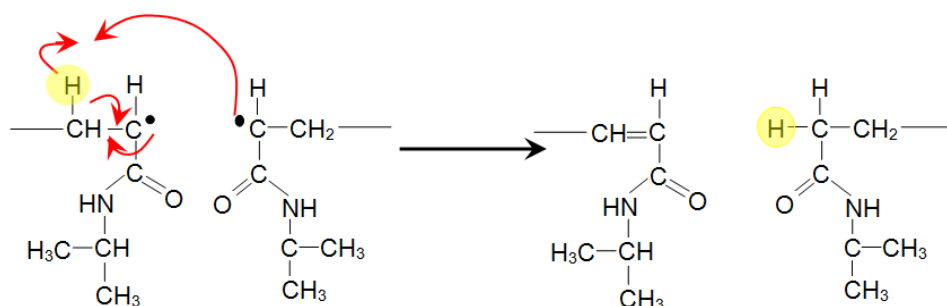
Figure 2.19 *The disproportionation mechanism for the NIPAm radical*

The mechanism of free radical polymerisation of polyNIPAm is summarised by Figure 2.20.

NIPAm monomer   MBAm cross-linker   Cross-linked polyNIPAm
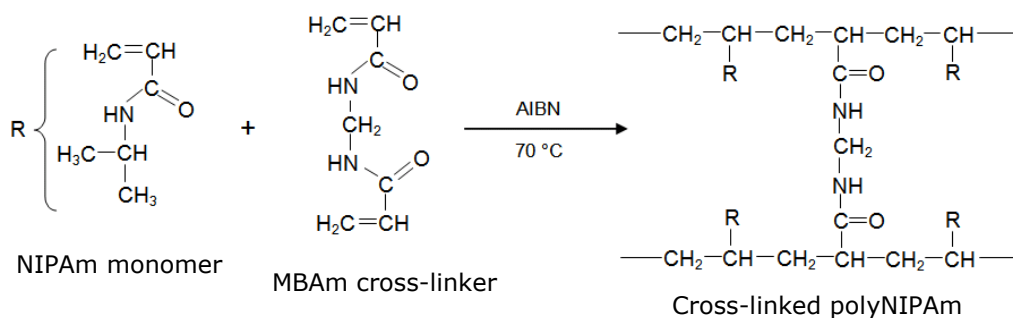
Figure 2.20 *The mechanism of free radical polymerisation of polyNIPAm*

28

2.4 Polymerisation Techniques

Three polymerisation techniques may be used to produce spherical particles, *i.e.* precipitation, emulsion and suspension polymerisation. The differences between these polymerisation techniques are now described.

Precipitation polymerisation is a single phase, homogeneous radical polymerisation process, with no stabilizer or surfactant required. It begins with a homogeneous mixture of monomer, initiator and solvent, but the formed polymer is insoluble in the solvent [84,85]. The propagating chains grow beyond their solubility limit in the solvent and precipitate out as particles, as depicted by Figure 2.21. Typically, the resultant nuclei aggregate into larger, polydispersed particles that continue to grow by capturing other particles, either by newly formed polymer chains or by absorption and polymerisation of the monomer.
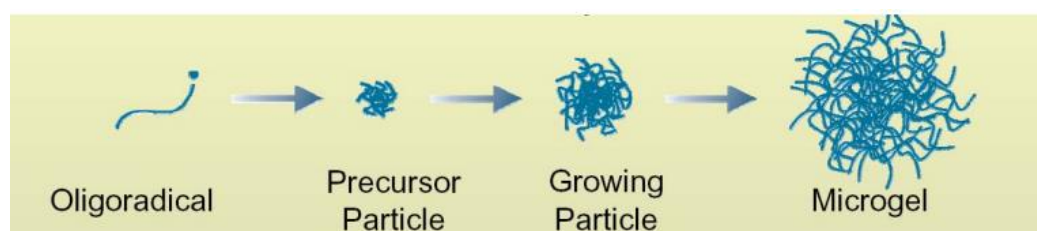
Figure 2.21 Polymer particle formation via precipitation polymerisation

Emulsion polymerisation is a type of heterogeneous radical polymerisation process whereby two different phases (usually oil and water) are involved. Droplets of monomer (oil) are emulsified with surfactants in a continuous phase of water. The initiator is not located in the monomer phase, and the polymerisation reaction is not initiated in the monomer phase. Instead, polymerisation takes place within the particles that spontaneously form during the first few minutes of processing. Figure 2.22 presents a depiction of emulsion polymerisation. An amphiphilic surfactant is required to stabilise the thermodynamically unstable emulsion. Micelles are formed as surfactant molecules adsorb onto small amounts of monomer molecules. Free radicals generated from the initiator in the aqueous phase diffuse into the micelles and react with the monomer droplets [86]. The growing polymer chains continue to propagate until a second radical diffuses into the micelle.
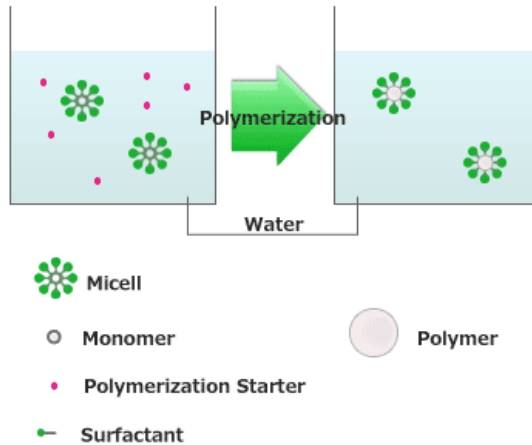
Figure 2.22 *Polymer particle formation via emulsion polymerisation*

Suspension polymerisation is another type of heterogeneous radical polymerisation process that utilises two different phases. In this case, the initiator is located within the monomer phase in suspension, and the polymerisation reaction occurs within the monomer droplets. The monomer droplets are converted into spherical polymer particles once the monomer has reacted with the radicals generated from the initiator, followed by propagation of the polymer chains. Figure 2.23 illustrates the formation of polymer particles via suspension polymerisation.
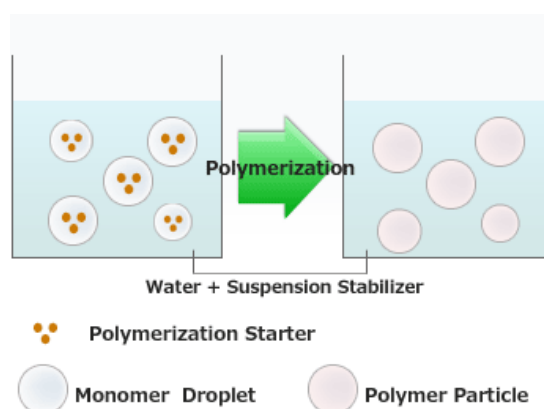
Figure 2.23 *Polymer particle formation via suspension polymerisation*

The key difference between emulsion and suspension polymerisation is that: In emulsion polymerisation, the water-soluble radicals are more likely to diffuse into micelles rather than monomer droplets. This is due to the presence of large numbers of micelles having much higher surface area (~ 1,000 times more) compared to monomer droplets. As a result, the size of the polymer particles produced from emulsion polymerisation is relatively small, *i.e.* between 0.05 and 2 μm [87]. Table 2.2 summarises the key features of precipitation, emulsion and suspension polymerisation.

Table 2.2 *Overview of precipitation, emulsion and suspension polymerisation [87]*

	Precipitation polymerisation	Emulsion polymerisation	Suspension polymerisation
Number of phases	One	Two	Two
Location of initiator	In monomer phase	In solvent	In monomer phase
Site of polymerisation	In solvent	In micelles	In monomer droplets
Particle size produced	0.1 - 10 μm	0.05 - 0.2 μm	20 - 2000 μm

2.5 Surfactant Classification

A surfactant is a surface active agent which adsorbs at a surface or interface. Surfactant molecules incorporate both hydrophilic and hydrophobic groups, referred to as "head" and "tail", respectively [88] (Figure 2.24).
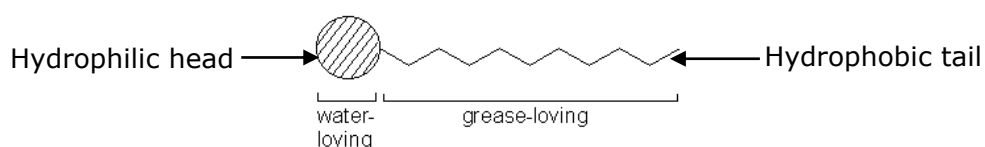
Figure 2.24 *Schematic representation of a surfactant*

The driving force for surfactant adsorption at an interface is the reduction of free energy at the phase boundary. When surfactants dissolve in aqueous media they orientate at the surface such that the hydrophobic components emanate from the aqueous environment (Figure 2.25). When the surfactant molecules replace some of the surface water molecules, the force of attraction between surfactant and water molecules is less than that between two water molecules, with consequent reduction in surface tension [89].
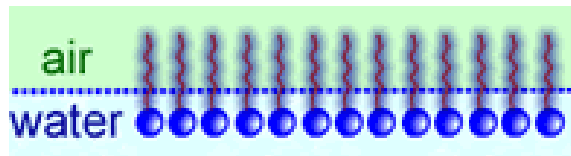
Figure 2.25 *Alignment of surfactant molecules at the water-air interface*

Surfactants will adsorb also at the interface between two immiscible liquids, such as oil and water. The surfactants orientate themselves with their hydrophilic groups in water and their hydrophobic groups in the oil phase (Figure 2.26). The interfacial tension arising because of a similar imbalance of attractive forces as at the water surface, will be reduced by the adsorption of surfactants [90].
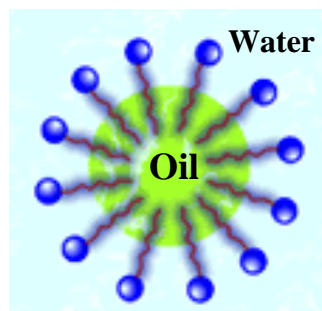
Figure 2.26 *Orientation of surfactant molecules at an oil-water interface*

Generally, surfactants can be classified into four categories, depending on the charge on the polar head group. Table 2.3 lists some examples of anionic, cationic, nonionic, and zwitterionic surfactants.

Table 2.3 *Classification of surfactants [91]*

Class	Examples
Anionic	Sodium stearate
	Sodium dodecyl sulfate
	Sodium dodecyl benzene sulfonate
Cationic	Laurylamine hydrochloride
	Trimethyl dedecylammonium chloride
	Cetyl trimethylammonium bromide
Nonionic	Polyoxyethylene alcohol
	Alkylphenol ethocylate
	Polysorbate 80
Zwitterionic	Dodecyl betaine
	Lauramidopropyl betaine

2.5.1 Anionic Surfactants

Negatively charged polar head groups in anionic surfactants normally originate from carboxylate, sulphate, sulfonate or phosphate groups. Typically, the counterions used are sodium, potassium, ammonium, calcium or various protonated alkyl amines. Sodium and potassium impart water solubility, whereas calcium and magnesium promote oil solubility. Amine or alkanol amine salts give products with both water and oil solubility [91]. Anionic surfactants are the most commonly used class of surfactant because of the ease and low cost of manufacture, but they are sensitive to water hardness. Sodium laureth sulfate is one of the most commonly used anionic surfactants in cleaning applications. It lowers the surface tension of liquids and promotes particles and impurities in suspension to bind together. Some examples of anionic surfactants are presented in Figure 2.27.
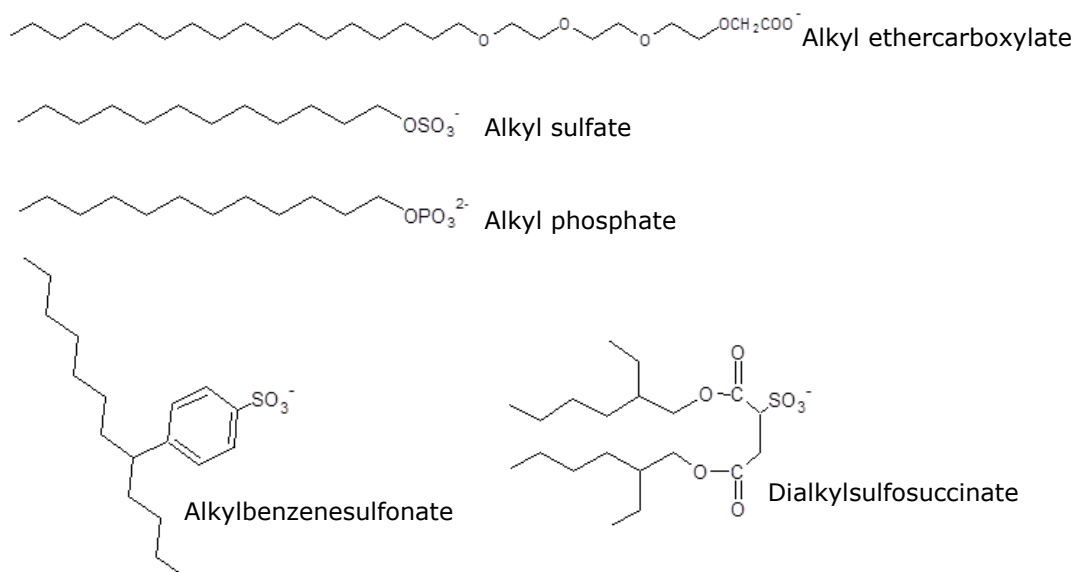
Figure 2.27 *Chemical structures of example anionic surfactants [91]*

2.5.2 Cationic Surfactants

The charge of cationic surfactants arises from the presence of nitrogen atoms from either amine or quaternary ammonium compounds. The quaternary ammonium compounds retain their charge over the whole pH range, whilst amine-based compounds are pH sensitive and only function as surfactants in the protonated state, and hence cannot be used at high pH. Cationic surfactants are generally not compatible with anionic surfactants. The majority of surfaces, which include metals, minerals, plastics, fibres and cell membranes are negatively charged [88]. The applications of cationic surfactants relate to their tendency to adsorb at these surfaces (Table 2.4). The chemical structures of some cationic surfactants are presented in Figure 2.28.

Table 2.4 *Applications of cationic surfactants [88]*

Surface	Application
Steel	Anticorrosion agent
Mineral ores	Flotation collector
Inorganic pigments	Dispersant
Plastics	Antistatic agent
Fibres	Fabric softener
Hair	Conditioner
Fertilizers	Anticaking agent
Bacterial cell walls	Bactericide
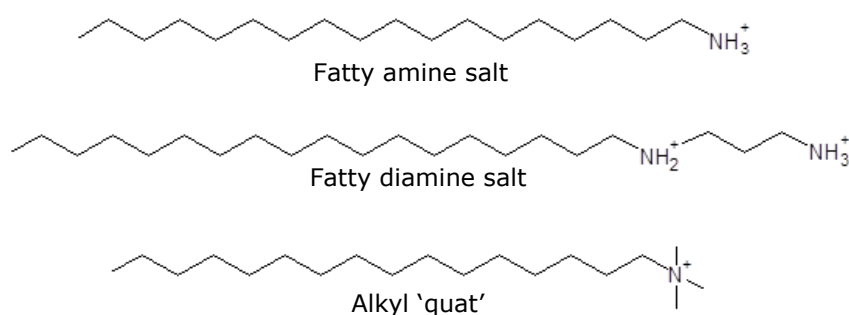
Figure 2.28 *Chemical structures of example cationic surfactants [91]*

2.5.3 Nonionic Surfactants

Nonionic surfactants incorporate a non-charged polar head group, such as polyether or polyhydroxyl chains. They are not sensitive to water hardness and are compatible normally with other types of surfactants. Contrary to ionic surfactants, their physicochemical properties are not influenced significantly by electrolytes [91]. For example, sorbitan ester is a polyhydroxyl-based non-ionic surfactant, commonly found in food and used in drug applications. Figure 2.29 presents the chemical structures of some non-ionic surfactants.

Fatty alcohol ethoxylate

Fatty acid ethoxylate

Sorbitanalkanoate

Alkyl glucoside
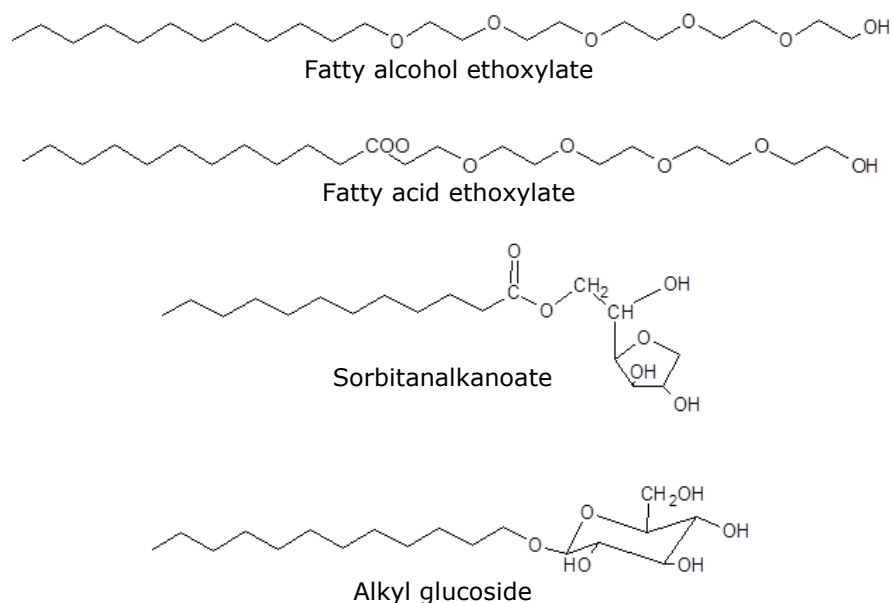
Figure 2.29 *Chemical structures of example nonionic surfactants [91]*

2.5.4 Zwitterionic Surfactants

Zwitterionic surfactants possess two differently charged polar head groups. The positive charge is carried normally by an ammonium group whilst the negative charge is often carried by a carboxylate. If the ammonium group is quaternary, the molecule will exist as a zwitterion over a wide pH range, being permanently charged. If not, the molecule will behave as an amphoteric surfactant, *i.e.* the molecule will change from net cationic to zwitterionic to net anionic as pH is increased. Such surfactants will only be zwitterionic over a certain pH range, depending on the p*K*a value, *i.e.* the acidity constant which corresponds to the strength of an acid in a solution [92]. At the isoelectric point, both charged groups will be fully ionised and the molecule will show properties similar to those of a non-ionic surfactant. As the pH shifts away from the isoelectric point, the molecule will gradually assume the properties of either a cationic or anionic surfactant [88]. In a similar fashion to nonionic surfactants, zwitterionic surfactants are compatible with other types of surfactants and are not sensitive to water hardness. Zwitterionic surfactants exhibit excellent dermatological properties, low eye irritation and are used frequently in shampoos and other cosmetic products [89]. *N*-alkyl

derivatives of simple amino acids such as glycine (NH_2CH_2COOH), amino propionic acid ($NH_2CH_2CH_2COOH$) and the alkyl betaines are common examples of zwitterionic surfactants. Chemical structures for some zwitterionic surfactants are presented in Figure 2.30.

Betaine

Amidobetaine

'Imidazoline'

Amine oxide
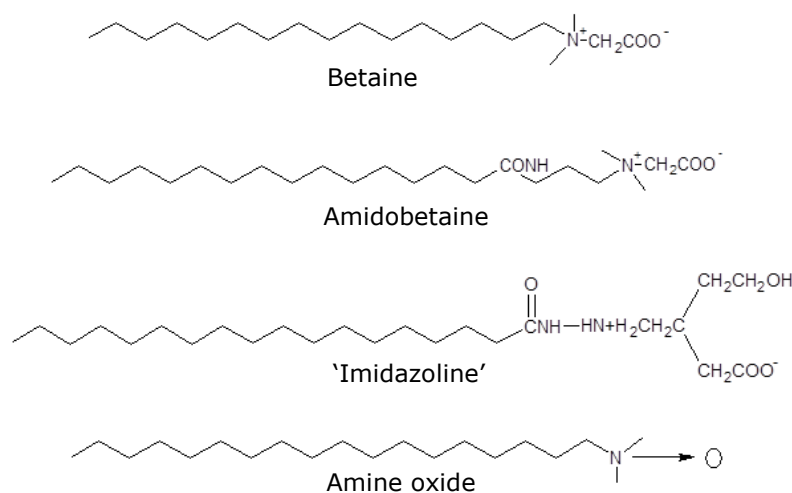
Figure 2.30 *Chemical structures of example zwitterionic surfactants [91]*

2.6 The Hydrophile-Lipophile Concept

The hydrophile–lipophile balance (HLB) concept was introduced by William C. Griffin in 1949 [88]. The HLB number represents the ratio of the hydrophilic to the hydrophobic part of the surfactant. The HLB number for a normal nonionic surfactant can be determined by simple calculation:

For alcohol ethoxylates and alkylphenolethoxylates:

$$HLB = \frac{Weight\ \%\ of\ ethylene\ oxide}{5}$$

For polyolethoxylates:

$$HLB = \frac{Weight\ \%\ of\ ethylene\ oxide + Weight\ \%\ polyol}{5}$$

For polyolethoxylates:

$$HLB = 20 \left(1 - \frac{Saponification\ number\ of\ ester}{Acid\ number\ of\ the\ fatty\ acid}\right)$$

The HLB number gives an indication of the solubility of a surfactant in liquids. Table 2.5 presents some surfactant applications based on Griffin's HLB concept. In general, a surfactant having low HLB number (0 to 10) tends to be oil-soluble, whereas a surfactant having high HLB number (greater than 10) tends to be water-soluble [89].

Table 2.5 *Surfactant applications based on Griffin's HLB number concept [88]*

HLB number	Application
3-6	Emulsifier for water-in-oil (W/O) emulsion
7-9	Wetting agent
8-18	Emulsifier for oil-in-water (O/W) emulsion
13-15	Detergent
15-18	Solubiliser

Griffin's HLB number concept is restricted to nonionic surfactants. However, the concept was extended by Davies [93] with the introduction of a scheme to assign HLB group numbers to chemical groups comprising a surfactant (Table 2.6).

Table 2.6 *HLB numbers according to the concept of Davies [88]*

Hydrophilic group	HLB number
-SO_4Na	35.7
-CO_2K	21.1
-CO_2Na	19.1
-N (tertiary amine)	9.4

Table 2.6 *(Continued)*

Hydrophilic group	HLB number
Ester (sorbitan ring)	6.3
Ester (free)	2.4
$-CO_2H$	2.1
-OH (free)	1.9
-O-	1.3
-OH (sorbitan ring)	0.5

Lipophilic group	HLB number
0	-0.87
$-CF_2-$	-0.87
0	-0.475
$-CH_2-$	-0.475
-CH-	-0.475

HLB = 7 + ∑(hydrophilic group numbers) +∑(lipophilic group numbers)

It is recognised that the combination of a more hydrophilic and a more hydrophobic surfactant is often superior to a single surfactant when making a stable emulsion. This is attributed to better packing at the oil-water interface provided by the two surfactants, having different critical packing parameters. The newly created oil-water interface can be furnished with water-soluble and oil-soluble stabilising surfactants from both sides simultaneously [88].

2.7 Surfactant Adsorption

The surface charge of a solid material can be modified by the adsorption of a surfactant [94]. Adsorption is a partitioning of the adsorbate species between the interface and the liquid media, and can occur if the interface is favoured by the surfactant in comparison to the liquid media. The driving force for surfactant adsorption is influenced by a number of forces such as electrostatic interaction, hydrogen bonding, covalent bonding, and hydrophobic interaction. [95]. The standard free energy of adsorption, ΔG^0_{ads} can be written as:

$$-\Delta G^0_{ads} = \Delta G^0_{elec} + \Delta G^0_H + \Delta G^0_{chem} + \Delta G^0_{C-S}$$

where ΔG^0_{elec} is the free energy due to electrostatic interaction; ΔG^0_H is the free energy due to hydrogen bonding; ΔG^0_{chem} is the free energy due to chemical bonding; and ΔG^0_{C-S} is the free energy due to hydrophobic interaction. The negative sign convention for ΔG^0_{ads} indicates that the reaction occurs spontaneously.

Electrostatic interaction is the major driving force for adsorption in systems involving ionic surfactants and charged solid particles. The adsorption of the cationic surfactant cetyltrimethyl ammonium bromide on negatively charged silica is an example of adsorption due to electrostatic interaction [96]. Conversely, hydrogen bonding plays an important role in systems containing nonionic surfactants. For example, the adsorption of ethoxylated alcohol onto oxides is attributed to hydrogen bonding between surfactant functional groups and the mineral surface [49]. Otherwise, chemical bonding is system specific, with covalent bonding between surfactant and solid. The adsorption of fatty acids on fluorite and hematite is an example of adsorption due to covalent bonding between surfactant and mineral surface [97]. Finally, the major driving force for adsorption onto a hydrophobic solid surface is the hydrophobic interaction between a surfactant alkyl chain and hydrophobic sites on the solid.

The interaction between different surfactants can produce significant interfacial effects, due to charge density and adsorption changes at the surface. The addition of small amount of one surfactant type to another can improve the adsorption process. For example, the adsorption of both anionic and cationic surfactants onto silica can be promoted by the co-adsorption of cationic surfactants [98]. For the case of nonionic-anionic

surfactant mixtures, they do not adsorb themselves but can co-adsorb in the presence of another component. In a study of the adsorption of tetradecyl-trimethyl-ammonium chloride (TTAC) and pentadecyl-ethoxylated-nonyl-phenol (NP-15) on alumina, TTAC adsorbed onto the negatively charged alumina (pH = 10), but NP-15 did not. However, the adsorption of NP-15 was improved significantly with increasing TTAC concentration in the surfactant mixture [98]. The mechanism for co-adsorption of nonionic-cationic surfactant mixtures is similar to that for nonionic-anionic surfactant mixtures. Xu *et al.* [99] reported that adsorption of the nonionic surfactant polyoxyethylene glycol onto hydrophilic surfaces was enhanced by the presence of the cationic surfactant dodecyltrimethylammonium chloride, due to hydrophobic interaction and a reduction of electrostatic repulsion between cationic head groups by the nonionic surfactant.

2.8 Mechanism of Protein Adsorption on Culture Substrate

Attachment of cells to a substrate is specifically promoted by a family of adhesive matrix proteins such as fibronectin, laminin, vitronectin and fibrinogen (Figure 2.31). The initial attachment of cells to a substrate is followed by a reorganisation of cytoskeletal components resulting in a flattening and spreading of the cell body. Subsequently, specialised adhesive structures like focal adhesions are formed [100].
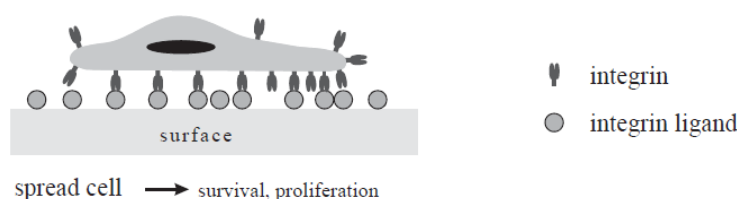
Figure 2.31 *Schematic representation of a cell-substrate interaction [101]*

In this context, initial protein adsorption plays an important role in cell adhesion and cell proliferation. Protein adsorption is defined as the partitioning of a protein between a bulk phase and an interface [102]. It was reported that cellular attachment increases with increasing protein adsorption [103]. According to Bollag *et al.* [104], the mechanism of

protein adsorption is based primarily on hydrophobic interactions between the hydrophobic portions of the adsorbed proteins and the substrate surface. Several studies on the effect of surface hydrophilicity on protein adsorption have been conducted. For example, protein adsorption on PEG-modified silicon surfaces was studied by Jeon *et al.* [105]. It was found that the amount of protein adsorbed on a PEG-modified silicon surface was lower than that on a unmodified silicon surface. This was due to steric repulsion exerted by the nonionic water soluble PEG film, which suppressed the direct contact of protein with the substrate. On the other hand, the O^- groups from the unmodified silicon surface allowed direct interaction between protein and the substrate surface through ionic and hydrogen bonding [106,107]. Similar findings were reported by Sawhney and Hubbell (1992) [108], in which the PEG chains hindered cellular attachment to the silicon substrate, leading to poor proliferation of cells. Further, Vogler (2006) [109] reported a decrease in protein adsorption with an increase in hydrophilicity of silanised glass. No protein adsorption was found on substrates having a water contact angle less than 65°. This is in agreement with the study of the effect of surface hydrophilicity on protein adsorption by Cha *et al.* (2008) [110].

2.9 Overview of Work on Surface Modification for Improved Cell Attachment

In general, membrane proteins can be classified as transporter, receptor or adhesion molecules, or as enzymes. These proteins play an important role in substrate transfer through cell membranes, connection and recognition amongst cells, interaction with the extracellular matrix (ECM), immune response to foreign objects, and matrix formation for cell embedding. These proteins are categorized into three domains, *i.e* the extracellular, transmembrane and cytoplasmic domain [111]. Amongst these three domains, the transmembrane proteins such as the adhesion integrin, selectin and cadherin molecules are essential for cell survival and growth [112].

Extensive studies have been performed to render the bio-adhesion of materials via functionalisation with molecules that are able to interact with transmembrane adhesion proteins. For example, Arg-Gly-Asp (RGD), tripeptide sequence, has been used to modify the surface chemistry of

culture substrates. Table 2.7 presents an overview of previous studies on the modification of materials using ECM proteins or RGD peptides. According to their findings, cell attachment and cell growth were improved after ECM or RGD functionalisation. However, there is a major drawback of using ECM or RGD peptides, *i.e.* a large amount of long chain peptides is required for functionalisation. In addition, peptides tend to diffuse undesirably from the interface [113]. Further, it is costly due to the complex synthesis procedure involved.

Table 2.7 *Overview of previous studies on the functionalisation of materials with peptides*

Reference	Substrate material	Conjugation material	Findings
[114]	Carboxylate-functionialised poly(*N*-isopropylacrylamide)-co-*N*-acryloylalanine	Fibronectin	Greater amount of endothelial cells spread on the fibronectin-immobilised substrate
[115]	Cellulose	Xyloglucan-GRGDS	*In vitro* studies showed that the adhesion of human endothelial cells was enhanced after cellulose modification with xyloglucan-GRGDS
[116]	Methylcellulose (MC)	Laminin	The laminin-functionalized MC exhibited enhanced adhesion of primary rat cortical neurons
[117]	Poly(*N*-isopropylacrylamide-co-polyethylene glycol)	Gly-Arg-Gly-Asp-Ser (GRGDS) peptides	The peptides-conjugated copolymer enhanced osteoblasts spreading by 600% as compared to the non-conjugated copolymer
[118]	Poly(ethylene oxide) and poly(propylene oxide) copolymer	Extracellular matrix (ECM)	The endothelial cells were found to adhere and grow on protein-coated surfaces

Table 2.7 *(continued)*

[119]	Poly(ethylene terephthalate)	Arg-Gly-Asp (RGD) peptides	The RGD-grafted PET membrane promoted cellular adhesion while the original membrane showed poor adhesion of human epithelial cells
[120]	Poly(*N*-isopropylacrylamide-co-2-carboxyisopropylacrylamide) grafted onto polystyrene dish	Arg-Gly-Asp-Ser (RGDS) peptides	Greater spreading of human umbilical vein endothelial (HUVE) cells was found for the RGDS-immobilised surfaces
[121]	Tissue culture polystyrene (TCPS) dish	RGD peptide	Cell adhesion and spreading on the modified TCPS dish increased significantly after the incorporation of RGD peptide
[122]	PolyNIPAm-co-Poly(*N*-aminoethyl methacrylate)	Cell-adhesion peptides GRGDY	The GRGDY-modified pNIPAM hydrogels presented improved cell attachment and temperature-dependent detachment of chondrocytes
[123]	Poly(NIPAM-co-acrylic acid)	Cell-adhesion peptides GRGDY	The rat calvarial osteoblasts spread more on the peptide-modified substrate
[124]	Poly-L-lactides	Arg-Gly-Asp (RGD) peptides	The cell attachment improved with increasing amount of immobilised RGD

The formation of covalent bonds between peptides and the functional groups of the substrate materials is required for stable linkages [125]. There are several conjugation strategies available for the binding of peptides and materials (Table 2.8). However, each conjugation strategy consumes a lot of chemical substances, most of which are harmful to the environment and aquatic lives. Further, if no functional groups are present in the material, a suitable functional group has to be incorporated to the material via chemical reaction [126]. This in turn will increase the complexity of the fabrication process and overall production cost.

Although RGD modification improved cell adhesion and growth, the preparation procedure was very complicated. For example, since polyNIPAm has no suitable functional group for RGD joining, the polyNIPAm must be modified with acrylic acid (AAc) and 2-carboxyisopropylacrylamide (CIPAm) to introduce a functional carboxylic group in order to form covalent bonds with RGD peptides. Hence, these RGD modification approaches were not used in the present study. This literature review only serves as a reference to show the pros and cons of work done by other research groups on improving cell attachment.

Table 2.8 *Conjugation strategies with respect to reactant functional groups [125]*

Strategy	Peptide and material's functional groups
Carbodiimide-conjugation	Amine and carboxylate
Reductive amination	Aldehyde and amine
Isothiocyanate reaction	Amine and amine
Maleimides reaction	Thiol and amine

2.10 Liquid/Liquid Dispersions

Dispersing two immiscible liquids in a turbulent system is a common process in the food, drug and cosmetic industry. The immiscible phases are separate from each other before stirring. The organic phase is dispersed into the aqueous phase when the liquid/liquid system is stirred [127]. Figure 2.32 illustrates the behaviour of a liquid/liquid system before and during stirring.

Energy input
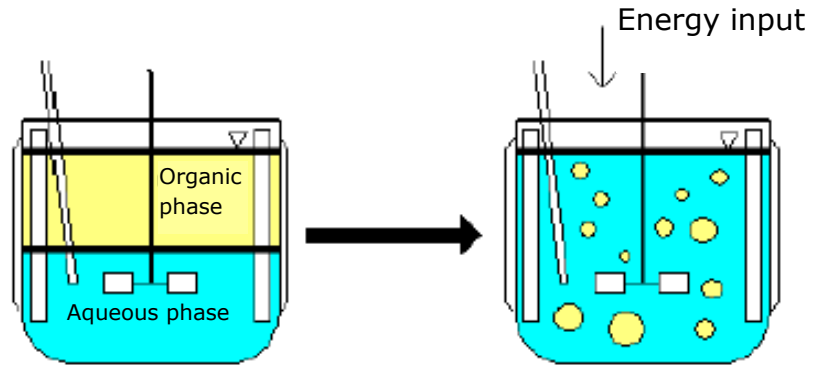
Figure 2.32 *Depiction of a liquid/liquid system before and during stirring [127]*

The drop size distribution (DSD) of the dispersed phase results from drop breakage and coalescence phenomena. Drop breakage occurs as the external forces and stresses exerted on the drops by the continuous phase exceed the internal forces and stresses that hold them together [128]. On the other hand, coalescence is a process of collision between two or more drops which depends on the collision frequency and coalescence efficiency between drops. According to the Kolmogorov's theory of turbulence [129], the maximum stable drop diameter results from dynamic pressure forces due to changes in velocity around the particles. It is essential to control the DSD as it determines the final properties of the product.

It was established that stirring rate has a significant impact on the drop size of a liquid/liquid dispersion [130]. In this context, the Sauter mean diameter, d_{32}, defined as the ratio of the third and second moments of a drop size distribution, is commonly used in describing the emulsion drop size because it is directly related to the volume fraction of the dispersed phase, Φ_d, and the interfacial area per unit volume, a_v [131]:

$$d_{32} = 6\Phi_d / a_v \qquad \text{…..................... Eq. (2.1)}$$

In a low viscosity dispersed phase liquid-liquid system, the stability of the emulsion drops is influenced only by the interfacial tension between the two immiscible liquids. The correlation between the mean energy dissipation rate, $\bar{\varepsilon}_T$ and the Sauter mean diameter, d_{32}, can be expressed as [132]:

$$d_{32}/D = K_1 \bar{\varepsilon}_T^{-\alpha} \qquad \text{…..………………..……Eq. (2.2)}$$

and $\quad \bar{\varepsilon}_T \ = N_{\mathrm{p}}\,\rho_c\,\omega^3\,D^5$ $\qquad$ …..…………………….…..Eq. (2.3)

where K_1 is a constant that depends on the tank geometry, and α is a constant that depends on the tendency of a system to coalesce, N_{p} is the power number of impeller, ρ_c is the density of continuous phase, ω is the angular speed, and D is the diameter of the impeller.

According to the Kolmogorov's theory of isotropic turbulence, the Sauter mean diameter of emulsion drops is dependent on the Weber number, We, which represents the ratio between the kinetic energy E_{kin} and surface energy E_γ. In other words, We represents the ratio of the external deforming forces to the stabilising surface forces.

$$We = \frac{E_{kin}}{E_\gamma} = \frac{\rho_c\omega^2 D^3}{\gamma} \qquad ………………………… \text{Eq. (2.4)}$$

where γ is the interfacial tension between the two liquids.

The correlation between the Sauter mean diameter and Weber number is described as [133]:

$$\frac{d_{32}}{D} = K_2 We^{-\alpha} \qquad ………………………….\text{Eq. (2.5)}$$

where K_2 is a constant that depends on the impeller type.

Numerous researches on two-phase liquid/liquid dispersions have been performed over the last decade. Table 2.9 summarises the correlations proposed by other research groups on the basis of the Kolmogorov's theory of turbulence to predict drop diameter.

Table 2.9 *Correlations proposed by various research groups for the prediction of drop diameter*

Reference	Stirrer type	System	Empirical correlation
[134]	Pilot scale Hanson mixer-settler extraction column	Toluene-acetone-water	$d_{32}/D = 0.197(1+3.04\Phi)We^{-0.6}(\mu_d/\mu_c)^{-1.27}$
		n-butyl acetate-acetone-water	$d_{32}/D = 0.23(1+2.24\Phi)We^{-0.6}(\mu_d/\mu_c)^{-1.14}$
[135]	Disk turbine and an open impeller	Kerosene as the dispersed phase; Distilled water as the continuous phase	$d_{32}\ \alpha\ N^{-a}$
[136]	Disk turbine impeller	Kerosene-distilled water	$d_{32}\ \alpha\ N^{-a}$
[137]	Pitched blade upflow turbine (PBTU) impeller	NiCl$_2$ as the dispersed phase; TBP-Sobesso 150 as the continuous phase	$d_{32}/D = 0.28(1+0.92\Phi)We^{-0.6}$

Table 2.9 *(Continued)*

[138]	Straight blade paddles with four blades	Sulfuric acid-diisobutylene diluted with benzene	$d_{32}/D = 0.0336(1+13.76\Phi)We^{-0.6}$
[139]	HEV impeller	Vaseline oil as the dispersed phase; Water as the continuous phase	$d_{32}/D = 0.57\ We^{-0.6}$
[140]	Pump-mix double shrouded impeller	Salicylaldoxime and ketoxime mixture as the dispersed phase; Sodium sulfonate solution as the continuous phase	$d_{32}/D = 0.353\ We^{-0.6}$
[133]	High shear (RT) impeller	Sunflower oil as the dispersed phase; Water as the continuous phase	$d_{32}\ \alpha\ \varepsilon^{b}$
[131]	High shear (RT) and high flow (HE3) impeller	Silicone oil as the dispersed phase; Water as the continuous phase	$d_{32} = 118.6\ (\varepsilon_{max}\ ND^{2})^{-0.270}$

As seen in Table 2.9, the correlation for each system is different. This suggests that the correlations are influenced by the relevant parameters such as stirrer type, stirring speed and the liquid/liquid dispersion system used. Amongst these processing parameters, stirring speed had the strongest effect on Sauter mean diameter [131]. The whole distribution shifted to smaller droplet sizes with increasing stirring speed. This trend in droplet size reduction was consistent with the findings of Desnoyer *et al.* (2003) [137] and Giapos *et al.* (2005) [136]. Further, the characteristics and physical properties of the liquid-liquid dispersions are different. For example, Torab-Mostaedi *et al.* (2012) obtained two different correlations for two different dispersion systems, *i.e.* toluene-acetone-water and n-butyl acetate-acetone-water, respectively [134]. Hence, it is not surprising that different correlations were developed by research groups.

Since Sauter mean diameter of the droplet is dependent mainly by stirring speed, the stirring speed applied in the polyNIPAm microcarrier synthesis was varied, in order to obtain a desirable size range of microcarrier for optimal cell yields in the present study.

2.11 Summary

In this Chapter, the development of cell culturing has been outlined. Mechanical scrapping and trypsinisation are the commonly used methods to harvest confluent cells from the growing surface. However, these harvesting methods cause cell damage and cell death, which subsequently reduce cell yield. Hence, the present research work is aimed at developing an alternative microcarrier that enables cell detachment without the use of trypsin. Based on the literature, polyNIPam is identified as a promising candidate material for use as microcarrier for non-invasive harvesting of cells without the use of trypsin, attributable to its reversible phase transition around physiological temperature. In particular, suspension polymerisation is selected for the production of polyNIPAm microspheres with diameters between 100 and 300 µm, *i.e.* the ideal size range for cell culturing. The polyNIPAm microcarrier synthesis in the presence of different initiators will be presented. In addition, the effect of surfactant composition on cell attachment to the microcarrier will be discussed. Further, a study on the incorporation of a hydrophobic comonomer into polyNIPAm microcarrier for the purpose of improving cell attachment will be documented. Finally, the effects of stirring rate and cross-linker content on the physical and mechanical properties of the polyNIPAm microcarrier are discussed.

CHAPTER 3

MATERIALS AND METHODOLOGY

3.0 Introduction

This Chapter presents the specifications of all the materials used to synthesise polyNIPAm microspheres investigated in this study. The experimental procedures for the synthesis of polyNIPAm microspheres and the cell seeding process are described. In addition, the basis of each characterisation technique used is outlined.

3.1 Materials

The starting materials used for the synthesis of polyNIPAm microspheres were *N*-iso-propylacrylamide (NIPAm), *N,N'*-methylenebisacrylamide (MBAm), azobis-isobutyronitrile (AIBN), ammonium persulfate (APS), *N,N,N',N'*-tetramethylethylene-diamine (TEMED), cyclohexane, poly(vinyl alcohol) (PVA), Span 80® and cetrylmethylammonium bromide (CTAB). All the reagents were analytical grade and used as received. A Merck Millipore water system was used to produce ultrapure water. The specifications of each starting material are presented in the following sections.

3.1.1 *N*-isopropylacrylamide

The *N*-isopropylacrylamide (NIPAm) monomer was purchased from Nacalai Tesque Incorporated, Japan. PolyNIPAm microspheres were synthesized via the polymerisation of NIPAm monomer in the presence of a cross-linker. The chemical structure of the NIPAm monomer is depicted by Figure 3.1, whilst the specifications of the NIPAm monomer are summarised in Table 3.1.
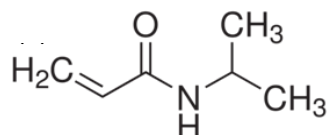
Figure 3.1 *Chemical structure of N-isopropylacrylamide*

Table 3.1 *Specifications of N-isopropylacrylamide provided by Nacalai Tesque Incorporated, Japan*

Property	Value
Molecular formula	$C_6H_{11}NO$
Molar mass	113.16 g/mol
Purity	99%
Appearance	White powder
Density	1.10 g/cm^3
Melting point	60-63°C
Boiling point	89-92°C
Solubility in water	69 g/L (at 20°C)

3.1.2 *N,N'-methylenebisacrylamide*

N,N'-methylenebisacrylamide (MBAm) is a commonly used cross-linker in the polymerization of polymers such as polyacrylamide. The MBAm used was purchased from Sigma-Aldrich (M) Sdn Bhd, Malaysia. Figure 3.2 depicts the chemical structure of MBAm, whilst Table 3.2 presents the specifications of MBAm.
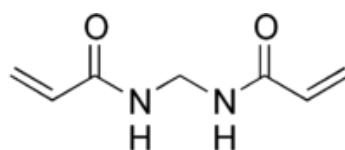
Figure 3.2 *Chemical structure of N,N'-Methylenebisacrylamide*

Table 3.2 *Specifications of N,N'-Methylenebisacrylamide provided by Sigma-Aldrich (M) Sdn Bhd, Malaysia*

Property	Value
Molecular formula	$C_7H_{10}N_2O_2$
Molar mass	154.17 g/mol
Purity	99%
Appearance	White powder
Density	1.24 g/cm^3
Melting point	> 300°C
Solubility in water	0.02 g/L (at 20°C)

3.1.3 Azobis-isobutyronitrile

Azobis-isobutyronitrile (AIBN) is a common radical initiator for polymerisation reactions. In the present study, the AIBN initiates the polymerisation reaction of NIPAm via the formation of free radicals at temperature above its decomposition temperatures, *i.e.* 65°C. The AIBN was purchased from Sigma-Aldrich (M) Sdn Bhd, Malaysia. The chemical structure of azobis-isobutyronitrile is depicted by Figure 3.3, whilst the specifications of azobis-isobutyronitrile are presented in Table 3.3.
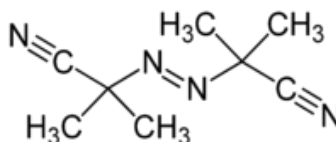
Figure 3.3 *Chemical structure of azobis-isobutyronitrile*

Table 3.3 *Specifications of azobis-isobutyronitrile provided by Sigma-Aldrich (M) Sdn Bhd, Malaysia*

Property	Value
Molecular formula	$C_8H_{12}N_4$
Molar mass	164.21 g/mol
Purity	98%
Appearance	White powder
Density	1.10 g/cm^3
Melting point	102-104°C

3.1.4 Ammonium Persulfate

Ammonium persulfate (APS) is a redox initiator used in the synthesis of polymers. It produces persulfate (SO_4^-) radicals spontaneously when it reacts with *N,N,N',N'*-tetramethylethylene-diamine (TEMED). The APS was purchased from Sigma-Aldrich (M) Sdn Bhd, Malaysia. Figure 3.4 presents the chemical structure of ammonium persulfate, whilst Table 3.4 lists the specifications of ammonium persulfate.
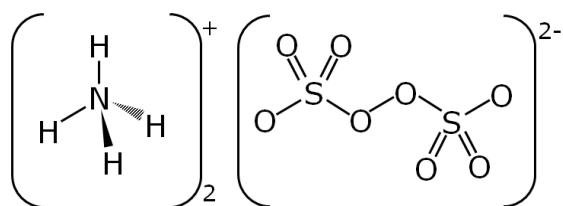
Figure 3.4 *Chemical structure of ammonium persulfate*

Table 3.4 *Specifications of ammonium persulfate provided by Sigma-Aldrich (M) Sdn Bhd, Malaysia*

Property	Value
Molecular formula	$H_8N_2O_8S_2$
Molar mass	228.20 g/mol
Appearance	White powder
Density	1.98 g/cm^3
Melting point	120°C
Solubility in water	228 g/L (at 20°C)

3.1.5 *N,N,N',N'*-tetramethylethylene-diamine

N,N,N',N'-tetramethylethylene-diamine (TEMED) was purchased from Sigma-Aldrich (M) Sdn Bhd, Malaysia. It acts as an accelerator in the production of persulfate (SO_4^-) radicals. The chemical structure of TEMED is depicted by Figure 3.5, whilst its specifications are summarised in Table 3.5.
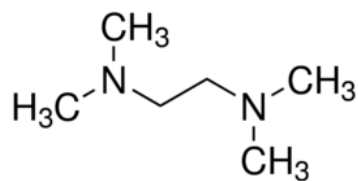
Figure 3.5 *Chemical structure of N,N,N',N'-tetramethylethylene-diamine*

Table 3.5 *Specifications of N,N,N',N'-tetramethylethylene-diamine provided by Sigma-Aldrich (M) Sdn Bhd, Malaysia*

Property	Value
Molecular formula	$C_6H_{16}N_2$
Molar mass	116.20 g/mol
Appearance	Colorless liquid
Density	0.78 g/cm^3
Melting point	-55°C
Boiling point	122°C
Solubility in water	Soluble

3.1.6 Cyclohexane

Cyclohexane was used as a solvent in the suspension polymerisation of NIPAm. It was purchased from Merck Sdn Bhd, Malaysia. Figure 3.6 presents the chemical structure of cyclohexane, whilst Table 3.6 lists the specifications of cyclohexane.
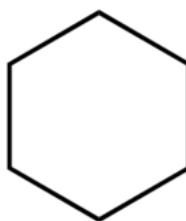
Figure 3.6 *Chemical structure of cyclohexane*

Table 3.6 *Specifications of cyclohexane provided by Merck Sdn Bhd, Malaysia*

Property	Value
Molecular formula	C_6H_{12}
Molar mass	84.16 g/mol
Appearance	Colorless liquid
Density	0.78 g/cm^3
Melting point	4°C
Boiling point	81°C
Solubility in water	0.003 g/L (at 20°C)

3.1.7 Poly(Vinyl Alcohol)

Poly(vinyl alcohol) (PVA) was used to stabilize the O/W emulsion. It was purchased from Sigma-Aldrich (M) Sdn Bhd, Malaysia. The chemical structure of PVA is depicted by Figure 3.7, whilst its specifications are listed in Table 3.7.
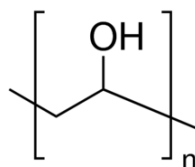
Figure 3.7 *Chemical structure of poly(vinyl alcohol)*

Table 3.7 *Specifications of poly(vinyl alcohol) provided by Sigma-Aldrich (M) Sdn Bhd, Malaysia*

Property	Value
Molecular formula	$(CH_2CHOH)_n$
Appearance	Colorless powder
Density	1.27 g/cm^3
Melting point	258°C
Glass transition temperature	99°C
Solubility in water	Soluble

3.1.8 Span 80®

Span 80® is a commonly used nonionic surfactant for stabilising W/O emulsions. The Span 80® used in the present study was purchased from Sigma-Aldrich (M) Sdn Bhd, Malaysia. Figure 3.8 presents the chemical structure of Span 80®, whilst Table 3.8 lists the specifications of Span 80®.
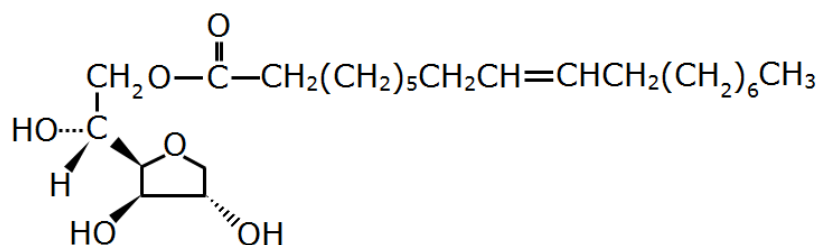
Figure 3.8 *Chemical structure of Span 80®*

Table 3.8 *Specifications of Span 80® provided by Sigma-Aldrich (M) Sdn Bhd, Malaysia*

Property	Value
Molecular formula	$C_{24}H_{44}O_6$
Molar mass	428.62 g/mol
Appearance	Brown liquid
Density	0.99 g/cm^3
Flash point	186°C
Boiling point	579°C

3.1.9 Cetrylmethylammonium Bromide (CTAB)

Cetrylmethylammonium bromide (CTAB) is a cationic surfactant used to stabilise the dispersed droplets in the W/O emulsion. The CTAB was purchased from Sigma-Aldrich (M) Sdn Bhd, Malaysia. The chemical structure of CTAB is depicted by Figure 3.9, whilst its specifications are summarised in Table 3.9.
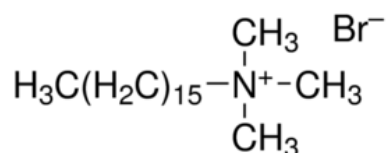
Figure 3.9 *Chemical structure of cetrylmethylammonium bromide*

Table 3.9 *Specifications of cetrylmethylammonium bromide provided by Sigma-Aldrich (M) Sdn Bhd, Malaysia*

Property	Value
Molecular formula	$C_{19}H_{42}BrN$
Molar mass	364.45 g/mol
Appearance	White powder
Density	0.97 g/cm^3
Melting point	250°C
Flash point	244°C
Solubility in water	36.4 g/L at 20°C

The main purpose of using a cationic surfactant was to modify the surface charge of the polyNIPAm microspheres. According to Troy and Beringer, there are two types of cationic surfactants available in the market, namely cetyl trimethyl ammonium bromide (CTAB) and cetyl pyridinium chloride (CPC) [89], as listed in Table 3.10. CTAB was selected to be used in the present study because CTAB possesses a HLB value of 10, which is more suitable for W/O emulsions. On the other hand, CPC is suitable for O/W emulsions.

Table 3.10 *HLB values and molecular formulae of the cationic surfactants*

Cationic surfactant	Molecular formula	HLB value
Cetyl trimethyl ammonium bromide (CTAB)	$(C_{16}H_{33})N(CH_3)_3Br$	10.0
Cetyl pyridinium chloride (CPC)	$C_{21}H_{38}ClN$	26.0

3.2 Methodology

3.2.1 Suspension Polymerisation of NIPAm Using a Thermal Initiator

PolyNIPAm particles were synthesised via suspension polymerisation using a methodology modified from Ma and Zhang [141]. Firstly, 1 g of NIPAm monomer, 0.15 g of MBAm cross-linker, and 0.01 g of AIBN initiator were mixed in 10 ml of cyclohexane using magnetic stirring. The continuous aqueous phase was prepared by mixing a predetermined amount (0.01 g, 0.02 g, 0.03 g, and 0.04 g, respectively) of PVA stabiliser with 100 ml of ultrapure water. The monomer phase was poured slowly into the PVA aqueous solution and mixed under constant stirring rate of 200 rpm for 1 h. The mixture was then heated up to 70°C to initiate the polymerisation reaction. The system was purged with N_2 gas to remove any remaining oxygen that might inhibit polymerisation. The resultant polyNIPAm microspheres were washed with excess ultrapure water and centrifuged at 7,000 rpm for 15 minutes, followed by decantation of the supernatant and resuspension within fresh water. The centrifugation process was repeated five times to ensure complete removal of unreacted monomer. The particles were filtered and dried in an oven at 40°C for 24 h and then stored in a desiccator in advance of characterisation. Four sets of polyNIPAm microspheres were produced using different concentrations of PVA stabiliser.

3.2.2 Suspension Polymerisation of NIPAm Using a Pair of Redox Initiators

Suspension polymerisation using a pair of redox initiators was performed at room temperature, *i.e.* ~ 25°C. Firstly, 1 g of NIPAm monomer, 0.15 g of MBAm cross-linker and 0.03 g of APS initiator were dissolved in 10 ml of ultrapure water and mixed using magnetic stirring. The oil phase was prepared by mixing 2 g of Span 80® with 100 ml of cyclohexane. The water phase was poured slowly into the oil phase under constant stirring rate of 200 rpm, and the system purged with N_2 gas for 1 h to remove unwanted oxygen that might inhibit polymerisation reaction. Next, 0.15 ml of TEMED was added to the suspension to initiate polymerisation. The resultant polyNIPAm microspheres were washed with excess ultrapure water and centrifuged at 7,000 rpm for 15 min, followed by decantation of

the supernatant and resuspension within fresh water. The centrifugation process was repeated five times to ensure complete removal of unreacted monomer. The microspheres were filtered and dried in an oven at 40°C for 24 h and then stored in a desiccator in advance of characterisation. The preparation of the polyNIPAm microspheres is depicted schematically by Figure 3.10.
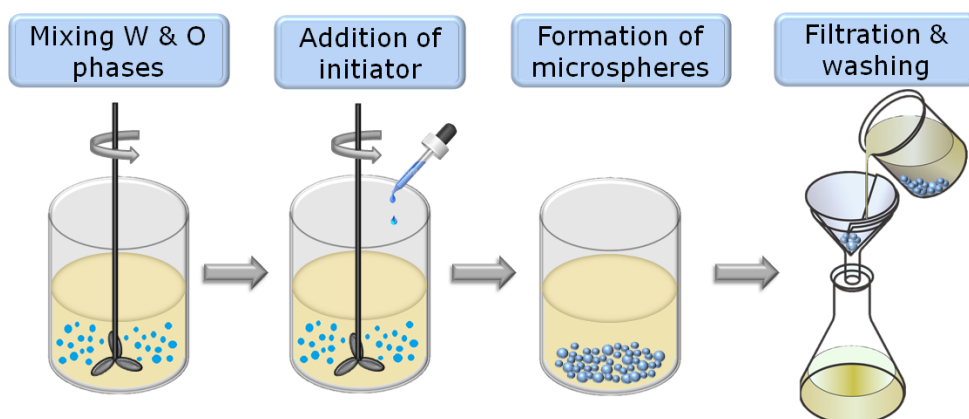
Figure 3.10 *Process for the preparation of polyNIPAm microspheres via suspension polymerisation*

3.2.3 Seeding of HEK Cells on PolyNIPAm Microspheres

Human embryonic kidney (HEK 293) cells were seeded onto polyNIPAm microspheres prepared from thermal and redox initiators. The objective was to appraise the level of HEK cell attachment to the polyNIPAm. The procedure for cell seeding was adopted from Tamura *et al.* [142]. HEK 293 cells were cultured in Dulbecco's modified Eagle medium (DMEM) with 10% fetal bovine serum (FBS), 4mM L-glutamine, 1% penicillin and streptomycin on a well-plate. Prior to cell seeding, the polyNIPAm microspheres were hydrated in phosphate-buffered saline (PBS) solution for at least 24 h. The hydrated microspheres were then sterilised by autoclaving at 121°C for 15 minutes and then washed with culture medium. Initial inoculations of 10^5 cells/ml were cultured with 3 mg/ml of the polyNIPAm microspheres. Cell culturing was performed at 37°C under a humidified atmosphere of 5% CO_2. Initial cell behaviour was monitored

using optical microscopy. The culture medium was changed every day to ensure sufficient supply of nutrient to the cells.

3.3 Characterisation techniques

Several complementary analytical techniques were used to characterise the prepared polyNIPAm microspheres, *i.e.* interfacial tension measurement using the pendant drop method, fourier transform infrared (FTIR) spectroscopy, scanning electron microscopy (SEM), energy dispersive X-ray spectroscopy (EDX), optical microscopy, zeta potential analysis, differential scanning calorimetry (DSC), thermogravimetric analysis (TGA), Trypan blue exclusion method, water drop contact angle measurement and compression testing. Brief descriptions of these characterisation techniques are presented in the following sections.

3.3.1 Interfacial Tension Measurement

Interfacial tension is defined as the amount of energy required to increase the interfacial area between two immiscible liquids. In the present study, the pendant drop method was used to measure the interfacial tension between cyclohexane and the PVA aqueous solution used for the synthesis of polyNIPAm microspheres. Figure 3.11 depicts the configuration for pendant drop method which consists of an experimental chamber, an illuminating system and a camera connected to a computer [143].
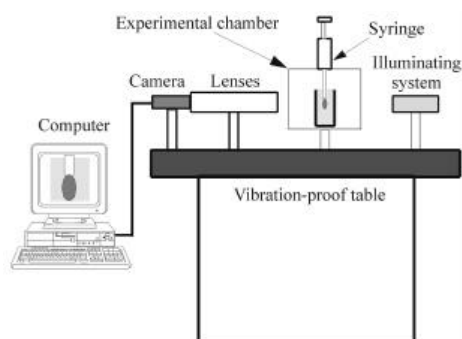
Figure 3.11 *Configuration for the pendant drop method*
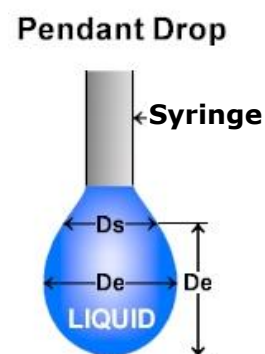
Figure 3.12 *Schematic of a pendant drop*

The shape profile of a pendant drop of PVA aqueous solution in cyclohexane was captured and analysed using a Ramé-hart Model 250 F1 Series standard goniometer with Ramé-hart DROPimage Advanced v2.4 software. Interfacial tension was calculated using the Young-Laplace equation (Equation 3.1):

$$\gamma = \frac{g \, D_e{}^2 \Delta\rho}{H}$$ ....(Eq 3.1)

where γ is the interfacial tension; g is the gravity constant; D_e is the equatorial diameter of the drop; $\Delta\rho$ is the density difference between the oil and water phases; and H is a correction factor which is inversely proportional to the shape factor of the pendant drop, S, as expressed by Equation 3.2:

$$S = \frac{D_s}{D_e}$$ ....(Eq 3.2)

where D_s is the minimum drop diameter measured horizontally at a distance D_e away from the apex of the drop, and is the maximum drop diameter measured horizontally at the centre of the drop, as depicted by Figure 3.12.

3.3.2 Fourier Transform Infrared Spectroscopy

Fourier transform infrared (FTIR) spectroscopy is a very useful analytical technique for identifying the types of chemical bonds or functional groups present in a molecule by producing an infrared absorption spectrum that is like a molecular "fingerprint" [144]. FTIR spectroscopy offers rapid and sensitive analysis of organic compounds, as well as the chemical structures of many inorganics. It can be applied to the analysis of solids, liquids, and gasses. FTIR spectroscopy deals with the infrared region of the electromagnetic spectrum that exhibits longer wavelength and lower frequency as compared to visible light (Figure 3.13).
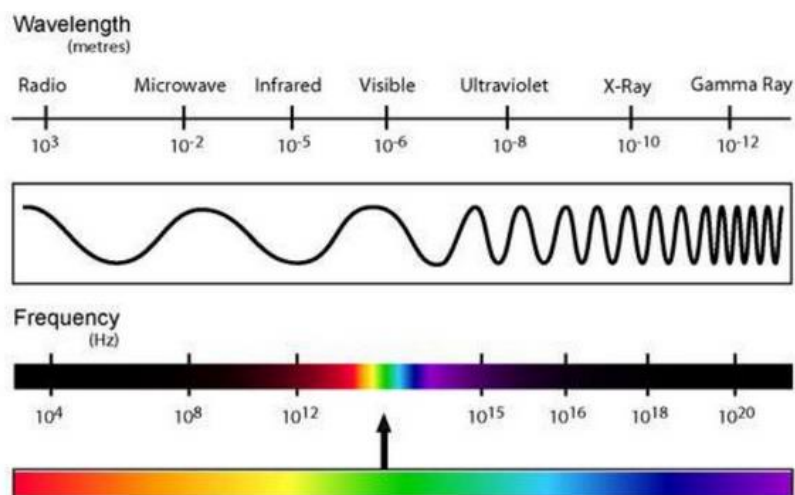
Figure 3.13 *Wavelength and frequency of electromagnetic spectrum [145]*

The mid-IR region (4000 – 400 cm^{-1}) is used because the frequencies of this region correspond to the fundamental vibrations of virtually all the functional groups in organic molecules. A molecule can be excited to a higher vibrational state by absorbing IR radiation. The probability of a particular IR frequency being absorbed is dependent on the actual interaction between this frequency and the molecule. Generally, a frequency will be strongly absorbed if its photon energy coincides with the vibrational energy levels of the molecule [146].

Figure 3.14 depicts the configuration of an FTIR spectrometer which consists of four main components, *i.e.* the IR radiation source, interferometer (a stationary mirror, a moving mirror and a beam-splitter), sample compartment and detector. IR radiation generated from the source is directed to the beam-splitter, which sends the IR radiation in two directions at right angles. Half of the IR beam is reflected and sent to a stationary mirror whilst the other half is transmitted and sent to a moving mirror. An interferogram, *i.e.* constructive and destructive interference is created when the reflected and transmitted beams recombine at the beam-splitter, due to the difference in path lengths between the two beams. Specific wavelengths from the interferogram are subtracted when the recombined beam passes through the sample, as absorption of the IR radiation occurs when the frequency of the IR is identical to the vibrational frequency of a bond in the molecule. The variation in energy as a function of time is recorded simultaneously by the detector [147].
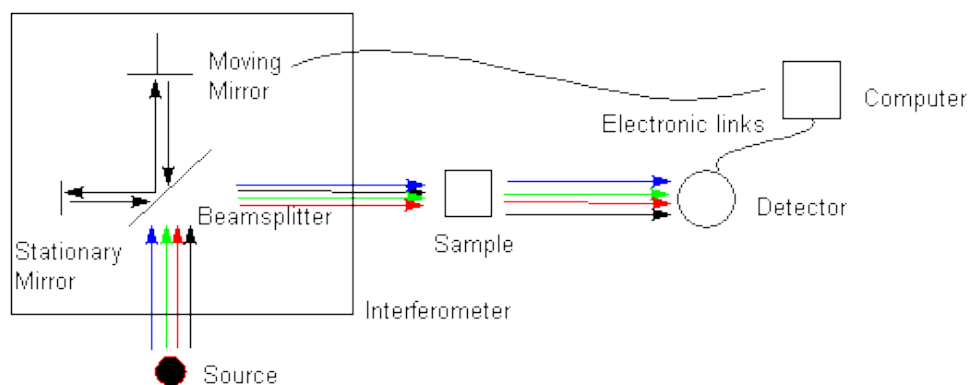
Figure 3.14 *Configuration of an FTIR spectrometer [147]*

The interferogram is translated to an FTIR spectrum, *i.e.* intensity versus frequency plot, via Fourier transform, as expressed in Equation 3.3 [146]:

$$A(r) = \sum X(k) \exp\left(-2\pi \frac{irk}{N}\right) \dots\dots\dots\dots\dots\dots\dots(\text{Eq 3.3})$$

where *A(r)* and *X(k)* are frequency domain and time domain points, respectively, for a spectrum of *N* points. Figure 3.15 presents an FITR spectrum of the NIPAm monomer obtained in the present study.
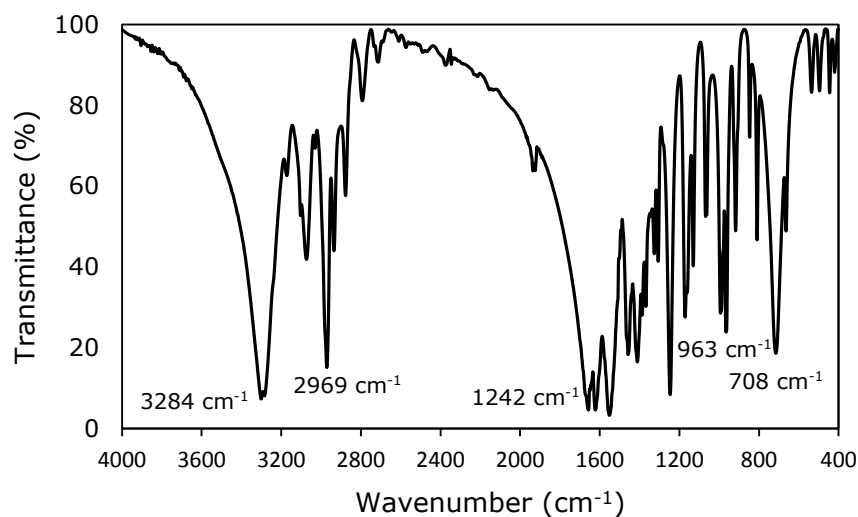
Figure 3.15 *FITR spectrum of the NIPAm monomer*

The chemical bonds of a molecule vibrate when the molecule absorbs infrared radiation. In this context, different chemical bonds possess different energies and hence the associated FTIR peaks appear at different wavenumbers. In general, wavenumber and vibration frequency are directly proportional to the bond energy. In other words, the higher the bond energy, the higher is the wavenumber. Table 3.11 lists functional groups corresponding to peaks present in the FTIR spectrum of the NIPAm monomer (Figure 3.15). N-H stretching vibrations occur at 3284 cm^{-1} due to the relatively high energy of the N-H bond. Conversely, the CH_2 bond possesses lower energy and its vibrations occur between 963 and 708 cm^{-1}.

Table 3.11 *Functional groups present in the NIPAm monomer [169-172]*

Wavenumber (cm^{-1})	Functional groups
3284	N-H stretching
2969	C-H stretching
1653	C=O stretching of Amide I
1617	N-H bending of Amide II
1544	N-H bending of Amide II
1455	C-H bending
1409	$CH(CH_3)_2$ stretching of isopropyl group
1242	Amide III
1164	CH_3 skeletal
963	CH_2 rocking
806	CH_2 rocking
708	CH_2 rocking

In the present study, the chemical bonding of the polyNIPAm microspheres was appraised using a Perkin Elmer Spectrum RX1 FTIR spectrometer. Prior to preparation, KBr powder was dried in an oven at 120°C for 24 h. A very small amount of dried polyNIPAm microspheres

were ground finely with ~ 0.225 g of potassium bromide (KBr) until homogenised, using a mortar and pestle. The fine powder mixture was then pressed into a thin, nearly transparent pellets having diameter of 13 mm, using a pellet press at a pressure of 49 kPa for 5 minutes. Background spectra that showed the instrument energy profile were acquired before the specimen pellet was placed onto the pellet holder for analysis, at a resolution of 4 cm^{-1} with 32 scans. Resolution is an indication of the degree of fineness of the data obtained, *i.e.* the minimum peak interval that can be distinguished. Thus, resolution of 4 cm^{-1} was used in the present study to increase the accuracy of the FTIR analyses.

3.3.3 Scanning Electron Microscopy

The scanning electron microscope (SEM) may be used to examine the microstructure of a material that is invisible to naked eye. Figure 3.16 depicts the configuration of an SEM. A primary electron beam is emitted from an electron gun fitted with a tungsten filament cathode. The electron beam, with energy ranging from 0.2 to 40 keV is focused by condenser lenses to a spot ~ 0.4 to 5 mm in diameter. The electron beam passes through scanning coils in the electron column under high vacuum, and bombards the sample. A high vacuum mode is used to minimise scattering of the electron beam before reaching the sample [148].
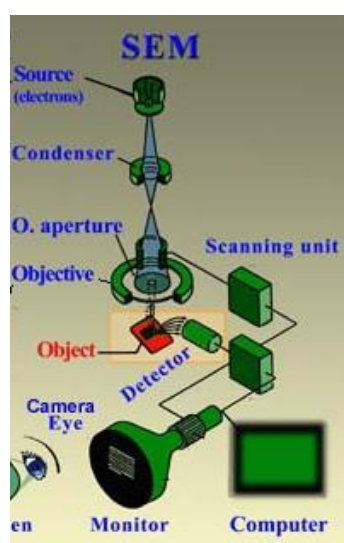
Figure 3.16 Configuration of an SEM [148]

The interaction between the primary electron beam and the atoms of the sample yields several types of signals, such as secondary electrons, backscattered electrons and characteristic X-rays [149], as illustrated by Figure 3.17.
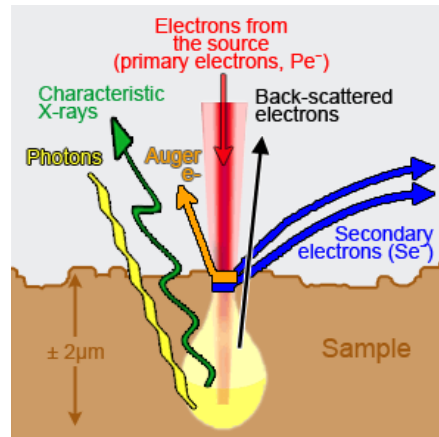
Figure 3.17 *Signals produced by the interaction of high energy electron beam and atoms in a sample [149]*

Secondary electrons are those electrons ejected from an atom with energies below 50 eV as a result of inelastic collisions between primary electrons and loosely bound electrons of the conduction band or tightly bound valence electrons. Since secondary electrons possess relatively low energies, only those produced near the surface of a sample can be detected. In particular, secondary electrons exhibit high spatial resolution relative to other available signals as the greatest density of secondary electrons is created by the primary beam before it has a chance to spread. Surface details on the scale of 1 nm can be revealed using the secondary electron (SE) detection mode. Hence, the secondary electron mode is used mainly for micrographic imaging, owing to its topographic sensitivity and high spatial resolution [150].

Conversely, backscattered electrons (BSE) arise due to elastic collisions between primary electrons and the nuclei of target atom, with little or no change in energy of the scattered electrons. The number of electrons backscattered increases with increasing atomic number (Z) of the sample. Owing to the (locally averaged) atomic number dependent intensity, the BSE detection mode provides information on the distribution of different elements in a sample. Furthermore, biological specimens, which would be

difficult to detect in secondary electron detection mode, can be revealed using the BSE detection mode [148].

In addition, characteristic X-rays are emitted when the primary electron beam removes an electron from the inner shell of atom, causing a higher-energy electron to fill the shell and release energy. These characteristic X-rays are used to identify composition and measure the abundance of elements in a sample [151].

An FEI XL30 SEM, equipped with a tungsten filament, was used to appraise the surface morphologies of the prepared polyNIPAm samples. Specimens held using double sided carbon tape were observed at an accelerating voltage of 5 kV as higher accelerating voltages caused charging effects and damaged the soft polymer. The secondary electron (SE) detection mode was used for morphological observations.

For the observation of cell-attached microspheres, the fixing and dehydration of cells were performed prior to morphological observation. Firstly, the cell-attached microspheres were washed with phosphate buffered saline (PBS) solution, and replaced with a fixing agent, *i.e.* 3% glutaraldehyde/PBS solution for 30 minutes. The fixed specimens were then washed three times with PBS, followed by dehydration using varying concentrations of ethanol solution: 20% ethanol for 2 minutes; 40% ethanol for 5 minutes; 60% ethanol for 5 minutes; 70% ethanol for 5 minutes; 80% ethanol for 2 minutes; 90% ethanol for 2 minutes; and 100% ethanol for 5 minutes. The dehydrated samples were left in a fume cupboard overnight [152].

Figure 3.18 shows an SE micrograph of a polyNIPAm microsphere prepared in the present study. A low accelerated voltage of 5 kV was used to minimise charging effects on this nonconductive specimen. A recommended working distance of 9.6 mm was used. If the working distance was too large, the specimen image would look blurred. Conversely, if the working distance was too near, the specimen might hit and damage the detector.
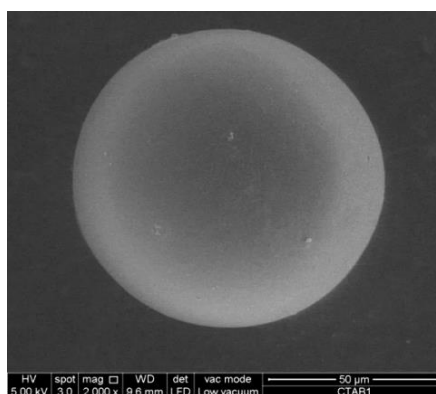
Figure 3.18 *SE micrograph of the polyNIPAm microsphere (Magnification: 2000 x)*

3.3.4 Energy Dispersive X-Ray Spectroscopy

Energy dispersive X-ray spectroscopy (EDX) is a chemical microanalysis technique used, in conjunction with SEM, to appraise the chemical composition of a material. EDX detects characteristic X-rays emitted from the sample during electron beam bombardment [153]. Each element has a unique atomic structure allowing X-rays that are characteristic of an element to be identified uniquely. A charge pulse that is proportional to X-ray energy is created when an incident X-ray strikes the EDX detector. The charge pulse is converted to a voltage pulse by a charge-sensitive preamplifier, and sent to a multi-channel analyser where the pulses are sorted by voltage. The energy for each incident X-ray is then recorded to a computer for data display and analysis. A spectrum of X-ray energy versus counts may be evaluated to determine the elemental composition of a sample [154]. In the present study, the elemental compositions of polyNIPAm microspheres were appraised using an FEI XL30 SEM configured with an Oxford Instruments INCA EDX system. EDX analyses were performed using BSE detection mode at an accelerating voltage of 20 kV. Firstly, the area of the specimen to be analysed was selected, as shown in Figure 3.19.
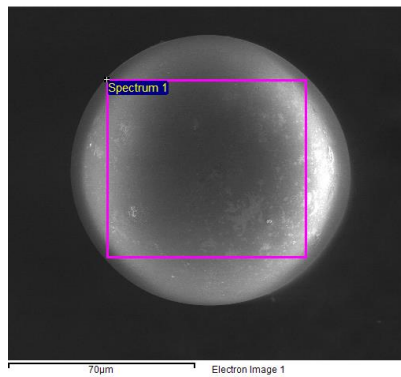
Figure 3.19 *Selected area of the polyNIPAm microsphere for EDX analysis*

Figure 3.20 shows EDX data for a polyNIPAm microsphere prepared in the present study. Since the atomic number of oxygen (O) is greater than that of carbon (C) and nitrogen (N), the peak for oxygen was detected at higher energy. Peak intensity corresponds to the atomic percentage of an element in the specimen. It was found that the peak intensity for carbon was the highest, followed by oxygen and nitrogen. This indicates that carbon was the majority element in the specimen, whilst nitrogen was the minority element.

Element	Weight%	Atomic%
C K	69.06	74.39
N K	5.15	4.76
O K	25.79	20.85
Totals	100.00	
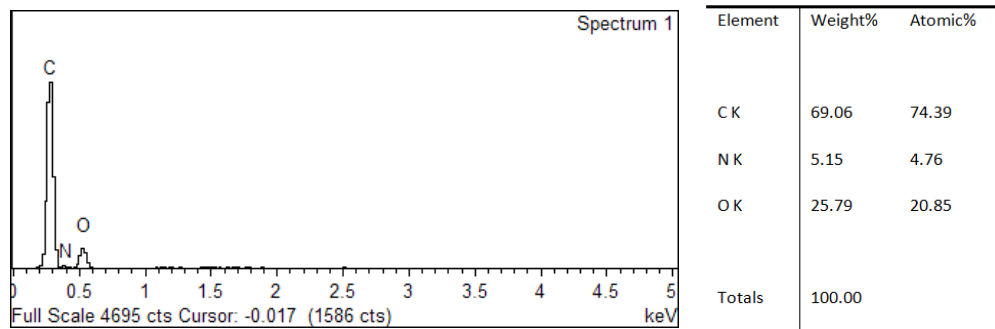
Figure 3.20 *EDX data for a polyNIPAm microsphere*

3.3.5 Optical Microscopy

Optical microscopes are used to obtain enlarged images of small objects and reveal structural details. Optical microscopes can be classified into two categories, *i.e.* upright and inverted transmission, based on the positions of the light source and the objective. Upright microscopes are constructed

with the tip of the objective pointing downward so as to view specimens from above. In transmission, light is directed on to the specimen from below, *e.g.* allowing the observation of prepared slides. Conversely, in an inverted microscope, light is directed on to the specimen from above, whilst the tip of the objective is pointing upward so as to view the specimen from below [155]. Inverted microscopes are widely used for viewing biological specimens in petri dishes [156]. Figure 3.21 depicts the configuration of inverted and upright microscopes, whilst Table 3.12 summarises the function of the basic components of an optical microscope.
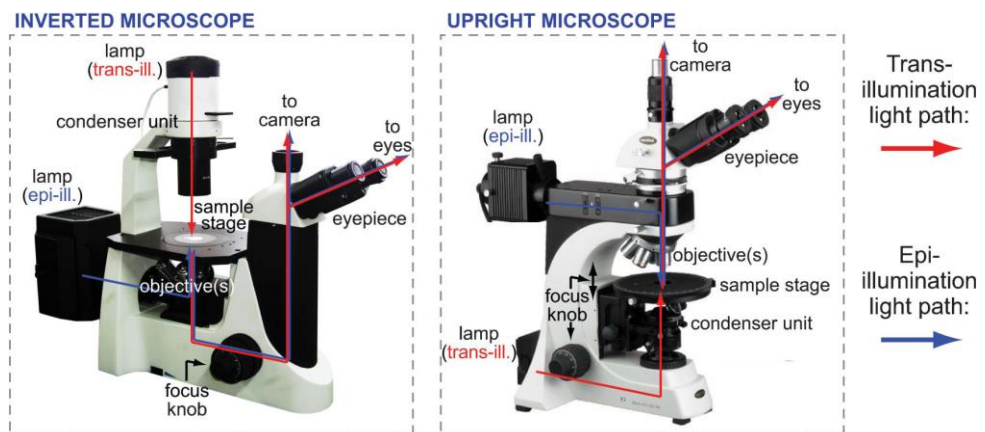
Figure 3.21 *Configuration of inverted and upright microscopes [155]*

Table 3.12 *Function of the basic components of an optical microscope [155]*

Basic component	Function
Lamp and condenser	Illuminate specimen
Objective and eyepiece	Create a magnified image of the specimen
Focus knob	Bring the specimen into focus
Sample stage	Mount the specimen and determine the location to be observed
Camera	Observe and record

Three main types of observation method are available for optical microscopes, *i.e.* bright field, phase contrast and fluorescence microscopy. The bright field observation mode is used commonly to observe colour and brightness information *e.g.* from a stained specimen. In bright field microscopy the entire field of view is illuminated. Alternatively, specimens stained with fluorescent dye can be viewed using fluorescence microscopy. A mercury lamp with high-intensity pressure is used as a light source for the generation of specimen fluorescence, which is viewed in a dark field mode [157]. Conversely, phase contrast microscopy may be used for viewing transparent and colourless specimens and live cells. The difference between light rays propagating directly from a light source and light rays refracted by a specimen imparts contrast to the images of transparent specimens. Specimens can be made to appear either dark against a bright background or bright against a dark background [158].

In the present study, a Nikon Eclipse TS100 inverted microscope in the phase contrast observation mode was used to observe cell suspensions throughout the cell culturing process. Cell suspensions were focused whilst magnification was adjusted through change of the objective lenses. Figure 3.22 shows an optical micrograph of microspheres and HEK cell suspension obtained in the present study.
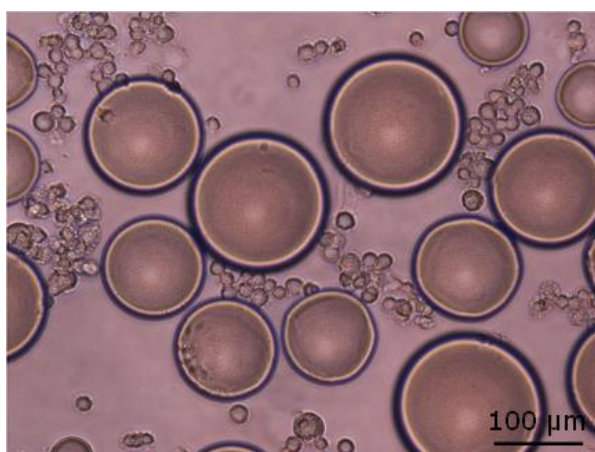
Figure 3.22 *Optical micrograph of microspheres and HEK cells*

3.3.6 Zeta Potential Analysis

The zeta potential is the electrical potential that exists at the shear plane of a particle in a solution (Figure 3.23). Colloidal particles are electrically charged due to their ionic characteristics and dipolar attributes. The development of a net charge at a particle surface affects the distribution of ions in the neighbouring interfacial region [159]. Typically, the first adsorbed monolayer of ions is defined as the inner Helmholtz layer, which consists of oppositely charged ions, whilst the second adsorbed monolayer is known as the outer Helmholtz layer, comprising ions of different polarities. The combination of both inner and outer Helmholtz layers is called the electrical double layer. The zeta potential of the double layer decays exponentially with distance from the surface, towards zero due to the oppositely charged counter ions.
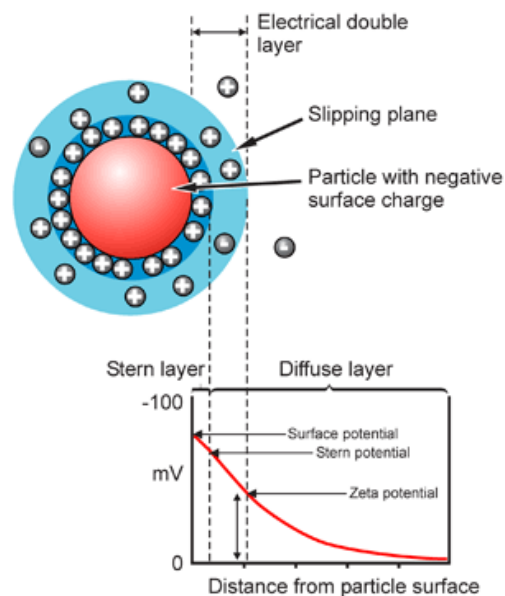
Figure 3.23 *Zeta potential at the shear plane of a negatively charged particle [159]*

The surface charge of prepared polyNIPAm microspheres was appraised by measuring the zeta potential using a Malvern Zetasizer Nano ZS. According to Ishikawa *et al.* [160], the surface charge of a cell culture substrate has a significant effect on the attachment of cells. Hence, the effect of surface charge of the prepared microspheres on cell attachment

74

during the cell trials was studied. The polyNIPAm microspheres were dispersed in PBS solution (pH = 7.4) at a concentration of 1 mg/ml. A zeta potential cuvette was filled with 150 µl of microsphere dispersion, and sonicated for 1 minute prior to analysis. Laser Doppler Micro-electrophoresis was used to measure the zeta potential of the dispersion by applying an electric field across the dispersion. The microspheres within the dispersion migrate toward the electrode of opposite charge with a velocity proportional to the magnitude of the zeta potential. Scattering of laser light occurs when the microspheres are moving (Figure 3.24).
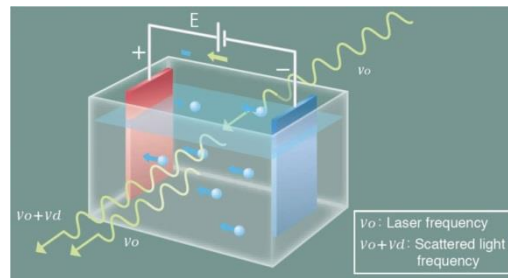
Figure 3.24 *Scattering of laser light under an applied electric field [159]*

Microsphere velocity was measured using a laser interferometric technique termed M3-PALS (Phase analysis Light Scattering), enabling the calculation of electrophoretic mobility (Equation 3.4):

$$U = \frac{\lambda\, V\, d}{2\, E\, \eta\, \sin(\frac{\theta}{2})}$$ …………………………………..(Eq 3.4)

where *U* is the electrophoretic mobility; *λ* is the wavelength of the laser light; *V* is the particle velocity; *d* is distance from the electrode; *E* is the electric field strength; *η* is the refractive index of the solvent used; and *θ* is the angle of scattered light.

The zeta potential was calculated using Equation 3.5:

$$\zeta = \frac{U\mu}{\varepsilon\, f\,(ka)'}$$ ………….………………………..(Eq 3.5)

where *ζ* is the zeta potential; *U* is the electrophoretic mobility; µ is the solvent viscosity; *ε* is the solvent dielectric constant; and *f(ka)'* is the Henry coefficient.

3.3.7 Differential Scanning Calorimetry

Differential scanning calorimetry (DSC) is a thermoanalytical technique used to determine phase transitions, such as the glass transition, melting and crystallisation of a material. The basic principle of DSC is that, when a sample undergoes a phase transition, more or less heat is required to flow to the sample than a reference material, to maintain both at the same temperature [161]. The difference in heat flow to the sample and reference, as a function of temperature, is recorded (Equation 3.6):

$$\Delta \frac{dH}{dt} = \left(\frac{dH}{dt}\right)_{sample} - \left(\frac{dH}{dt}\right)_{reference} \quad \ldots\ldots\ldots\ldots(Eq\ 3.6)$$

The heat flow difference can be positive or negative, depending on the type of phase transition occurring. A positive heat flow difference is obtained during an endothermic process, such as melting, as heat is absorbed by the sample to break down the crystalline lattice. Conversely, the heat flow difference is negative in an exothermic process, such as crystallisation as heat is released from a sample [162].

The output obtained from DSC analysis is a graph of heat flow versus temperature. The enthalpy of a particular phase transition can be calculated by integrating the corresponding peak area, as expressed in Equation (3.7):

$$\Delta H = KA \qquad \ldots\ldots\ldots\ldots\ldots\ldots\ldots\ldots..(Eq\ 3.7)$$

where ΔH is the enthalpy of transition, K is the calorimetric constant, and A is the peak area. The K value varies with instrument type, and can be determined by analysing a well-characterised sample with known transition enthalpies.
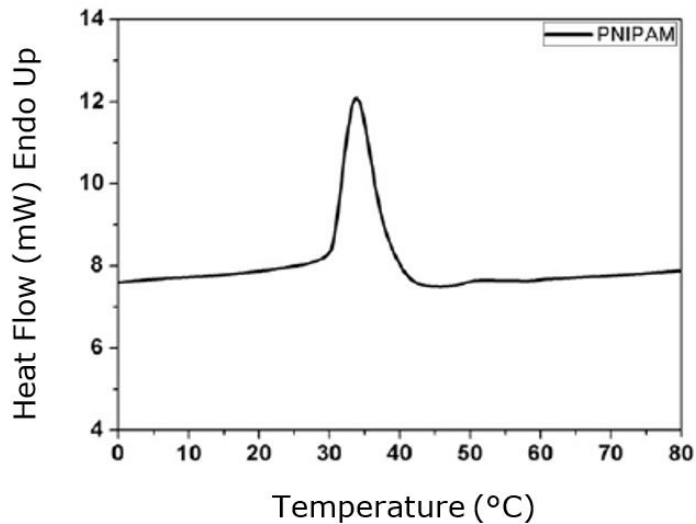
Figure 3.25 *DSC thermogram of polyNIPAm microspheres [46]*

Figure 3.25 presents a DSC thermogram of the polyNIPAm microspheres ontained during the heating scan from 0 to 80°C. A sharp endothermic peak appeared at a temperature of ~ 32°C during the heating scan. This peak represents the lower critical solution temperature (LCST) of polyNIPAm. The specimen absorbed heat from the surroundings in order to undergo a coil-to-globule phase transition. A DSC instrument consists of a furnace and an integrated sensor with designated positions for sample and reference crucibles (Figure 3.26). The sample holder is connected to an ultra-microbalance and a thermocouple, allowing for the recording of temperature difference between sample and reference. An empty alumina crucible is used commonly as the reference.
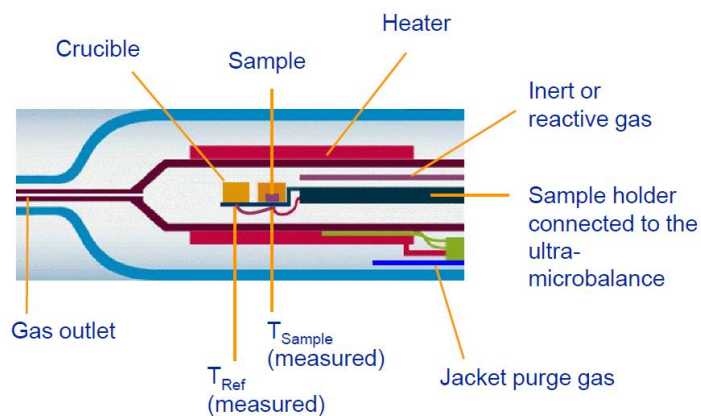
Figure 3.26 *Configuration of a DSC furnace*

The intensity of an endothermic or exothermic peak in a DSC thermogram is influenced by initial sample mass and the heating rate. The effect of sample mass on peak intensity is illustrated by Figure 3.27, with reference Indium peaks becoming broader as more sample mass is used [163].
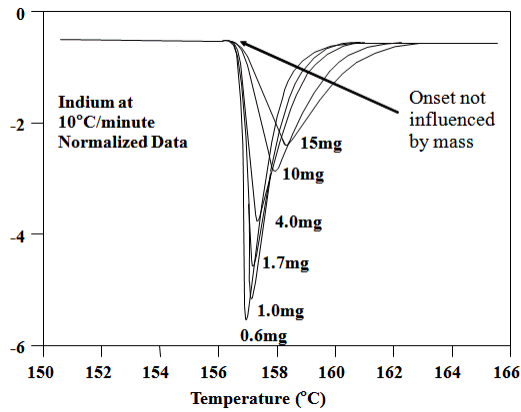
Figure 3.27 *Effect of sample mass on peak intensity in DSC*

Figure 3.28 presents exothermic peaks for reference material Indium scanned at different heating rates. It is observed that peak intensity increases with increasing heating rate.
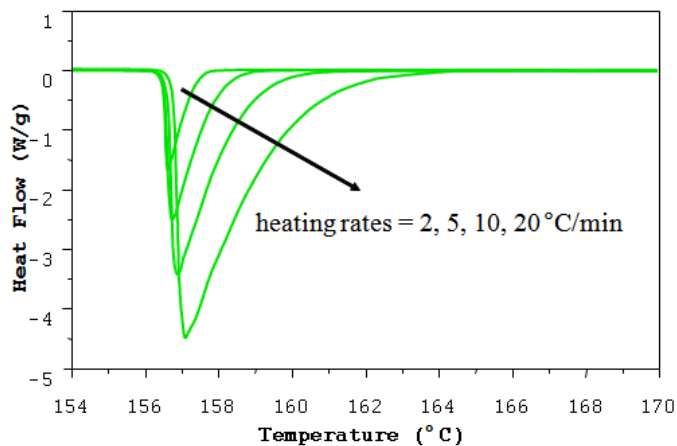
Figure 3.28 *Effect of heating rate on peak intensity during DSC measurement*

A Mettler-Toledo STAR System DSC was employed to investigate the phase transition temperature or the LCST of the polyNIPAm microspheres. The DSC was calibrated with indium as a standard. Prior to DSC analysis, the polyNIPAm microspheres were immersed in ultrapure water overnight. An alumina crucible containing ~10 mg of hydrated microspheres was placed in the sample holder located in the DSC furnace. Samples were heated from 25 to 80°C at a scanning rate of 5°C/minute. The scanning was run under a nitrogen gas atmosphere at a standard purging rate of 20 ml/minute.

3.3.8 Thermogravimetric Analysis

Thermogravimetric analysis (TGA) is used to determine the thermal stability and composition of a material by monitoring the weight change that occurs when the material is heated under an inert or reactive atmosphere [161]. In general, an inert atmosphere such as argon, helium, or nitrogen gas is used to standardise the conditions of the experiment without affecting the sample. Conversely, a reactive atmosphere such as air or oxygen plays an important role in the chemical reactions taking place in the sample. A sample loses weight due to decomposition, reduction or evaporation, whilst gaining weight due to oxidation or absorption. Figure 3.29 depicts the configuration of a TGA instrument that consists of a furnace, thermostated balance chamber and gas controller. An alumina crucible containing ~10 mg of sample was placed on the sample holder in the TGA furnace. The sample was heated consistently up to a maximum temperature where the sample weight remained constant to the end of the analysis. The temperature was monitored via a thermocouple, whilst weight change was recorded by an ultra-microbalance. The gas that flows over the sample and exits through an exhaust was controlled [164].
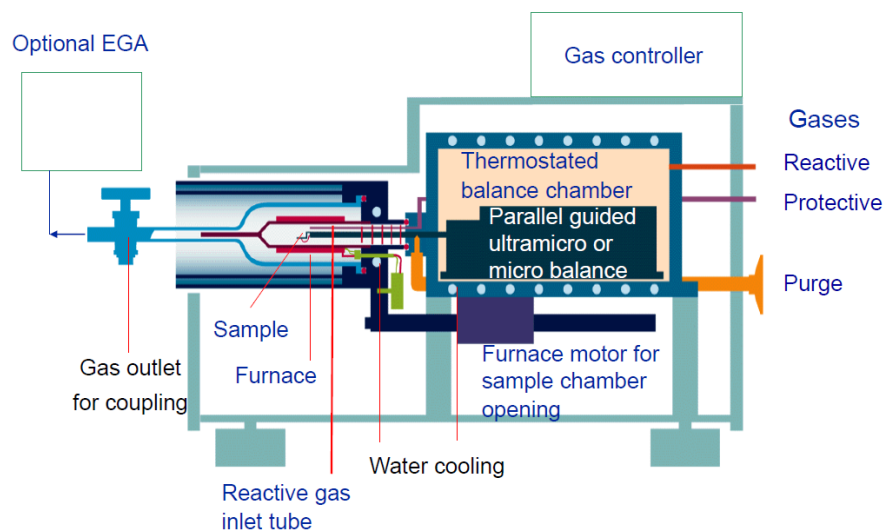
Figure 3.29 *Configuration of a TGA instrument*

Data was plotted as weight percent versus temperature or time. Figure 3.30 presents a TGA thermogram of polyNIPAm microspheres throughout constant heating from 25 to 500°C.
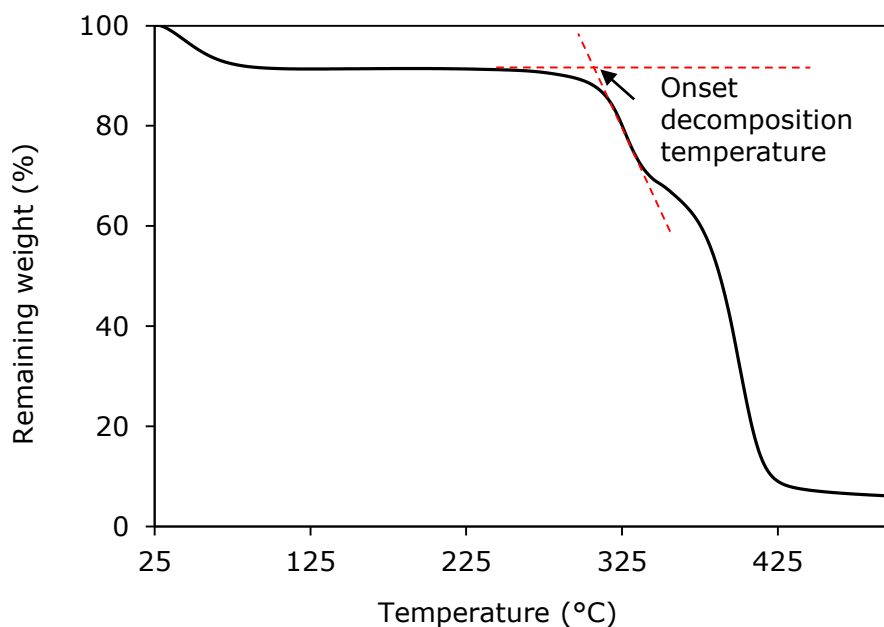
Figure 3.30 *TGA thermogram showing the onset decomposition temperature of polyNIPAm microspheres*

The onset decomposition temperature (T_{onset}) is denoted as the temperature at which weight loss begins. The weight change characteristics of a material are dependent on the experimental conditions, such as the type of sample crucible used, the nature and pressure of atmosphere in the sample chamber, and the heating rate [165]. Aluminium sample crucibles are used commonly for low temperature investigations, up to 600°C. Conversely, platinum and alumina crucibles are used for higher temperatures ranging from 600 – 1500°C. TGA analyses can be performed under a variety of atmospheric conditions, including vacuum (3 – 10 Pa), high pressure (up to 300 MPa) and atmospheric pressure in the presence of inert or reactive gases. A metal casing and high-pressure sealing around the sample housing are required for high-pressure heating. Alternatively, heating under vacuum requires a quartz housing around the sample, whilst diffusion pumps are used for evacuating the chamber. The thermal stability of the polyNIPAm microspheres was appraised using Thermogravimetric analysis (TGA, Mettler-Toledo STAR System) with a heating rate of 5°C/minute under nitrogen atmosphere.

3.3.9 Trypan Blue Exclusion Method

The Trypan blue exclusion method is used commonly for viable cell counting. This method is accomplished by a dye exclusion stain, whereby live cells with an intact membrane are able to exclude the dye and dead cells are permeated by the dye (Figure 3.31). Trypan blue is the recommended stain for the dye exclusion method as it enters across the membranes of dead cells only. Staining facilitates the visualisation of the cell morphologies [24].
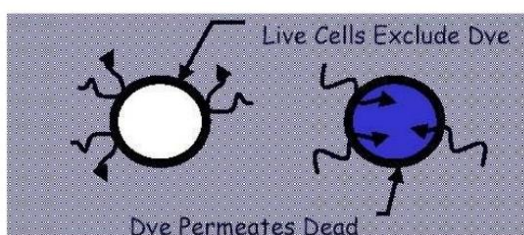
Figure 3.31 *Comparison of live and dead cells in the Trypan blue exclusion method*

To determine cell density during the sub-culturing process, the number of viable cells and dead cells in the culture flask were counted using a hemocytometer. 50 µl of the cell suspension was aspirated into a vial using a sterilised micropipette. 50 µl of Trypan blue was added into the same vial. The Trypan blue-cell suspension mixture in the vial was mixed thoroughly using a vortex mixer. 10 µl of the mixture was transferred to each chamber of the hemocytometer by touching the edge of the cover-slip with the micropipette tip to allow each chamber to fill by capillary action. Figure 3.32 presents the chambers of a hemocytometer. The number of viable and non-viable cells in each chamber was counted separately.
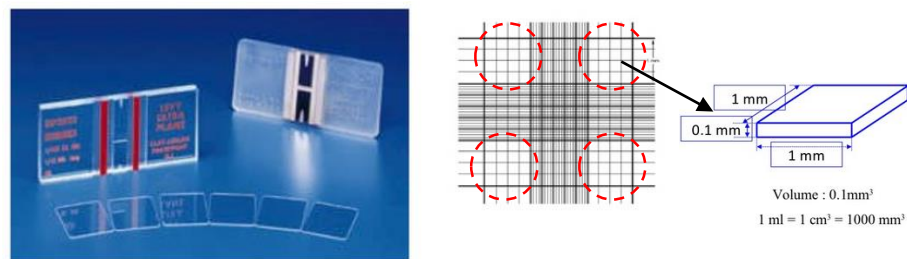
Figure 3.32 *Chambers of a hemocytometer*

Each chamber of the hemocytometer represents a total volume of 0.1 mm^3 or 10^{-4} cm^3. Since 1 cm^3 is equivalent to approximately 1 ml, the cell density, *i.e.* cell concentration per ml, was calculated using Equation 3.8 [166]:

$$\text{Cell density} = [\text{Total number of viable cells/Number of chambers}] \times \text{dilution factor} \times 10^4 \quad \ldots\ldots\ldots\ldots(Eq\ 3.8)$$

3.3.10 Water Contact Angle Measurement

Since the microspheres are too small for common contact angle measurement, the microspheres were pressed into a pellet form with a diameter of ~ 13 mm and a thickness of ~ 3 mm. A similar procedure was reported by Brandriss and Margel [167]. The water contact angle of the PNIPAm pellets was measured by the sessile drop method using a Ramé-hart Model 250 F1 Series standard goniometer equipped with Ramé-hart DROPimage Advanced v2.4 software. A drop of Millipore ultrapure water

was placed gently onto the pellet's surface using a micro-syringe. Ten images were taken at 1 s intervals. The drop profile was fitted using the Young/Laplace equation and a linear regression was used to estimate the initial water contact angle at the point the drop first contacted the surface [168]. Triplicate measurements were carried out for each sample. Figure 3.33 shows the drop profile on a polyNIPAm surface. The angles on both sides of a drop were measured to assure symmetry. The mean water contact angle was obtained by averaging the left and right theta values (θ_L and θ_R) within 1 s, as presented in Table 3.13.
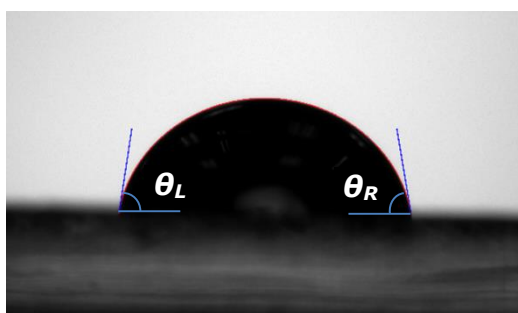
Figure 3.33 *Drop profile on a polyNIPAm surface*

Table 3.13 *Water contact angle data recorded in 1 s*

No. Messages	Time	Tilt	Theta(L)	Theta(R)	Mean	Dev.
1	0.0	0.0	80.78	79.78	80.28	0.50
2	0.1	0.0	80.73	79.72	80.23	0.50
3	0.2	0.0	80.72	79.82	80.27	0.45
4	0.3	0.0	80.73	79.77	80.25	0.48
5	0.4	0.0	80.75	79.75	80.25	0.50
6	0.5	0.0	80.85	79.74	80.29	0.55
7	0.6	0.0	80.88	79.76	80.32	0.56
8	0.8	0.0	80.84	79.76	80.30	0.54
9	0.8	0.0	80.73	79.80	80.26	0.47
10	0.9	0.0	80.64	79.80	80.22	0.42
Mean:		80.77	79.77	80.27	0.50	1.420
Stand.dev.:		0.02	0.01	0.01	0.01	0.000

3.3.11 Compression Test

Compression tests were performed to determine the compressive strength and modulus of the polyNIPAm microspheres, using an Instron Universal Tester. Specimens were placed between the compressive plates parallel to the surface. The specimens were compressed with a preload of 5 N at a constant rate of 1 mm/minute. Maximum load was recorded along with stress-strain data. Measurements were repeated three times per specimen, and average values for compressive strength and modulus were computed. Figure 3.34 shows the graph of compressive stress versus strain for the polyNIPAm microspheres synthesised in the study. It was found that the compressive stress was almost constant at strain below 20%. Further increase in strain resulted in a gradual increase in the compressive stress. This result indicates that the polyNIPAm microsphere is a ductile material that exhibits a large range of strain under compression.
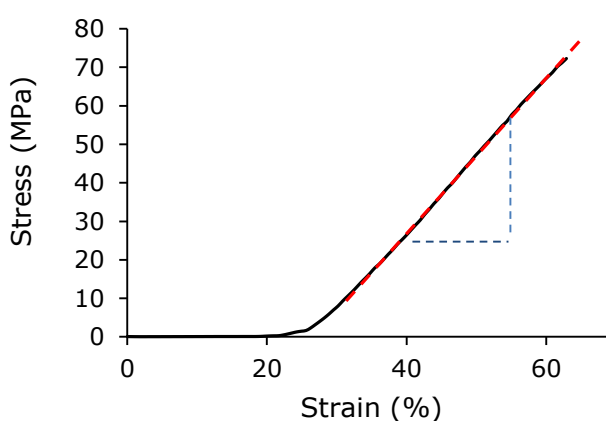
Figure 3.34 *Stress versus strain graph for the polyNIPAm microspheres*

The compressive modulus of the polyNIPAm microspheres was calculated from the slope of the stress-strain graph in Figure 3.34, as follows:

$$Compressive\ modulus = \frac{(55.92-18.86)}{(54.39-36.08)} \times 100 = 200 \text{ MPa}$$

3.4 Summary

The experimental procedures for the synthesis of polyNIPAm microspheres and cell seeding have been presented. Furthermore, the characterisation techniques used were described. The interfacial tension between the cyclohexane and PVA aqueous solution was measured using the pendant drop method. FTIR was used for the chemical bonding analysis of the polyNIPAm microspheres. SEM and EDX were used to appraise surface morphologies and elemental compositions, respectively. The zeta potential of the polyNIPAm microspheres was measured using the Laser Doppler Micro-electrophoresis method. DSC was used to assess phase transition temperature, whilst TGA was used to investigate the thermal stability of the polyNIPAm microspheres. Cell counting was performed using the Trypan blue exclusion method with an optical microscope. Water contact angle measurements were used to appraise the wettability of the microspheres. The compressive modulus of the samples was determined using an Instron Universal Tester in compression mode.

CHAPTER 4

CHOOSING A SUITABLE INITIATOR:
THERMAL VS REDOX INITIATORS

4.0 Introduction

This Chapter compares the synthesis of polyNIPAm microspheres using two different types of initiator. In order to use as microcarriers to support cell growth, the microspheres must be larger than *e.g.* the size of a Human Embryonic Kidney (HEK) cell, *i.e.* 12 µm. Hence, the suspension polymerisation technique was chosen to synthesise polyNIPAm microspheres in the present study. The properties of the polymer products were characterised using FTIR, SEM, and zeta potential, respectively. HEK cell seeding on the polymer products was performed using the methodology described in Chapter 3 (Section 3.2.3). The effectiveness of the polyNIPAm microspheres, as microcarriers in anchorage-dependent cell culture, was evaluated through cell behaviour observations using optical microscopy. The preliminary characterisation data were utilised to determine the most suitable initiator for the production of polyNIPAm microspheres.

PolyNIPAm microspheres were synthesised via suspension polymerisation, according to the experimental procedure presented in Chapter 3 (Section 3.2.1). Four sets of samples were prepared at varying concentrations of PVA continuous phase, under heating at 70°C. Table 4.1 summarises the chemical quantities used for the synthesis of polyNIPAm microspheres using an AIBN thermal initiator.

Table 4.1 *Quantities used in the synthesis of polyNIPAm microspheres using an AIBN thermal initiator.*

Sample code	Quantity in 10 ml cyclohexane (g)			PVA (g/ml)
	NIPAm	MBAm	AIBN	
A1	1.00	0.15	0.10	0.01
A2	1.00	0.15	0.10	0.02
A3	1.00	0.15	0.10	0.03
A4	1.00	0.15	0.10	0.04

For suspension polymerisation using a pair of redox initiators (APS and TEMED), the experiment was performed at room temperature, *i.e.* ~ 25°C. As mentioned in Chapter 3 (Section 3.1.5), APS generates sulfate radicals when reacts with TEMED via reduction-oxidation process. Otherwise, no radicals are generated from APS without the presence of TEMED that acts as an accelerator in the initiation of polymerisation. This explains why a pair of redox initiators was used. Since the redox initiators were water-soluble, ultrapure water was used as the inner phase whilst cyclohexane was used as the outer phase. The concentration of Span 80® surfactant was selected based on measurement of the interfacial tension between the oil and water phase (Figure 4.1). The critical micelle concentration of Span 80® in cyclohexane at 25°C was reached at 0.02 g/ml. The addition of 0.02 g/ml of Span 80® resulted in a significant decrease in the interfacial tension between the oil and water phase. This effect was attributed to the adsorption of the Span 80® surfactant molecules between the oil and water phase, which subsequently stabilised the dispersing water droplets in the continuous oil phase. At concentrations above 0.02 g/ml, an insignificant change in the interfacial tension between the oil and water phase was recorded. This suggests that the aqueous droplets have been stabilized by the Span 80® and thus, further addition of surfactant would have no effect on the interfacial tension between these immiscible liquids. The chemical quantities used for the synthesis of polyNIPAm microspheres using a pair of redox initiators (APS and TEMED) are listed in Table 4.2.
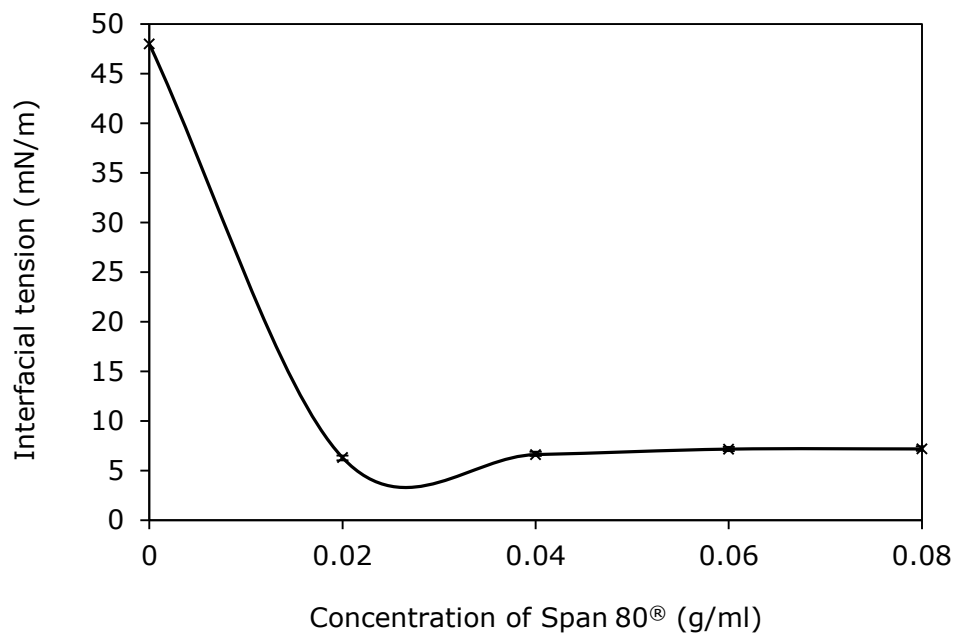
Figure 4.1 *Variation of interfacial tension between water and cyclohexane as a function of Span 80® concentration*

Table 4.2 *Quantities used in the synthesis of polyNIPAm microspheres using a pair of redox initiators (APS and TEMED)*

Sample code	Quantity in 10 ml ultrapure water (g)				Quantity in 100 ml cyclohexane (g)
	NIPAm	MBAm	APS	TEMED	Span 80®
B1	1.00	0.15	0.10	0.10	2.00

To determine the most suitable initiator for the synthesis of polyNIPAm microspheres, the polymer products synthesised using AIBN and APS/TEMED were compared in terms of particle size and surface charge. The following section is divided into two main parts: part one provides an account of the characterisation of the synthesised polyNIPAm microspheres using FTIR analysis, scanning electron microscopy (SEM), and zeta potential measurements; part two presents the cell trial results obtained from the polyNIPAm microspheres. The effectiveness of the polyNIPAm microspheres synthesised using AIBN and APS/TEMED, as microcarriers, is compared and discussed.

4.1 Results and Discussion

4.1.1 Characterisation of PolyNIPAm Microspheres

The chemical bonds present in the synthesised polyNIPAm microspheres were appraised using FTIR analysis, to confirm the progression of polymer synthesis. Figure 4.2 presents FTIR spectra of polyNIPAm samples prepared using the thermal (A1-A4) and redox (B1) initiators. The characteristic peaks present in the FTIR spectra of the NIPAm monomer and polyNIPAm samples are summarized in Table 4.3. All the polyNIPAm samples exhibited similar FTIR patterns, with two strong characteristic peaks at 1640 cm^{-1} and 1530 cm^{-1}, attributable to carbonyl (C=O) stretching of the primary amide group and N-H bending of the secondary amide group, respectively [169]. Comparison of FTIR spectra of the NIPAm monomer and polyNIPAm samples showed that the strong, sharp characteristic peak at 3300 cm^{-1}, being attributable to N-H stretching of the amide group in the NIPAm monomer, became broader after polymerisation. This reflected peak overlap with signatures due to the O-H stretching of water molecules, being attributable to interactions between polymer chains and neighbouring water molecules [170]. The peaks between 600 and 1000 cm^{-1} in the FTIR spectrum of the NIPAm monomer, disappeared in the FTIR spectra of the polyNIPAm microspheres. This confirmed that the polymerisation of NIPAm had progressed successfully, with breakdown of carbon double bonds in the NIPAm monomer and the formation of polyNIPAm polymer chains, in agreement with the reports of Zhang *et al.* [171] and Costa *et al.* [172]. The chemical structures of the NIPAm monomer and the polyNIPAm polymer are depicted by Figure 4.3.
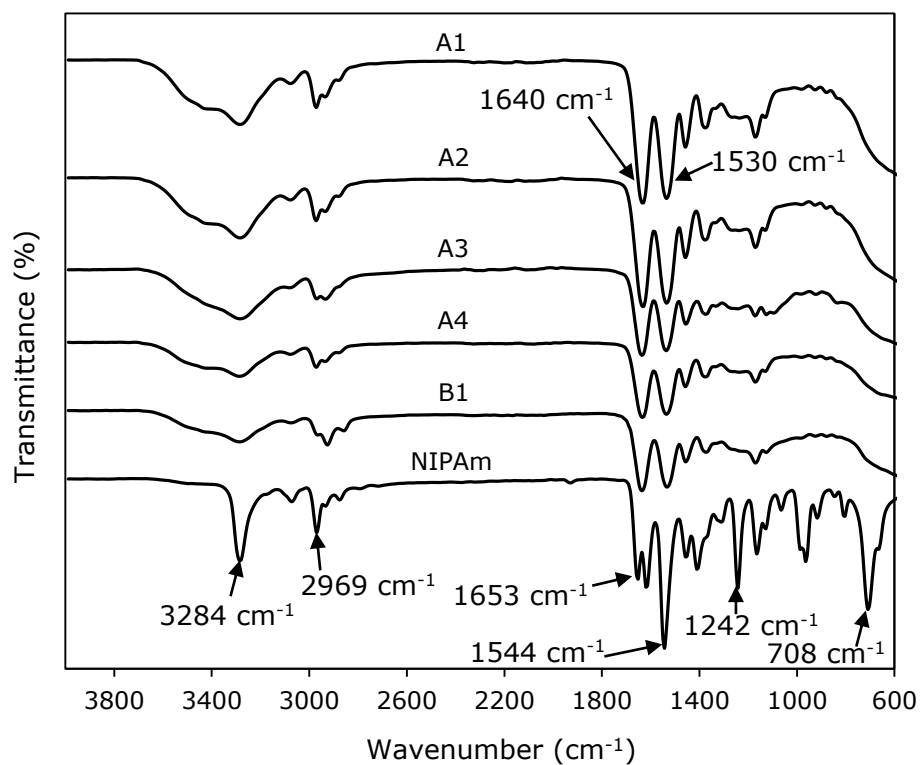
Figure 4.2 *FTIR spectra of polyNIPAm samples prepared using thermal (A1-A4) and redox (B1) initiators, and the NIPAm monomer*
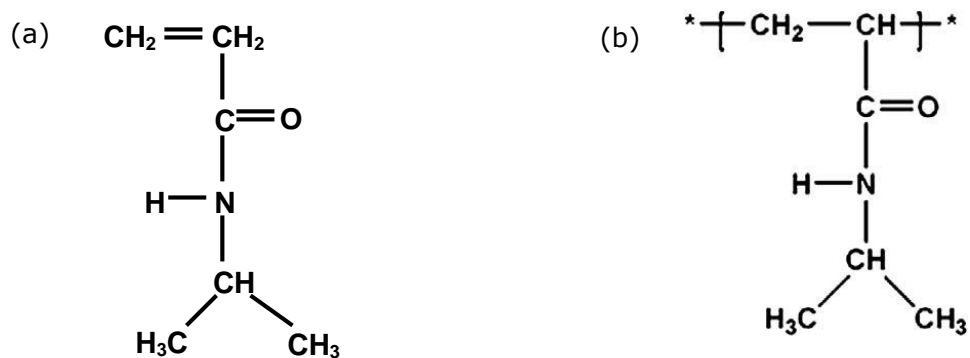
Figure 4.3 *Chemical structures of (a) the NIPAm monomer, and (b) the polyNIPAm polymer*

Table 4.3 *Characteristic peaks in the FTIR spectra of the NIPAm monomer and the polyNIPAm microspheres [169-172]*

NIPAm monomer		PolyNIPAm microspheres	
Wavenumber (cm^{-1})	Functional groups	Wavenumber (cm^{-1})	Functional groups
3284	OH-stretching	3287	OH-stretching
2969	C-H stretching	2927	C-H stretching
1653	C=O stretching of Amide I	1640	C=O stretching of Amide I
1617	N-H bending of Amide II	1530	N-H bending of Amide II
1544	N-H bending of Amide II		
1455	C-H bending	1456	C-H bending
1409	CH(CH$_3$)$_2$ stretching of isopropyl group	1393	CH(CH$_3$)$_2$ stretching of isopropyl group
1242	Amide III		
1164	CH$_3$ skeletal	1170	CH$_3$ skeletal
963	CH$_2$ rocking		
806	CH$_2$ rocking		
708	CH$_2$ rocking		

To appraise the effect of PVA stabiliser concentration on the size and shape of the polyNIPAm microspheres prepared using a thermal initiator (A1-A4), four sets of polyNIPAm samples were produced via suspension polymerisation. PVA was used to stabilize the oil droplets in the aqueous phase, by creating a repulsive force to prevent coalescence of the oil droplets [173]. Without a stabiliser, the O/W emulsion becomes unstable, and the oil droplets coalesce with each other due to the high interfacial tension between the immiscible oil and aqueous phases (Figure 4.4).
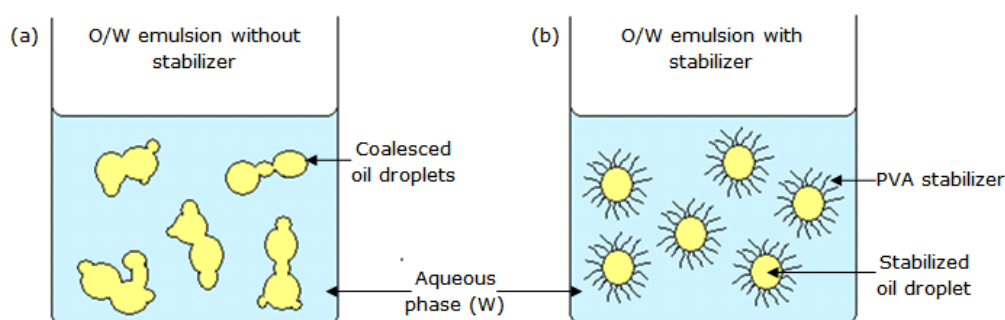
Figure 4.4 *Schematic overview of an O/W emulsion (a) without; and (b) with a stabiliser*

For practical applications, the aim was to produce spherical polyNIPAm microspheres with diameters > 12 µm. However, all four products consisted of relatively small spherical microspheres with diameters in the range ~ 0.6 - 1.5 µm, as shown by the secondary electron (SE) micrographs of Figures 4.5. Agglomeration of the polyNIPAm microspheres was characteristic for each sample, attributable to the high surface area to volume ratio of the small microspheres. In order to minimize the high surface energy, the microspheres tended to form agglomerates via attractive van der Waals forces [174].
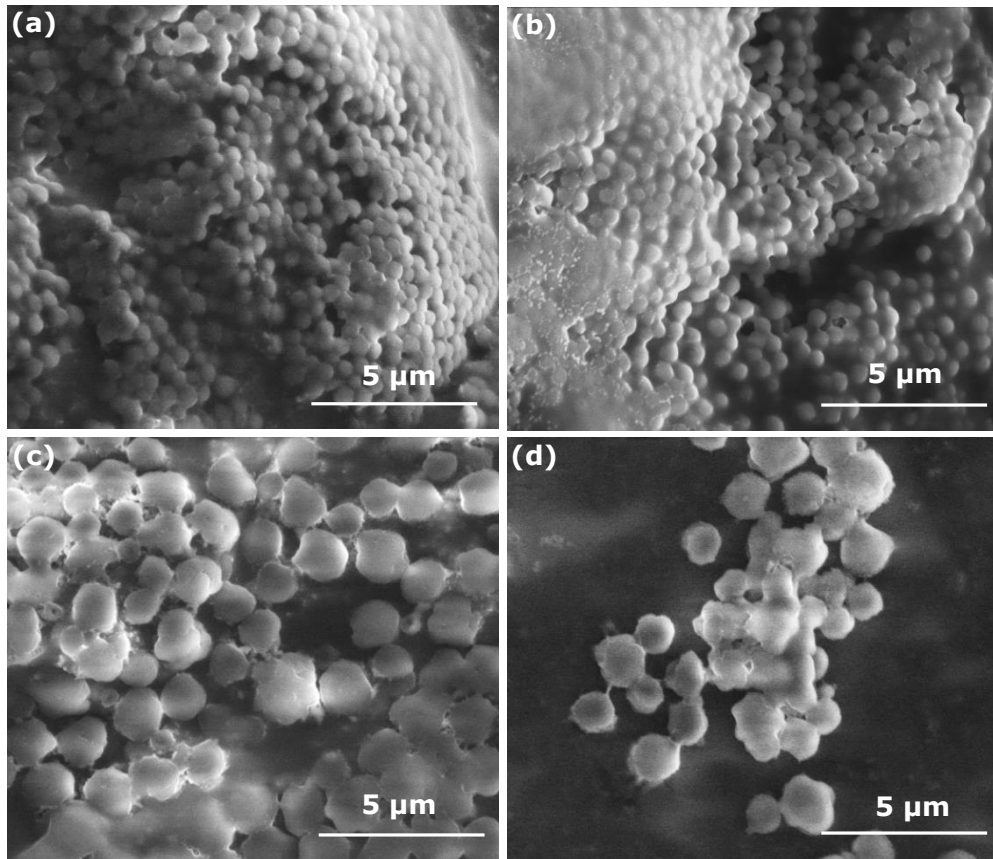
Figure 4.5 *SE micrographs of polyNIPAm samples prepared using a thermal initiator as a function of PVA stabiliser concentration: (a) A1 (0.01 g/ml PVA); (b) A2 (0.02 g/ml PVA); (C) A3 (0.03 g/ml PVA); and (d) A4 (0.04 g/ml PVA)*

According to Israelachvili [175], van der Waals forces are electrodynamic interactions resulted from fluctuating electric dipoles and decay asymptotically as r^{-7}, where r is the distance between the centres of two particles. Over a short distance, the particles diverge as $d^{-2} = (r-2a)^{-2}$, where a is the particle radius and d is the distance between the surfaces. The van der Waals forces dominate over short distances for particles smaller than a few micrometers (Figure 4.6). Similar findings were reported by Leong *et al.* [176] and Mandzy *et al.* [177] on studies of polymer composite and titanium dioxide nanoparticles, respectively.
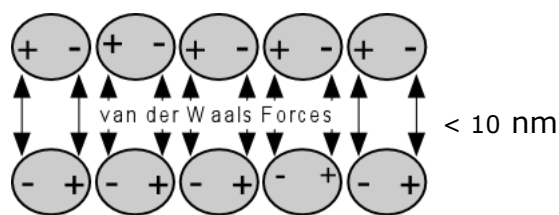
Figure 4.6 *Depiction of van der Waals forces between particles in close proximity*

The root cause of the production of < 2 µm polyNIPAm microspheres was the high polymerisation temperature of 70°C. Ideally, oil droplets containing the monomer phase become well-dispersed in PVA aqueous solution at room temperature. However, as the temperature increased up to 70°C, the O/W emulsion changed to a W/O emulsion (Figure 4.7), being attributable to a change in lipophilicity of the PVA stabiliser at elevated temperature [178]. As a result, the stabilizer became more soluble in the oil phase leading to the formation of the W/O emulsion. Since the AIBN initiator, NIPAm monomer and MBAm cross-linker were dissolved in the oil phase, precipitation polymerisation then took place with the formation of oligoradical and precursor particles, followed by particle growth via monomer capture by the growing oligomers until a critical chain length was reached [179]. Subsequent precipitation occurred when the particles with critical chain length became insoluble in the solvent (Figure 4.8). It is noted that the size of polyNIPAm microspheres synthesised from the AIBN thermal initiator, between 0.6 and 1.5 µm, is a typical size range for the products of precipitation polymerisation [180].
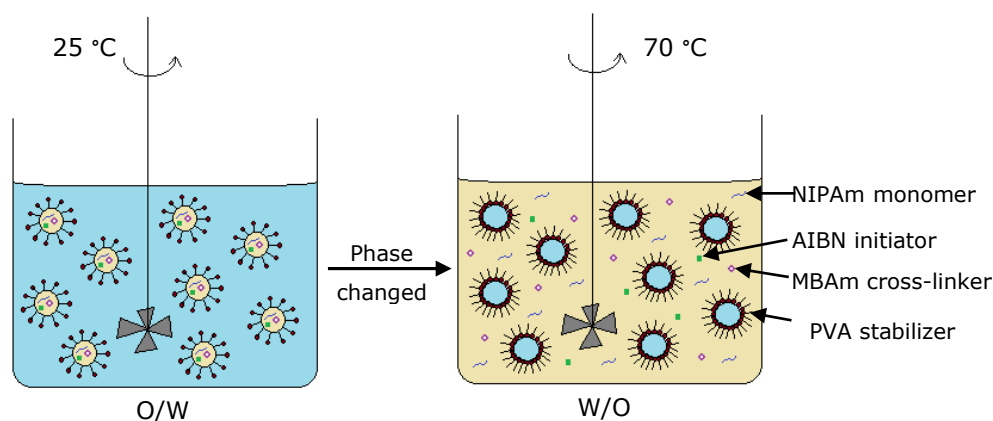
Figure 4.7 *Depiction of suspension polymerisation of NIPAm at 25°C and 70°C*
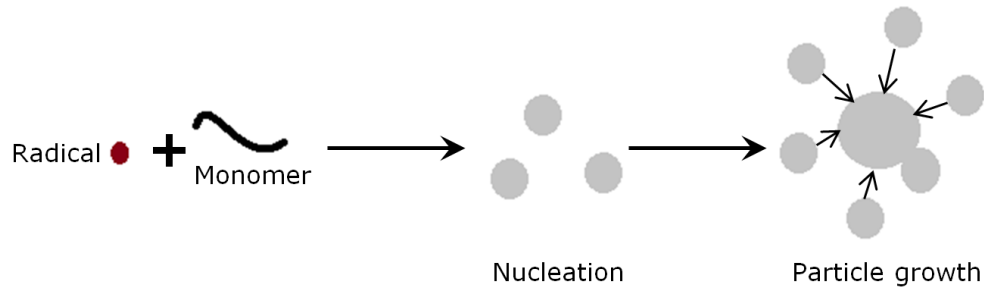
Figure 4.8 *Mechanism for polyNIPAm particle formation via precipitation polymerisation*

In contrast, relatively large polyNIPAm microspheres with smooth surfaces were prepared via suspension polymerization at room temperature (25°C) using a redox initiator (Figure 4.9), with the average size of 100 particles from this sample being 54 ± 8 µm. Such large microspheres, as prepared at room temperature, are considered to be potentially more suitable for practical applications, as compared to the submicron-particles prepared at 70°C using a thermal initiator.
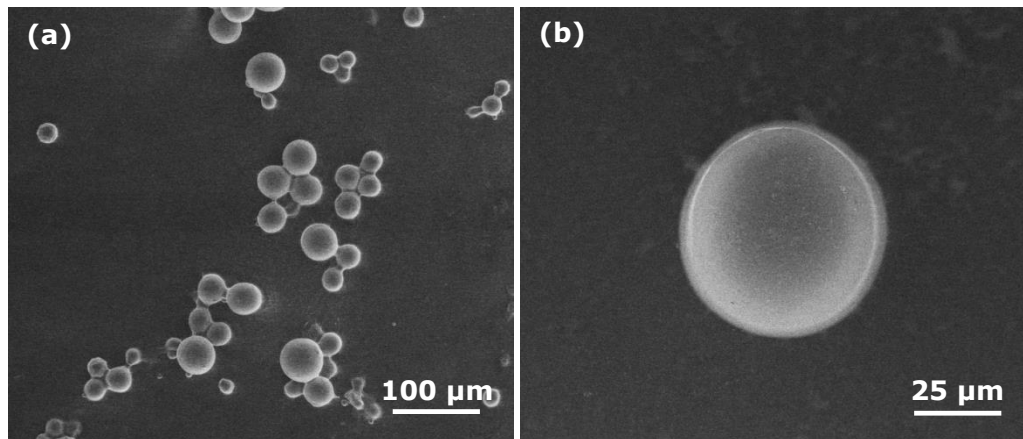
Figure 4.9 *SE micrographs of polyNIPAm microspheres prepared using a redox initiator: (a) at low magnification (500 x); (b) at high magnification (2000 x)*

In suspension polymerisation, polymer particles are formed via a chain reaction mechanism involving initiation, propagation and termination [87]. Figure 4.10 depicts the mechanism for polyNIPAm particle formation via suspension polymerisation. Generally, the initiator is soluble in the monomer droplet stabilized by surfactant molecules. Free radicals are generated from the decomposition of the initiator. The monomer radicals are then activated by the free radicals, forming new polymer chains. Propagation of the growing chains takes place as the activated monomers react with other monomers [181]. Cross-linked polymer particles are formed when chain termination occurs, as described in Chapter 2 (Section 2.2.3). Unlike precipitation polymerisation, the particle size produced via suspension polymerisation is dependent on the size of the stabilized monomer droplet. Hence, particles produced via suspension polymerisation are much larger than those produced via precipitation polymerisation.
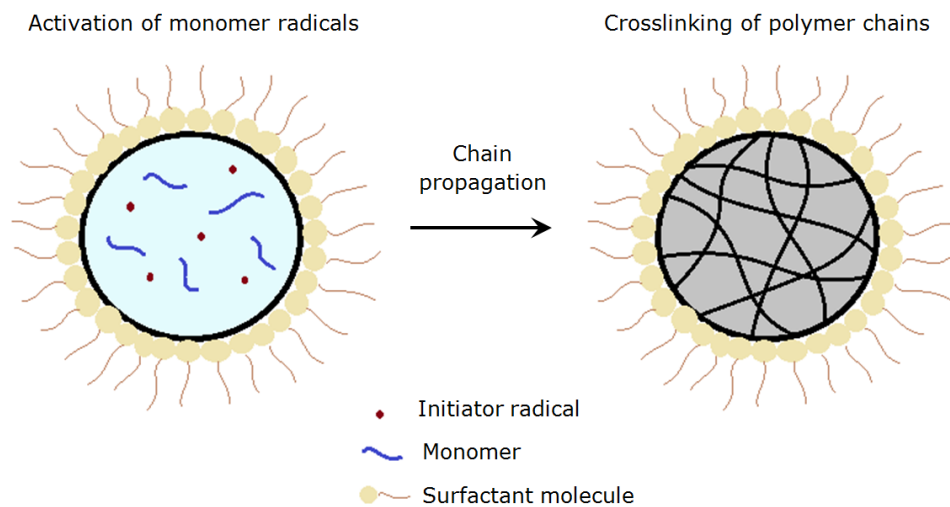
Figure 4.10 *Schematic overview of polyNIPAm particle formation via suspension polymerisation of a W/O system*

4.1.2 Cell Attachment

To assess the potential of the synthesised polyNIPAm microspheres as microcarriers in anchorage-dependent cell culture, HEK cells were cultured with the microspheres for seven days. Figure 4.11 presents optical micrographs of HEK cell suspensions containing polyNIPAm microspheres produced using the thermal initiator and different PVA stabiliser concentrations (A1-A4), on Days 2 and 7 of the culturing process. No cell attachment to the polyNIPAm microspheres was observed throughout the seven days of cell culture. This was attributed partly to the small size of the polyNIPAm microspheres, being much smaller than the 12 μm size of the HEK cell. According to Senuma *et al.* [182], the ideal size of a microcarrier for anchorage-dependent cell culture is between 100 and 300 μm. In this case, it appears that HEK cells are unable to attach to templates smaller than the cell size. Similar finding was reported by Chen *et al.* [183], in which the large microcarrier with a mean diameter of 190 μm demonstrated greater cell yield than the smaller microcarrier having a mean diameter of 10 μm. This is in agreement with the previous report of Re *et al.* [184], stating that peptide-coated microcarrier beads larger than 100 μm exhibited human endothelial cell adhesion and spreading, whereas small beads with diameter of 4.5 μm did not support cell adhesion and resulted in cell death within 12 h of cell seeding.

It was observed that the structure of the HEK cells changed from Day 2 to 7. On Day 2 of culturing, the HEK cells were of rounded shape, indicating that the cells were still in a detached state. While on Day 7 of culturing, the HEK cells exhibited elongated shapes, indicative of cell attachment and proliferation at the bottom of the culture flask. Furthermore, the small polyNIPAm microspheres were found to form agglomerates due to Brownian motion, *i.e.* the continuous random movement of particles suspended in a fluid.
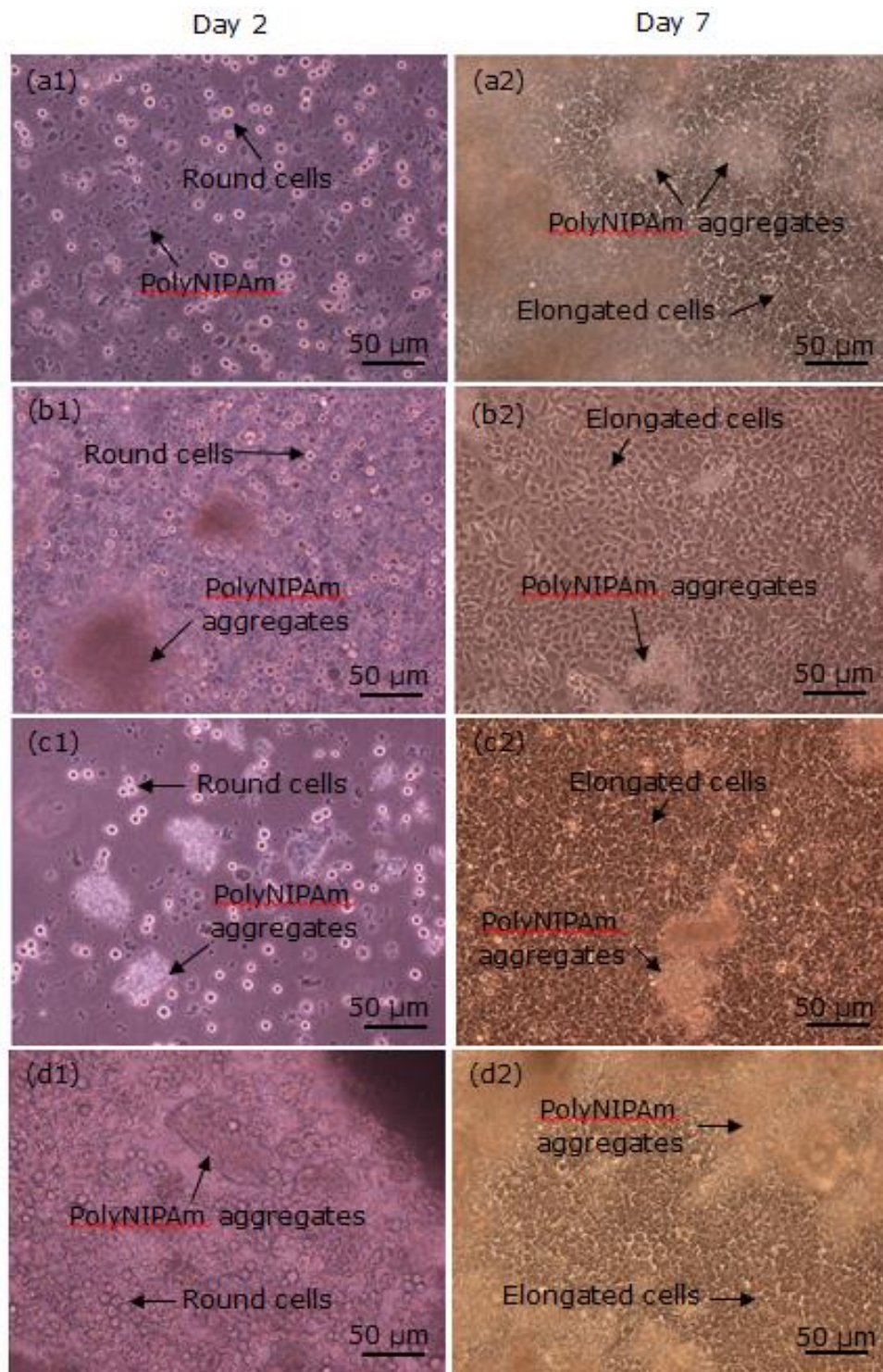
Figure 4.11 *Optical micrographs of HEK cells and polyNIPAm microspheres (A1-A4) produced using: (a1,a2) 0.01 g/ml PVA; (b1,b2) 0.02 g/ml PVA; (c1,c2) 0.03 g/ml PVA; and (d1,d2) 0.04 g/ml PVA, in culture media on Day 2 and Day 7 of the culturing process*

Optical micrographs of HEK cell suspensions containing polyNIPAm microspheres produced using a pair of redox initiators (B1) at room temperature, are presented in Figure 4.12. Again, no cell attachment to the polyNIPAm microspheres was observed throughout the seven days of the culturing process. Instead, the HEK cells clumped together and formed aggregates. This effect was attributed to the negative surface charge of the polyNIPAm microspheres (Table 4.4). According to Ishikawa *et al.* [160], surface charge is the main factor affecting cell behaviour. Since cells are negatively charged due to the presence of a glycocalyx carbohydrate on the cell surface. Accordingly, the microcarrier surface charge ideally should be positive, in order to promote cell adhesion. Lee *et al.* [185] and Schneider *et al.* [186] found that cell culture substrates with positive charge promoted more cell adhesion and spreading compared to neutral or negatively charged surfaces.
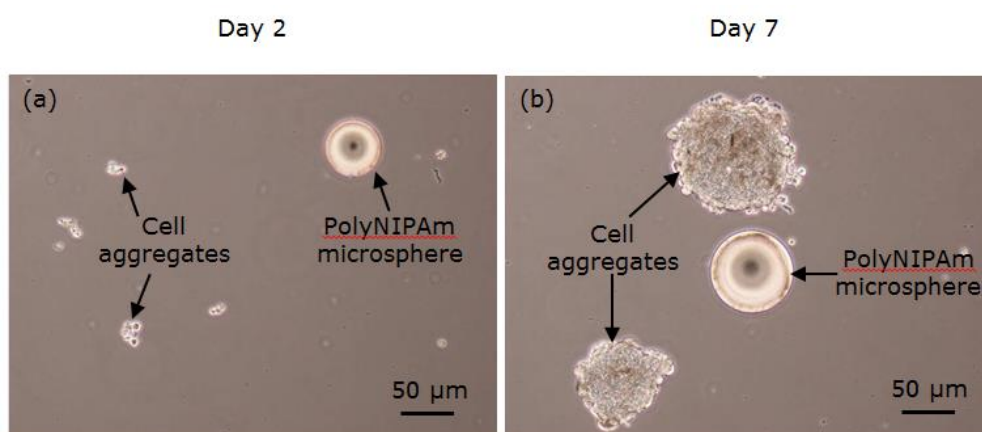
Figure 4.12 *Optical micrographs of HEK 293 cells and polyNIPAm microspheres produced using a redox initiator on Day 2 and Day 7 of the culturing process*

Zeta potential data for polyNIPAm microspheres synthesised using the different initiators is presented in Table 4.4. It was found that the zeta potential of polyNIPAm particles produced using the thermal initiator (AIBN) was less negative as compared to polyNIPAm microspheres produced using the redox initiators (APS/TEMED). When the AIBN thermal initiator was used, the zeta potential of the polyNIPAm microspheres was ~ -3 mV. When the APS/TEMED redox initiator was used, the zeta

potential of the polyNIPAm microspheres was ~ -29 mV. This was attributed to the difference in surface charge associated with AIBN and APS. AIBN is a neutral initiator having zero net charge, whereas APS is negatively charged due to the presence of persulfate anions (SO_4^-) generated from the decomposition process, as depicted by Figure 4.13 [187].

Table 4.4 *Zeta potential data for polyNIPAm microspheres produced using thermal (A1-A4) and redox (B1) initiators*

Sample code	Zeta potential (mV)
A1	-2.8 ± 3.4
A2	-2.9 ± 3.9
A3	-2.6 ± 3.4
A4	-3.0 ± 3.9
B1	-28.7 ± 1.3

$$S_2O_8{}^{-2} \xrightarrow{\text{Decomposition}} SO_4 \bullet^{-1} + SO_4 \bullet^{-1}$$
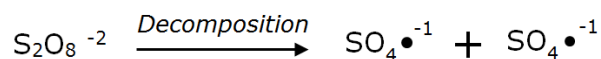
Figure 4.13 *Anionic persulfate radical formation from APS decomposition*

Upon decomposition of the APS initiator, persulfate radicals diffuse into the monomer droplets to initiate polymerisation by reacting with the oligomers, as depicted by Figure 4.14. This explains why these synthesised polyNIPAm microspheres are so strongly negatively charged. Similar findings were reported by van Berkel *et al.* [188], from a study of the effect of a potassium persulfate initiator on polymer surface charge. The present study demonstrates similarly that the surface charge of polymer microspheres is affected strongly by the type of initiator used in the polymerisation reaction.
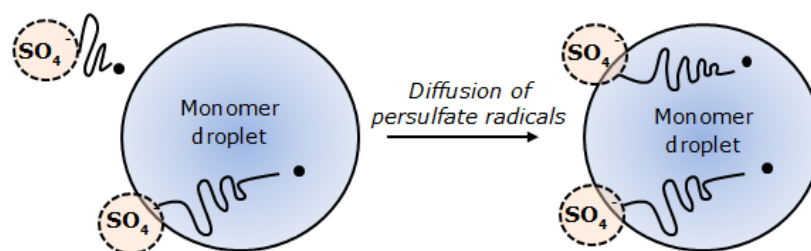
Figure 4.14 *Depiction of the diffusion of persulfate radicals into a monomer droplet during suspension polymerisation*

4.2 Summary

PolyNIPAm microspheres with two different size ranges were produced using different initiators and polymerization temperatures. PolyNIPAm microspheres < 2 μm in size were synthesised at 70°C using a thermal initiator, whilst relatively large (~ 50 μm) polyNIPAm microspheres were synthesised at 25°C using a redox initiator. Since the synthesized polyNIPAm microspheres were intended for use as microcarriers for anchorage-dependent cell culture, there is a requirement for the microspheres to be larger than the cell size. However, no cells attached to the polyNIPAm microspheres, even when microspheres larger than the cells were produced using the redox initiator. The negative surface charge of the polyNIPAm microspheres was considered dominant in hindering cell attachment. Accordingly, the route of suspension polymerisation of NIPAm using a redox initiator at 25°C was selected as the process of choice for the following studies, seeking to enhance cell attachment through surface charge modification of the polyNIPAm microspheres.

CHAPTER 5

EFFECT OF SURFACE CHARGE ON HEK CELL ATTACHMENT TO POLYNIPAM MICROSPHERES

5.0 Introduction

To enhance cell attachment to the polyNIPAm microspheres, modification of the surface charge of the microspheres using differently charged surfactants was investigated. In the present study, the cationic surfactant cetyl trimethyl ammonium bromide (CTAB) was identified as being suitable for addition to the system containing the nonionic surfactant Span 80®. It was hypothesised that adsorption of the cationic-nonionic surfactant mixture onto the negatively charged surfaces of the polyNIPAm microspheres would be enhanced, thereby reducing the negativity of the surface charge on the polyNIPAm microspheres. The objective of this part of the study was to appraise the effect of surfactant mixtures on the surface charge of the polyNIPAm microspheres. Additionally, the effect of surface charge on the attachment of human embryonic kidney (HEK) cells was investigated.

Four sample sets of polyNIPAm microspheres were prepared via suspension polymerisation with varying surfactant composition at room temperature (25°C). The effect of surfactant composition on the physical and thermal properties of the polyNIPAm microspheres were investigated using FTIR, TGA, DSC SEM, and zeta potential. HEK cells were seeded on the polyNIPAm microspheres and the cellular response to the microspheres with different surface charges was studied through the appraisal of cell density as a function of culturing time, using the Trypan blue exclusion method as described in Chapter 3 (Section 3.3.9). The surfactant compositions used in the synthesis of the polyNIPAm microspheres are listed in Table 5.1.

Table 5.1 *Quantities used in the synthesis of polyNIPAm microspheres prepared in the presence of varying CTAB/Span 80® surfactant composition*

Sample code	Quantity in 10 ml ultrapure water (g)				Quantity in 100 ml cyclohexane (g)	
	NIPAm	MBAm	APS	TEMED	Span 80®	CTAB
S1	1.00	0.15	0.10	0.10	2.00	0.00
S2	1.00	0.15	0.10	0.10	1.80	0.20
S3	1.00	0.15	0.10	0.10	1.60	0.40
S4	1.00	0.15	0.10	0.10	1.40	0.60

The chemical bonds present in the four samples prepared with different *CTAB/Span* 80® surfactant compositions were characterized using FTIR spectroscopy. The thermal stabilities and transition temperatures of the polyNIPAm microspheres as a function of surfactant composition were appraised using TGA and DSC, respectively. The microstructures of the four samples were studied using SEM, and an appraisal of the elemental composition of each sample was performed using EDX. The surface charges of the polyNIPAm microspheres prepared with different surfactant compositions were compared. Cell trial was performed to appraise effectiveness of the synthesised microspheres for cell culture application, using HEK cells, cultured for seven days. Optical microscopy and scanning electron microscopy were performed to study cell attachment and growth, as a function of culturing time. Cell detachment from the polyNIPAm microspheres was assessed using optical microscopy. Detailed explanation of the results obtained using each characterisation technique is presented in the following section.

5.1 Results and Discussion

5.1.1 PolyNIPAm Microsphere Synthesis and Characterisation

FTIR spectroscopic analysis was used to appraise chemical bonding and thereby study the influence of surfactant composition on the structure of the polyNIPAm microspheres. FTIR analysis provided evidence for the successful polymerization of polyNIPAm. Spectra for the CTAB surfactant, the Span 80® surfactant, the MBAm cross-linker, and the NIPAm monomer are included for comparison in Figure 5.1.
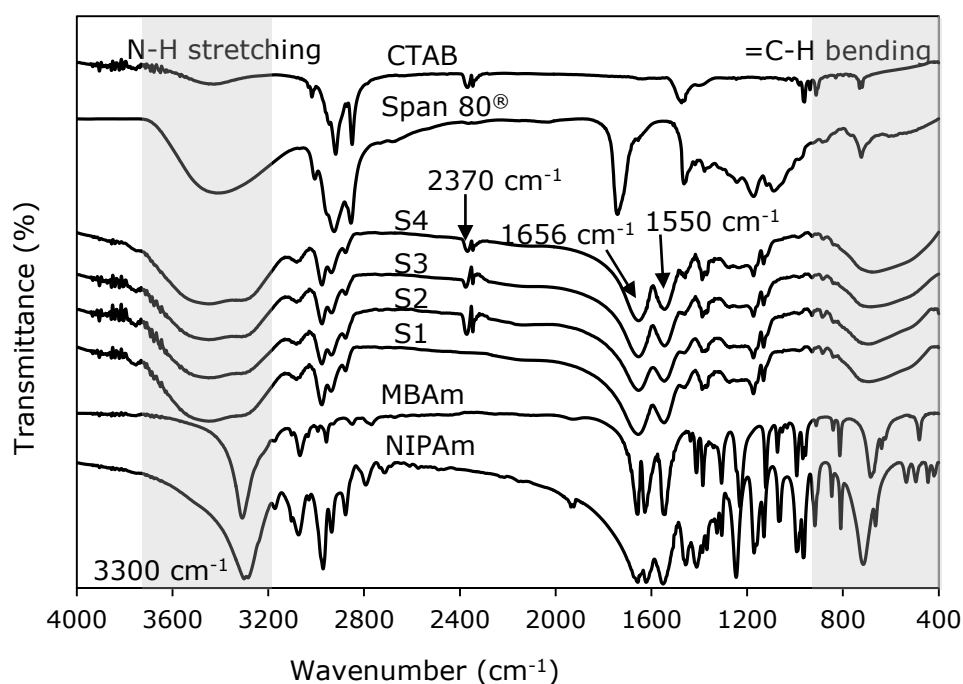
Figure 5.1 FTIR spectra of polyNIPAm microspheres prepared using four different surfactant compositions, along with reference spectra for the NIPAm monomer, MBAm cross-linker and CTAB surfactant
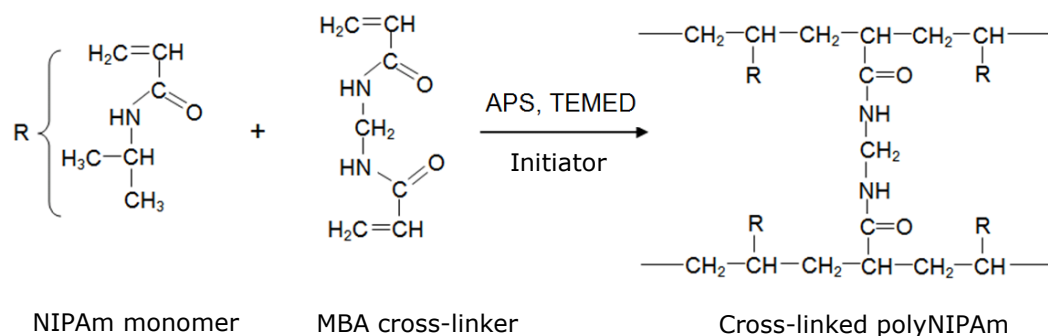
Figure 5.2 *Chemical reaction for NIPAm polymerisation*

Figure 5.2 illustrates the chemical reaction for NIPAm polymerisation at room temperature in the presence of APS/TEMED redox initiators. Briefly, NIPAm polymerisation is initiated by SO_4^- radicals generated from the spontaneous decomposition of the redox initiators added. The NIPAm monomer was subsequently polymerised via a chain propagation process and cross-linked by the MBAm cross-linker [189]. The NIPAm monomer and MBAm cross-linker possess similar chemical structures, *i.e.* both NIPAm and MBA contain alkene group (CH_2=CH-) and amide group (-C=O-NH-) (Figure 5.2) and hence exhibit similar FTIR spectra (Figure 5.1) with a strong, sharp characteristic peak at 3300 cm^{-1} attributable to N-H stretching of the amide group [190]. This peak became broader after NIPAm polymerisation due to interactions between the polymer and neighbouring water molecules, leading to peak overlap with characteristic attributable to the O-H stretching of water molecules [170]. In particular, all the polyNIPAm samples featured a double peak at 1550 and 1656 cm^{-1}, attributable to N-H bending of the secondary amide group and carbonyl (C=O) stretching of the primary amide group, respectively. The sequence of peaks between 400 and 900 cm^{-1} shown by the NIPAm monomer, corresponding to =C-H bending of the alkenes, was absent for polyNIPAm, confirming that the polymerisation reaction had progressed successfully, with free radical breakdown of carbon double bonds from the NIPAm monomer and MBAm cross-linker and subsequent formation of polyNIPAm polymer chains [78, 172]. Two minor peaks at 2345 and 2370 cm^{-1} in the FTIR spectra for the polyNIPAm microspheres prepared from the different CTAB contents (S2-S4) were characteristic of CTAB, suggesting that some surfactant CTAB molecules remained on the polyNIPAm surfaces.

TGA analyses were performed to appraise the thermal stability of the polyNIPAm microspheres prepared using the different surfactant mixtures. Each sample was heated from 25 to 500°C at a constant heating rate of 5°C/min under an inert N_2 atmosphere (Figure 5.3). All the samples exhibited a three-step thermal decomposition process.
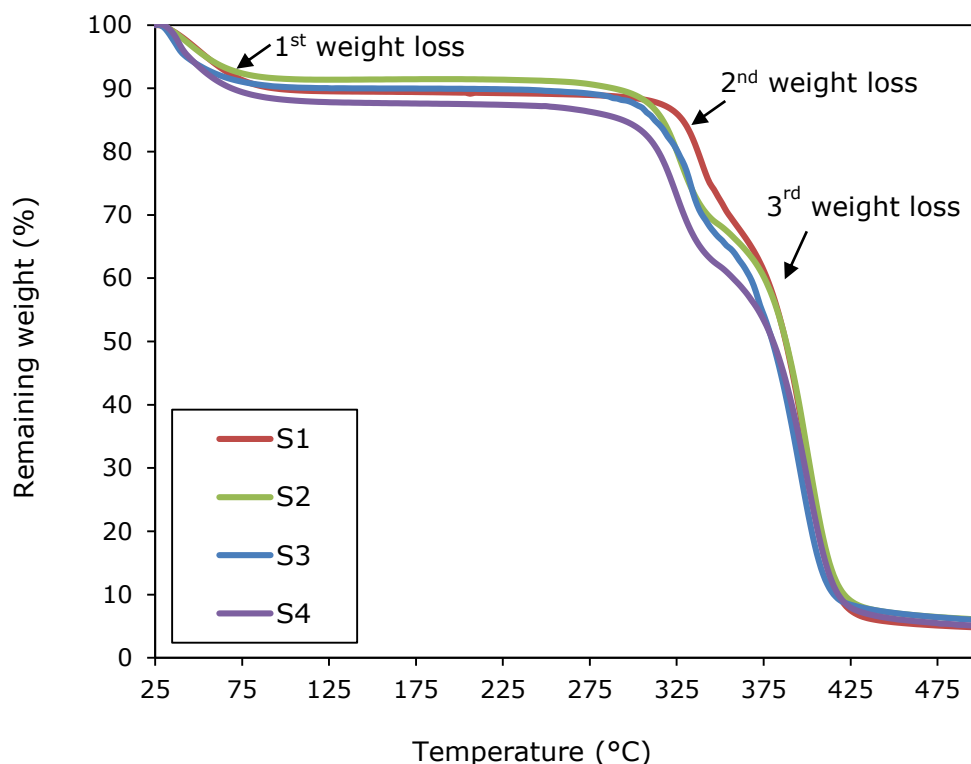
Figure 5.3 *TGA thermograms of the polyNIPAm microspheres prepared using different surfactant compositions (S1-S4)*

The first thermal decomposition slope, with minor weight loss of ~ 10%, was detected below 100°C and attributed to the evaporation of absorbed water. This indicated that the polyNIPAm samples were hydrophilic with a tendency to absorb moisture from the surroundings [191]. A second weight loss process in the range 300 and 350°C, with a weight loss of ~ 20% was attributed to the breakdown of hydrogen bonds that possess a relatively low bonding energy [192]. A third thermal decomposition process at ~ 400°C was attributed to decomposition of the polyNIPAm polymer backbone along with other functional groups. All four samples

106

exhibited similar weight of residue, *i.e.* ~ 5% upon heating up to 500°C. Similar findings were reported by Yang *et al.* (2009) [192] and Su *et al.* (2013) [190]. In particular, it was found that the onset decomposition temperature decreased with increasing concentration of cationic surfactant (CTAB). Sample S1 without CTAB exhibited an onset decomposition temperature at 350°C whilst Sample S3 with 30% CTAB started to decompose thermally at 300°C. This was because CTAB begins to decompose thermally at 250°C, in turn reducing the onset decomposition temperature of polyNIPAm. These TGA results are in agreement with the studies of Shinde *et al.* [193] and Bauri *et al.* [194], and confirm that polyNIPAm microspheres can be autoclaved at 121°C for sterilisation prior to cell seeding, with the microspheres being thermally stable up to ~ 300°C.

The DSC technique was used to appraise the transition temperature (LCST) of the synthesised polyNIPAm microspheres. As outlined in Chapter 2 (Section 2.1), polyNIPAm exhibits a reversible phase transition above the LCST. Hydrogen bonding between water molecules and the amide groups of polyNIPAm dominates at temperatures below the LCST [195]. Conversely, an increase in temperature facilitates the release of water molecules surround the hydrophobic isopropyl groups, promoting polymer-polymer association by hydrophobic interactions (Figure 5.4).
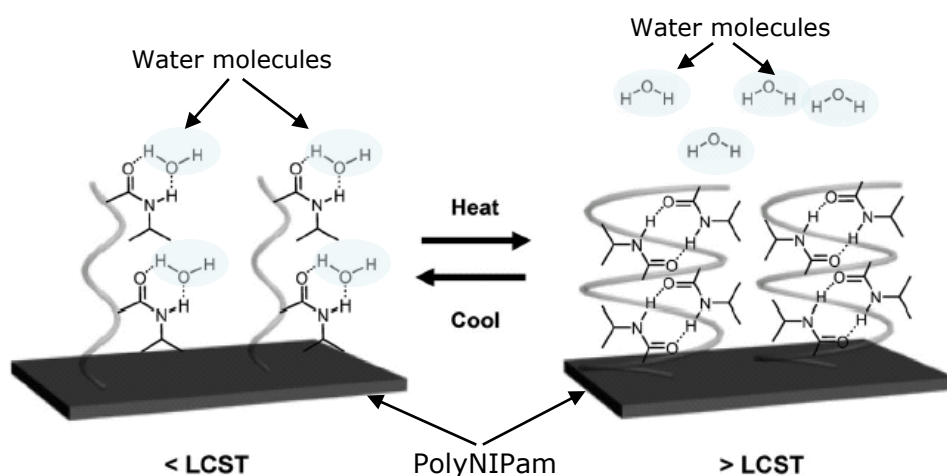
Figure 5.4 *Phase transition of polyNIPAm around the LCST [196]*

The LCST corresponds to the temperature of the endothermic peak in the DSC thermogram [197]. Figure 5.5 presents DSC thermograms of the polyNIPAm microspheres obtained when the samples were heated from 20 to 60°C. It was found that the endothermic peak shifted to higher temperatures as the amount of CTAB surfactant added was increased. Sample S1 (without CTAB) exhibited an endothermic peak at 32.4°C, corresponding to the transition temperature of these polyNIPAm microspheres. This is consistent with the previous findings of Schild [46] and Yoshida *et al.* [198]. However, the transition temperature was raised from 32.8 to 39.5°C when the amount of CTAB was increased from 10% to 30%. According to Haba *et al.* [199], the LCST increases with increasing hydrophilic content due to an increase in hydrogen bonds formed between the amide groups and water molecules, suppressing the dehydration of the polymer chains. A similar finding was reported by Purushotham and Ramanujan [200] on a study of hydrophilic effect on the LCST of polyNIPAm.
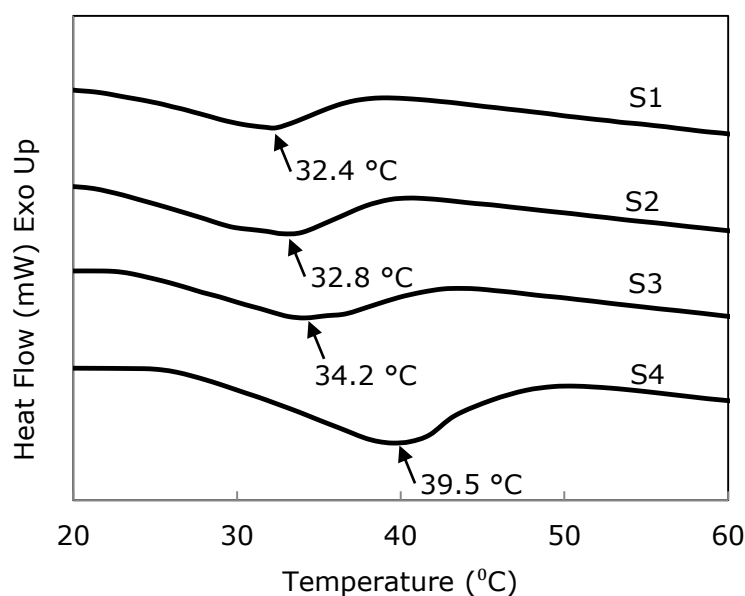
Figure 5.5 *DSC thermograms of the polyNIPAm microspheres prepared using different surfactant compositions (S1-S4)*

The EDX technique was used to appraise the effect of surfactant composition on the elemental composition of the polyNIPAm microspheres. Table 5.2 presents EDX data for the four samples (S1-S4). Only carbon, nitrogen and oxygen were detectable in each sample, indicating that all the samples were clean and free of impurities. The C/O ratios obtained from the EDS analyses were close to the theoretical C/O ratio (3:1) for polyNIPAm. In particular, it was found that the experimental ratio of N/C increased gradually with increasing amounts of CTAB surfactant, indicating that the amount of CTAB molecules adsorbed on the polyNIPAm samples increased as the addition of CTAB was increased.

Table 5.2 *Elemental compositions of the polyNIPAm microspheres*

Sample	Span 80® / CTAB ratio	Atomic %			N/C ratio
		C	N	O	
S1	100/0	74.4	4.4	21.2	0.059
S2	90/10	74.7	4.9	20.4	0.066
S3	80/20	73.8	5.8	20.4	0.079
S4	70/30	71.8	7.5	20.7	0.104

The effect of surfactant composition on the morphological changes of the polyNIPAm microspheres was appraised using SEM. Representative secondary electron (SE) micrographs of oven-dried polyNIPAm microsphere morphologies, as a function of surfactant composition, are presented in Figure 5.6. It was found that Samples S1 and S2 were spherical in shape, whilst samples S3 and S4 were more irregular. The suggestion here is that increased additions of the CTAB surfactant acted to decrease the stability of the monomer droplets during polymerization reaction. This was attributed to the increased interfacial tension between the oil and aqueous phase as the amount of CTAB was increased (Table 5.3). According to Sjoblom (2005) [201], the higher the interfacial tension of two immiscible liquids, the lower the stability of the dispersed droplets,

leading to a higher probability of droplet coalescence. As a result, larger particles are formed due to more frequent droplet coalescence.
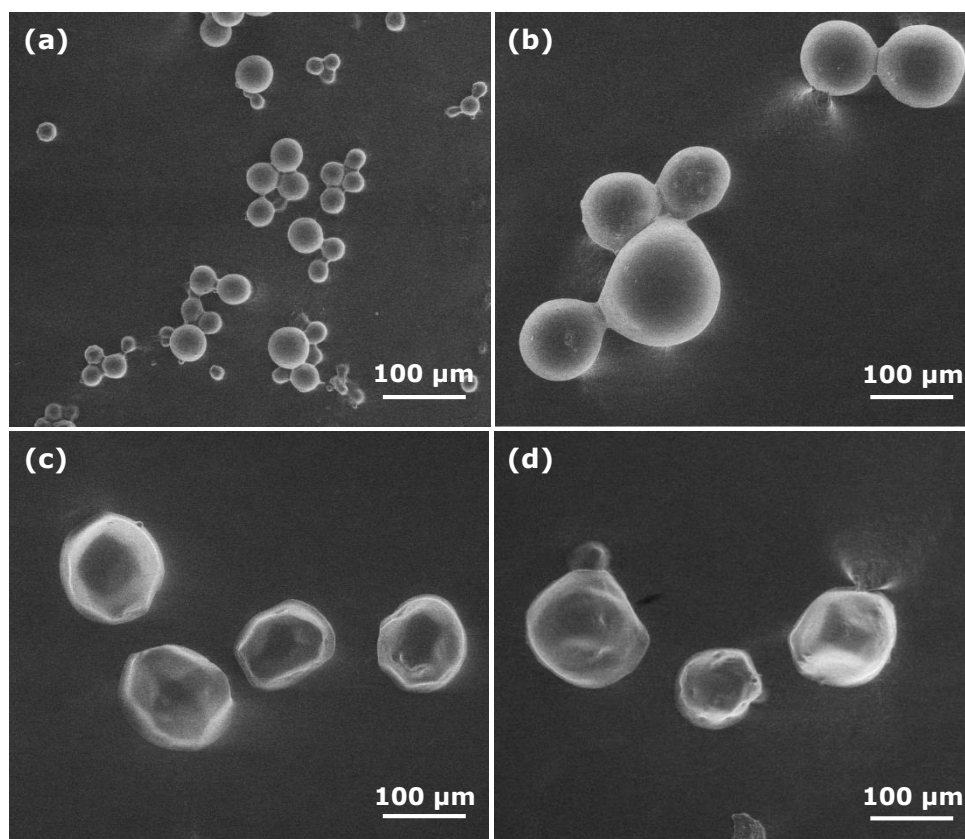
Figure 5.6 *SE micrographs of polyNIPAm microspheres prepared using different Span 80®/CTAB ratios: (a) S1 (100/0); (b) S2 (90/10); (c) S3 (80/20); and (d) S4 (70/30)*

Table 5.3 *Interfacial tension between water and cyclohexane containing different surfactant compositions*

Span 80®/CTAB ratio	Interfacial tension (mN/m)
100/0	6.30 ± 0.03
90/10	6.58 ± 0.13
80/20	7.34 ± 0.12
70/30	9.94 ± 0.23

The SE micrographs were used to determine the mean sizes of the polyNIPAm microspheres (S1–S4), based on ~ 100 different particles in each case, to quantify the effect of surfactant composition (Table 5.4). The polyNIPAm microspheres exhibited mean particle sizes ranging from 54 µm (S1) to 112 µm (S4), with increasing amounts of CTAB addition. According to Shahin *et al.* (2011) [202], emulsion droplet size reduces as the stability of the emulsion increases, being attributable to a decreased probability of droplet coalescence. This indicates that the stability of the NIPAm monomer droplet reduces with increasing amounts of CTAB surfactant. These results are corroborated by the interfacial tension measurement presented in Table 5.3.

Table 5.4 *Effect of surfactant composition on the mean particle size of polyNIPAm microspheres prepared by suspension polymerisation*

Sample	Span 80® / CTAB ratio	Mean particle size (µm)
S1	100/0	54 ± 8
S2	90/10	90 ± 19
S3	80/20	109 ± 19
S4	70/30	112 ± 31

The effect of surfactant composition on the surface charge of the polyNIPAm microspheres is summarized in Table 5.5. In particular, it was found that the zeta potential of the microspheres changed from negative (-29 mV) to positive (+17 mV) values as the amount of the CTAB cationic surfactant was increased up to 30 wt%.

Table 5.5 *Zeta potentials of the polyNIPAm microspheres for different Span 80®/CTAB ratios: (a) S1 (100/0); (b) S2 (90/10); (c) S3 (80/20); and (d) S4 (70/30)*

Sample	Span 80® / CTAB ratio	Zeta potential (mV)
S1	100/0	-28.7 ± 1.3
S2	90/10	-0.8 ± 0.4
S3	80/20	+7.5 ± 0.3
S4	70/30	+17.4 ± 0.5

It is evident that an increase in the amount of CTAB cationic surfactant caused a decrease in the negativity of the microspheres. This effect was attributed to the presence of cationic polar groups in the CTAB molecules adsorbed onto the surface of the negatively charged polyNIPAm microspheres via electrostatic attraction (Figure 5.7). A similar finding was reported by Desai and Dixit [203], stating that the surface charge of a polymer was dependent on the surfactant type. Since Span 80® is a nonionic surfactant with zero net charge, the zeta potential of polyNIPAm without CTAB addition was attributed solely to the effect of negatively charged sulfate end groups from the APS initiator. This is in agreement with a study reported by Lim *et al.* [204], in which the zeta potential of gold nanoparticles changed from negative to positive with increasing additions of CTAB cationic surfactant.
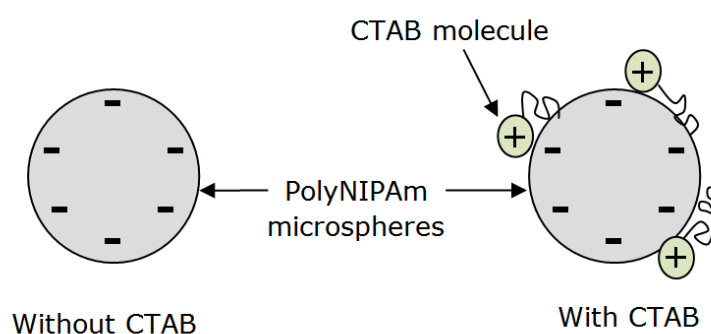
Figure 5.7 *The adsorption of CTAB molecules onto a polyNIPAm microsphere surface via electrostatic attraction*

5.1.2 Cell Attachment to PolyNIPAm Microspheres

HEK cells were seeded on the polyNIPAm microspheres in culture medium at an incubation temperature of 37°C. To study the effect of surface charge on cell attachment, suspensions of the cells and microspheres were monitored using an inverted optical microscope. Figure 5.8 presents optical micrographs of the association of HEK cells with polyNIPAm microspheres on Day 2 and Day 7 of the culturing process, respectively. Unlike the previous samples, as presented in Chapter 4 (Section 4.1.2), significantly more cell attachment to the microspheres prepared in the presence of CTAB was observed.
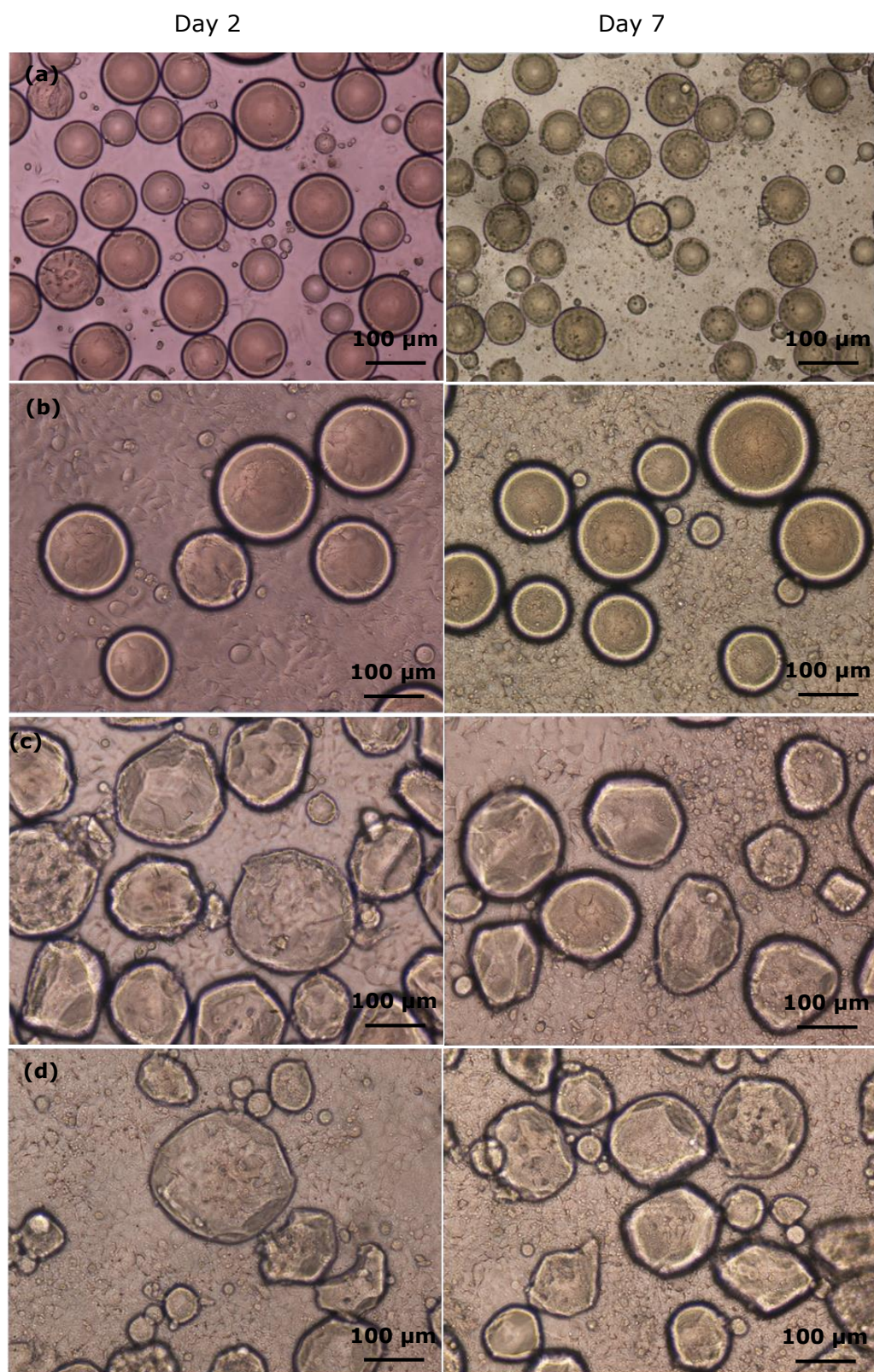
Figure 5.8 *Optical micrographs of HEK cell growth on polyNIPAm microspheres prepared using different Span 80® to CTAB ratios: (a) S1 (100/0); (b) S2 (90/10); (c) S3 (80/20); and (d) S4 (70/30), on Day 2 and Day 7 of the culturing process, respectively*

Sample S1 exhibited the poorest cell attachment, as shown in Figure 5.8 (a), whereby very few cells attached on the surface of the polyNIPAm microspheres. This effect was attributed to electrostatic repulsion between the cells and the high negative surface charge of these microspheres. Intriguingly, Sample S2 showed the best cell attachment (Figure 5.8 (b)), followed by Samples S3 and S4, in apparent contradiction to the suggestion that cell attachment improves continuously with decreasing negative surface charge of the culture substrate – the point being that cells are negatively charged and hence more likely to attach to positively charged surfaces [160]. Chun and co-workers (2004) [205] found that positively charged poly(lactic-co-glycolic acid) (PLGA) microspheres exhibited higher cell attachment as compared to the negatively charged microspheres.

As indicated by the optical micrographs of Figure 5.8, cell attachment did not improve continuously with increasing positive surface charge of the culture substrate in this study. It is considered that an increase in surface hydrophilicity of the microsphere was responsible for the reduced cell attachment found in Samples S3 and S4. Poncin-Epaillard *et al.* [206] suggested that cells are more likely to attach to hydrophobic culture substrates. Accordingly, cell attachment reduces as the hydrophilicity of the substrate increases, being attributable to increased hydrogen bonding between water molecules and the substrate surface which acts to inhibit interaction between cells and the substrate.

To investigate the effect of surfactant composition on the surface hydrophilicity of the polyNIPAm microspheres, the contact angles of water drops on the samples were measured using a goniometer. Table 5.6 presents contact angle measurement data for the microspheres. A gradual decrease in contact angle with increasing CTAB content was observed. According to Yuan and Lee [207], a contact angle < 90° means a hydrophilic surface whilst a contact angle > 90° means a hydrophobic surface. In other words, the higher the contact angle, the greater the material hydrophobicity. This suggests that the hydrophilicity of the polyNIPAm microspheres increased with increasing CTAB content. A similar finding was reported by Bink and Rodrigues [208], where the contact angle of water drops on silica reduced from 150° to 80° upon CTAB adsorption.

Wei *et al.* [209] reported that the optimal contact angles for fibroblast cell adhesion were between 60° and 80°. Although the contact angle of Sample S1 falls into this desired range, the sample exhibited relatively less cell attachment, because the negative surface charge of Sample S1. On the other hand, Samples S3 and S4 were more hydrophilic as compared to Sample S2. As a result, Sample S3 and S4 exhibited less cell attachment, even though the surface charge of these two samples was more positive as compared to Sample S2. This is in agreement with the study conducted by Vogler [109], that more hydrophilic surfaces with contact angle < 65° hindered the attachment of Madin-Darby Canine Kidney (MDCK) cells, consistent with argument that cell attachment is influenced by the surface hydrophilicity of the microspheres.

Table 5.6 Contact angle measurement data for the microspheres prepared using varying Span 80®/CTAB surfactant compositions

Sample	Span 80®/CTAB ratio	Contact angle (°)
S1	100/0	80.3 ± 0.2
S2	90/10	74.1 ± 0.8
S3	80/20	59.6 ± 0.3
S4	70/30	42.2 ± 0.5

Figure 5.9 presents representative SE micrographs of all the polyNIPAm microspheres prepared using different Span 80®/CTAB ratios on Day 7 of the culturing process. Sample S1 exhibited least cell attachment whilst Sample S2 showed most cell attachment, being consistent with the optical micrographs of Figure 5.8. This result is also corroborated by the measurement of viable cell density, as presented in Figure 5.10. The highest number of viable cells was found for Sample S2, whilst the least number of viable cells was found for Sample S1.
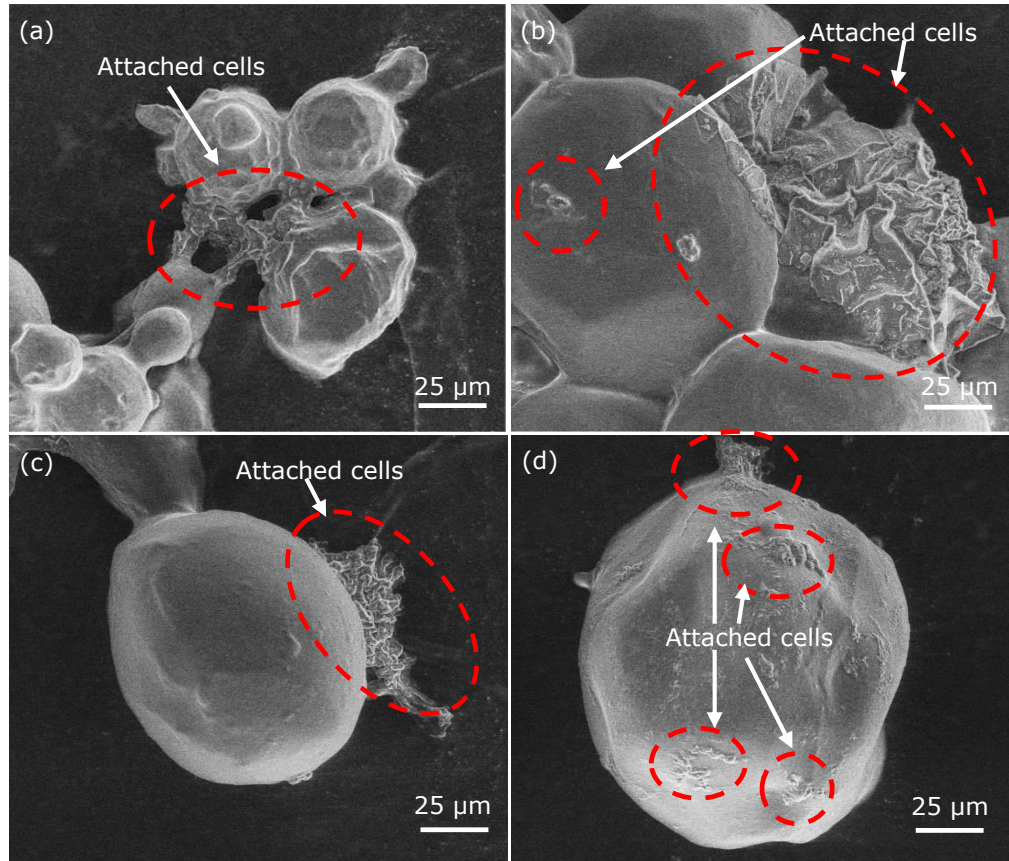
Figure 5.9 *SE micrographs of polyNIPAm microspheres, for different Span 80®/CTAB ratios, attached with HEK cells: (a) S1 (100/0); (b) S2 (90/10); (c) S3 (80/20); and (d) S4 (70/30), on Day 7 of the culturing process*

Cell counting was performed to appraise cell proliferation on the polyNIPAm microspheres. Figure 5.10 presents a summary of viable cell density as a function of culture time for HEK cells on the four polyNIPAm microsphere samples (S1-S4), as determined using Eq. 3.8. It was found that the viable cell density in all four samples increased with increasing culturing time, demonstrating that all the samples were compatible with cells [210]. However, Sample S1 was associated with the lowest number of viable cells, whilst Sample S2 was associated with the highest number of viable cells.
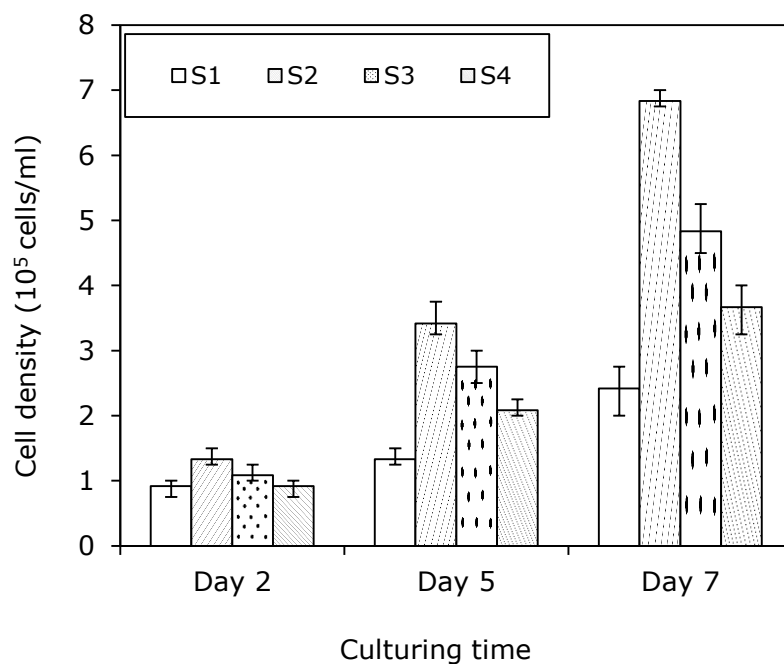
Figure 5.10 *HEK cell density on polyNIPAm microspheres prepared in the presence of different Span 80® to CTAB ratios: (a) S1 (100/0); (b) S2 (90/10); (c) S3 (80/20); and (d) S4 (70/30), on Days 2, 5 and 7 of the culturing process, respectively*

5.1.3 Cell Detachment from the PolyNIPAm Microspheres

To evaluate the capability for cell detachment from the polyNIPAm microspheres without the use of trypsin, suspensions of the cultured microspheres (S1-S4) were incubated at 20°C for 2 h. Optical micrographs showed detachment of the cells following low temperature incubation (Figure 5.11).
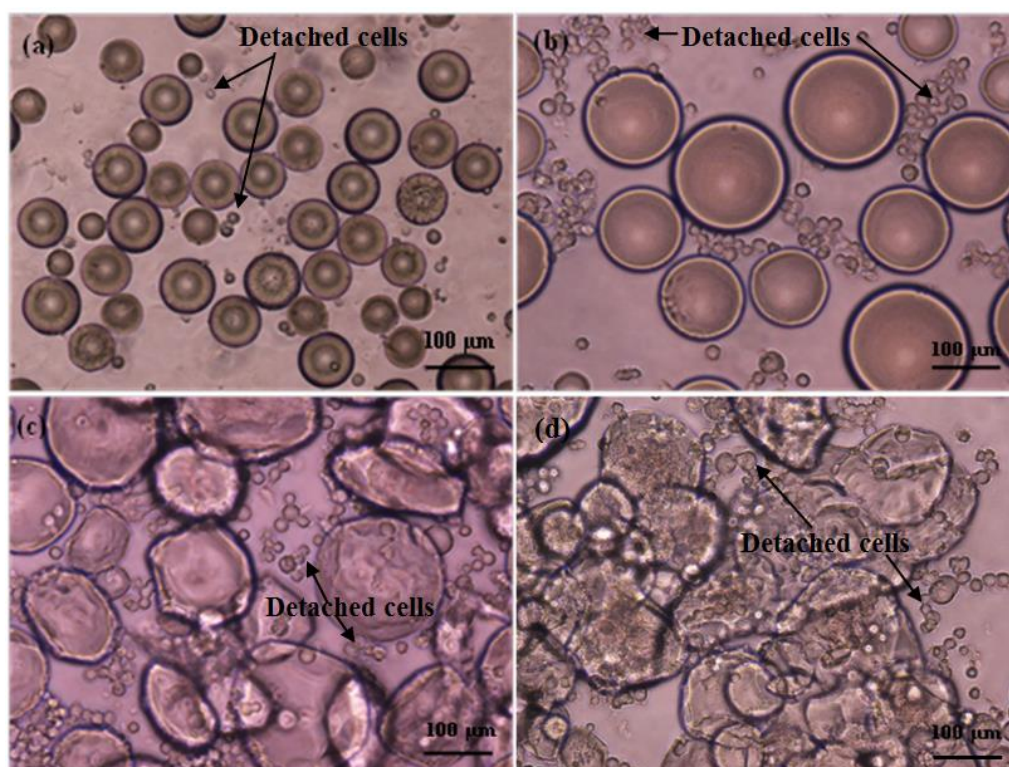
Figure 5.11 *Optical micrographs of detached HEK cells from the polyNIPAm microspheres prepared using different Span 80®/CTAB ratios: (a) S1 (100/0); (b) S2 (90/10); (c) S3 (80/20); and (d) S4 (70/30), on Day 7 of culturing, after incubation at 20°C for 2 h*

It is evident that the detached cells were all round in shape, being distinct from the spread cells of Figure 5.8. This suggests that the harvestment of cells can be done without using trypsin, as the HEK cells detached automatically from the polyNIPAm microspheres (S1-S4) by simply reducing the culturing temperature from 37°C to 20°C. This effect was attributed to a change in hydrophilicity of polyNIPAm as a function of temperature. According to Schild and Tirrel [211], polyNIPAm exhibits a reversible phase transition from globular to coil structure as the temperature is reduced below its LCST (32°C), *i.e.* when the polymer becomes hydrophilic and its chains become more extended. Conversely, polyNIPAm is relatively hydrophobic with a globular, packed conformation at temperatures above the LCST, as depicted by Figure 5.12. In other words, polyNIPAm undergoes a reversible change from a hydrophobic to a hydrophilic state when the temperature is reduced below the LCST, being mediated by hydrogen bonding between water molecules and amide groups as a function of temperature [212]. Indeed, Okano *et al.* [11] reported that culture substrates with hydrophilic surfaces inhibited cell

attachment due to the presence of hydrogen bonds between the polymer chains and water molecules, which acted to reduce the interaction between cells and the culture substrate surface. As surface hydrophilicity increases, cell shape changes from elongated to round, while cell metabolism reduces, leading to cell detachment from the culture substrate (Figure 5.11). Similar findings were reported by Cooperstein and Canavan [213], in which confluent Madin-Darby canine kidney (MDCK) cell sheet detached from tissue culture polystyrene (TCPS) dish grafted with polyNIPAm when the working temperature was reduced to 20°C.
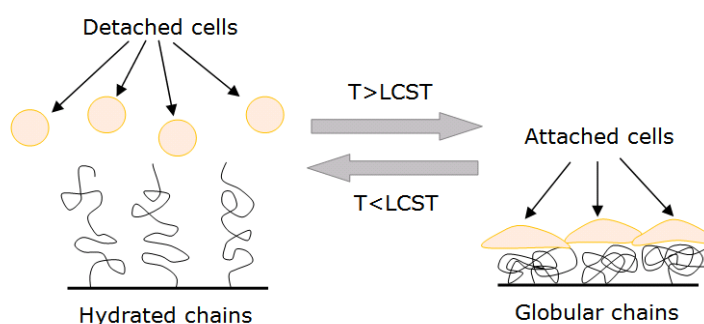
Figure 5.12 Cell behavior relatives to the phase change of polyNIPAm below and above the LCST

5.2 Summary

PolyNIPAm microspheres having various surface charges were synthesised successfully via free radical suspension polymerisation. The addition of a CTAB cationic surfactant was found to reduce the high negative surface charge of the microspheres. However, it was found that HEK cells attachment to the polyNIPAm microspheres was influenced not only by the surface charge but also by the hydrophilicity of the microspheres. On the basis of the data presented, Sample S2 (90% Span 80® and 10% CTAB) exhibited the greatest potential to be used as an alternative material for non-invasive microcarrier cell culture. However, the cell yields obtained in the present study was not as good as those for commercial microcarriers products on the market. Hence, further modification of the polyNIPAm microspheres via copolymerisation with a hydrophobic comonomer, was investigated, as described in the following Chapter.

CHAPTER 6

Modification of surface hydrophobicity for enhanced cell attachment

6.0 Introduction

The polyNIPAm microspheres prepared in Chapter 5 demonstrated cell attachment and showed good potential for use as an alternative microcarrier for anchorage dependent cell culture. However, further improvement of cell yield is necessary in order to be competitive with the commercial microcarriers available on the market. As outlined in Chapter 2, cellular attachment increases with increasing protein adsorption due to the interactions between the hydrophobic portions of the adsorbed proteins and the substrate surface [103,104]. In the present study, butyl methacrylate (BMA) was used as a comonomer to adjust the surface hydrophobicity of the polyNIPAm microspheres. BMA was chosen for the present study because of the presence of two methyl groups ($-CH_3$) per molecule, which promotes more hydrophobic interactions for better cell attachment. Poly(*N*-isopropyl acrylamide – *co* – butyl methacrylate) microspheres containing different compositions were synthesized via free radical suspension polymerisation (Table 6.1). The objective of this part of the study was to investigate the effect of BMA content on the physical and thermal properties of the microspheres. The chemical bonds present in the microspheres were appraised by Fourier transform infrared (FTIR) spectrometry analysis, whilst the thermal stabilities of the microspheres were evaluated by thermogravimetric analyses (TGA). The phase transition temperatures of the microspheres were appraised using differential scanning calorimetry (DSC). The morphologies of the microspheres were observed using scanning electron microscopy. Protein adsorption onto the microspheres was appraised using EDX. Additionally, the effect of surface hydrophobicity on HEK cell attachment was appraised using contact angle measurement, whilst cell growth as a function of culturing time was assessed using the Trypan blue exclusion method.

Table 6.1 *Quantities used in the synthesis of polyNIPAm microspheres*

Sample code	Quantity in 10 ml ultrapure water (g)					Quantity in 100 ml cyclohexane (g)	
	NIPAm	BMA	MBAm	APS	TEMED	Span 80®	CTAB
M1	0.9	0.1	0.15	0.1	0.1	1.8	0.2
M2	0.8	0.2	0.15	0.1	0.1	1.8	0.2
M3	0.7	0.3	0.15	0.1	0.1	1.8	0.2
M4	0.6	0.4	0.15	0.1	0.1	1.8	0.2

Since the polyNIPAm microspheres with positively charged surface did not exhibit significant improvement on cell attachment (Chapter 5, Section 5.1.2), another factor, *i.e.* surface hydrophobicity of the material, was studied. This section demonstrates again that surface hydrophobicity plays an important role in cell adhesion and proliferation. To investigate the effect of BMA comonomer on the properties of polyNIPAm microspheres, the samples were characterised using FTIR, TGA, DSC, contact angle measurement, zeta potential measurement and SEM. Then HEK cell seeding on the four sample set was performed for seven days. Characterisation of the surface chemistry of the samples was important to interpret the cell culture results. An appraisal of the cell response to the microspheres, as a function of BMA comonomer content, was performed using optical microscopy and SEM.

6.1 Results and discussion

6.1.1 Effect of BMA Comonomer Content

6.1.1.1 Chemical Bonding

FTIR analysis was performed to appraise the copolymer composition of the samples. Figure 6.1 presents FTIR spectra of the copolymers containing different amounts of BMA.
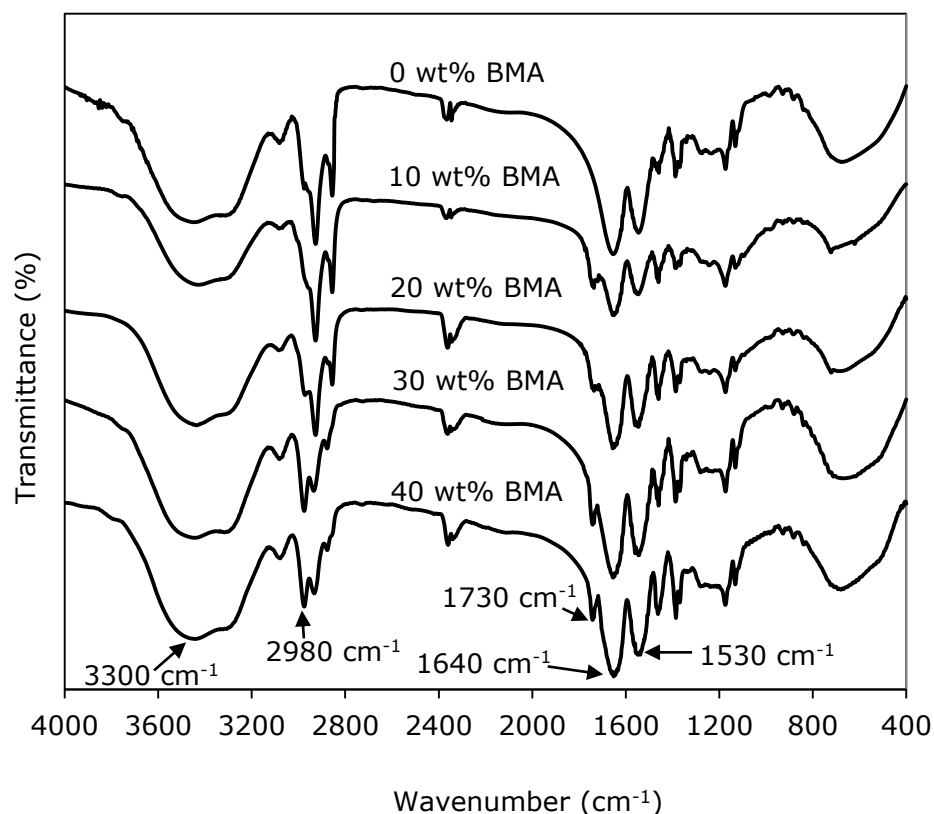
Figure 6.1 *FTIR spectra of poly(NIPAm-co-BMA) microspheres containing different amounts of BMA*

Similar to the FTIR spectra of the polyNIPAm samples presented (Chapter 5, Section 5.1.1), a characteristic doublet at 1530 cm^{-1} and 1640 cm^{-1} (Figure 6.1, arrowed), attributable to N-H bending of the secondary amide group and carbonyl (C=O) stretching of the primary amide group from polyNIPAm [214], was found in each sample. Moreover, all the copolymer samples exhibited a broad peak around 3300 cm^{-1}, assigned to N-H stretching of the amide group [190]. However, there were several differences in the FTIR spectra between the samples containing different amounts of BMA. The distinguishing feature of the poly(NIPAm-*co*-BMA) samples was the appearance of a new peak at 1730 cm^{-1}, characteristic of methacrylates due to C=O stretching of the ester group (-COOCH$_3$). It was found that the intensity of this peak increased slightly with increasing BMA content. This is in agreement with the findings reported by Akiva and Margel [215] and Bakhshi *et al.* [216]. Additionally, the peak intensity at 2980 cm^{-1}, attributable to the asymmetric stretching of methyl group (-CH$_3$) [217], was found to increase with increasing BMA content. This

123

confirms that the copolymerisation of NIPAm and BMA was successful. Figure 6.2 presents the synthesis route for the copolymerisation of NIPAm and BMA.
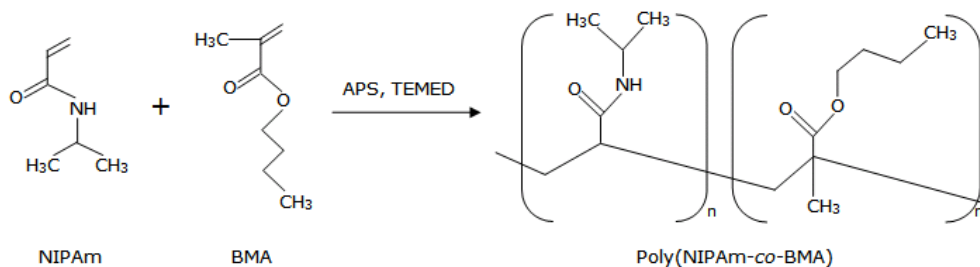
Figure 6.2 *Synthesis route for the copolymerisation of NIPAm and BMA*

6.1.1.2 Thermal Stability

The thermal stability of the poly(NIPAm-*co*-BMA) samples was appraised by TGA from 25 to 500°C at a heating rate of 5°C/min under an inert N_2 atmospheres. Figure 6.3 shows the TGA thermograms of the samples containing varying amounts of BMA. It was found that all samples exhibited a three-step thermal decomposition process. The first decomposition slope appeared at temperature between 30°C and 125°C, with minor weight loss of about 10%, being attributable to evaporation of moisture from the samples [191].

The second decomposition feature was associated with a weight loss of ~ 20%. It was found that the onset of the second decomposition temperature of the copolymers varied from 290 to 320°C, depending on the BMA comonomer content. This second thermal decomposition process was attributed to the breakdown of C-C and C-H bonds in the copolymer, forming carbon dioxide (CO_2) gas and water vapour. This is in agreement with the finding reported by Trivedi *et al.* [218], from a study of a copolymer of polyBMA and guar gum.

The third decomposition feature occurred at ~ 380°C, being attributable to side chain decomposition or random chain scission in the backbone. It was found that the onset of the second and third decomposition features shifted to lower temperatures as the BMA comonomer content increased. This suggests that the addition of BMA comonomer reduced the thermal

124

stability of the polyNIPAm samples. A similar weight of residue upon heating up to 500°C was found in all the samples, *i.e.* ~ 5%. According to the TGA data reported by Ozlem and Hacaloglu [219] , the onset decomposition temperature for polyBMA is ~ 380°C. This is consistent with the findings reported by Choi and Chung [220], whereby the onset temperature of decomposition for butyl methacrylate copolymer appeared between 358 and 450°C.
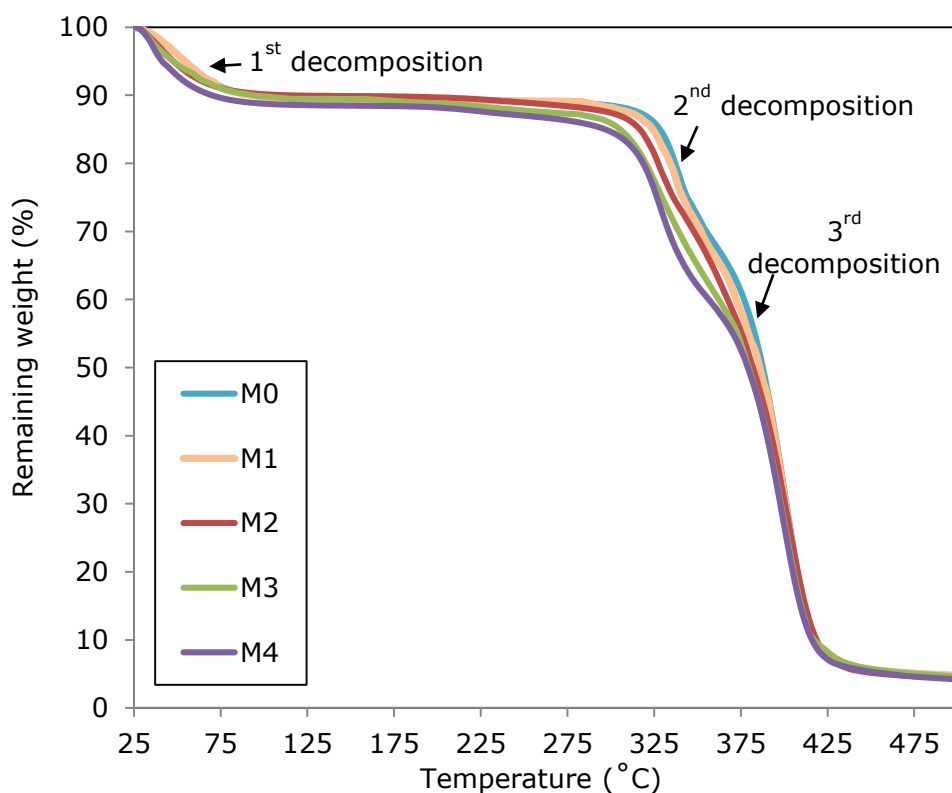
Figure 6.3 *TGA thermograms of poly(NIPAm-co-BMA) microspheres prepared using varying BMA comonomer content: M1 (10 wt% BMA); M2 (20 wt% BMA); M3 (30 wt% BMA); and M4 (40 wt% BMA)*

6.1.1.3 LCST

To study the effect of BMA comonomer content on the transition temperature of these copolymer microspheres, the microspheres were heated from 15 to 60°C at scanning rate of 5°C/min under inert N_2 atmospheres. DSC thermograms of the PNIPAm microspheres prepared from different BMA comonomer content are presented in Figure 6.4.
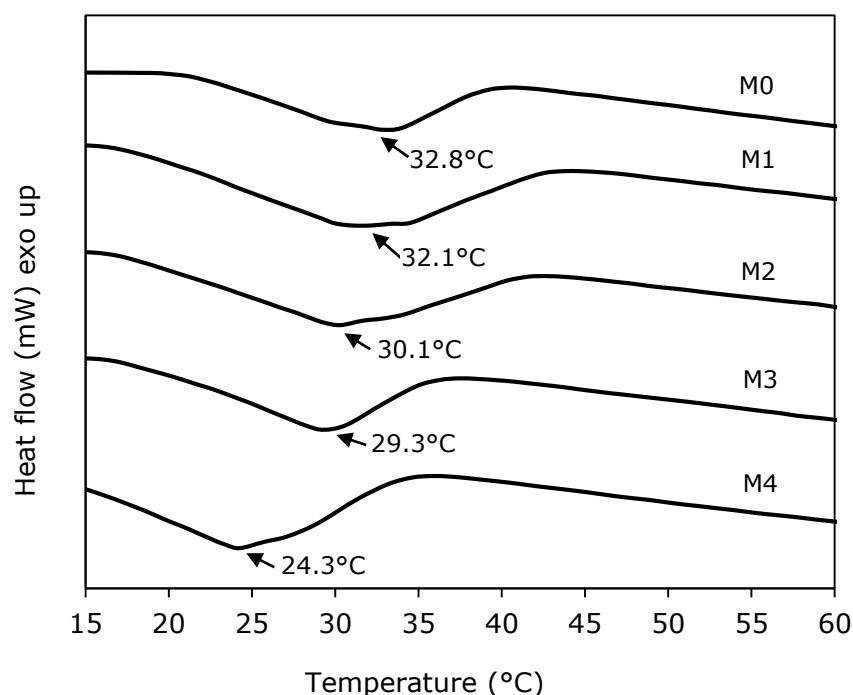
Figure 6.4 *DSC thermograms of poly(NIPAm-co-BMA) microspheres prepared using varying BMA comonomer content: M1 (10 wt% BMA); M2 (20 wt% BMA); BM (30 wt% BMA); and BM (40 wt% BMA)*

The endothermic peaks of the DSC curves for Samples M1-M4 (Figure 6.4), which corresponds to the lower critical solution temperature (LCST) of the PNIPAm microspheres, shifted to lower temperature as the hydrophobic BMA comonomer increased. Sample B1 containing 10 wt% BMA exhibited a LCST of 32.1°C whilst the LCST of Sample B4 containing 40 wt% BMA was 24.3°C. This effect was attributed to an increase in the number of hydrophobic isopropyl ($-CH(CH_3)_2$) groups, facilitating dehydration of the polymer chains when the temperature was raised above the LCST. The copolymerisation of NIPAm with the hydrophobic BMA

monomer resulted in an increase in hydrophobicity of the copolymer due to increased intra- and intermolecular hydrophobic interactions between the isopropyl groups. As a result, the release of water molecules from the copolymer was promoted upon increasing the temperature across the LCST [171]. A similar finding was reported by Chung *et al.* [221], based on a study of polymethacrylic acid stearyl ester and polyNIPAm copolymer, in which the incorporation of hydrophobic comonomer reduced the phase transition temperature of the copolymer. With increasing hydrophobic comonomer content, the copolymer associates to form more stable globular structure, isolating hydrophobic segments from aqueous solution as much as possible by intra- and intermolecular hydrophobic aggregation. Consequently, the dehydration of the copolymer chains is accelerated.

6.1.1.4 Surface Hydrophobicity

To investigate the change in surface hydrophobicity of the microspheres with varying BMA comonomer content, water contact angle measurements were performed. Table 6.2 presents contact angle data for the microspheres containing different amounts of BMA. An increase of $\sim$ 8% in contact angle was observed when the BMA comonomer content was increased from 10 to 20 wt%. Further increase of BMA content up to 40 wt% resulted in a greater contact angle, *i.e.* 122°. A hydrophobic surface exhibits a contact angle > 90° [207]. This indicates that the incorporation of BMA comonomer increased the surface hydrophobicity of the polyNIPAm microspheres, being attributable to an increase in the number of hydrophobic isopropyl ($-CH(CH_3)_2$) groups. As the number of isopropyl ($-CH(CH_3)_2$) groups present in a material increases, the extent of hydrogen bonding between water molecules and the material's surface reduces, resulting in greater contact angle [222]. This is in agreement with the study reported by Zobrist *et al.* [223], stating that the incorporation of hydrophobic *ter*-butylacrylate monomer to titanium surface increased the contact angle of titanium surface. The result was corroborated by the DSC data presented above.

Table 6.2 *Contact angles of poly(NIPAm-co-BMA) microspheres prepared using varying BMA comonomer content: M1 (10 wt% BMA); M2 (20 wt% BMA); M3 (30 wt% BMA); and M4 (40 wt% BMA)*

Sample code	Contact angle (°)
M1	89.6 ± 0.9
M2	96.5 ± 1.1
M3	103.3 ± 0.9
M4	122.0 ± 2.9

6.1.1.5 Surface Charge

The effect of BMA content on the surface charge of the microspheres was appraised by zeta potential measurements, as summarised in Table 6.3. It was found that all four samples exhibited a similar value for zeta potential, *i.e.* between -0.65 and -0.55 mV. This suggested that the surface charge of the poly(NIPAm-*co*-BMA) microspheres remained effectively unchanged, irrespective of the amount of BMA added. This is because the BMA comonomer is nonionic, possessing neutral charge [224], which is why it did not affect the surface charge of the microspheres.

Table 6.3 *Zeta potentials of poly(NIPAm-co-BMA) microspheres prepared using varying BMA comonomer content: M0 (0 wt% BMA), M1 (10 wt% BMA); M2 (20 wt% BMA); M3 (30 wt% BMA); and M4 (40 wt% BMA)*

Sample code	Zeta potential (mV)
M0	-0.80 ± 0.40
M1	-0.59 ± 0.11
M2	-0.55 ± 0.46
M3	-0.59 ± 0.17
M4	-0.65 ± 0.65

6.1.1.6 Microsphere Morphology

The microstructures of the microspheres containing varying amounts of BMA were compared using SEM with low vacuum mode. Figure 6.5 shows SE micrographs of the respective copolymer microspheres. As distinct from the samples reported on Chapter 5 (Section 5.1.1), all four sets of copolymer microspheres exhibited slightly irregular shapes with concave surfaces. This effect was attributed to uneven shrinkage of the polymer chains upon removal of water molecules during the drying process. According to Mujumdar and Devahastin [225], water molecules are removed from a polymer surface through evaporation, and hence polymer chain shrinkage occurs when water molecules evaporate during an oven drying process. When the poly(NIPAm-*co*-BMA) microspheres were immersed in aqueous solution, the polyNIPAm chains tended to absorb water via hydrogen bonding between the amide end groups and water molecules, leading to the recovery of a more rounded, spherical structure (Figure 6.7). Accordingly, when these hydrated copolymer microspheres were oven dried, adsorbed water was removed mainly from the polyNIPAm chains, having a greater effect on the shrinkage of the microspheres as compared to the polyBMA chains.
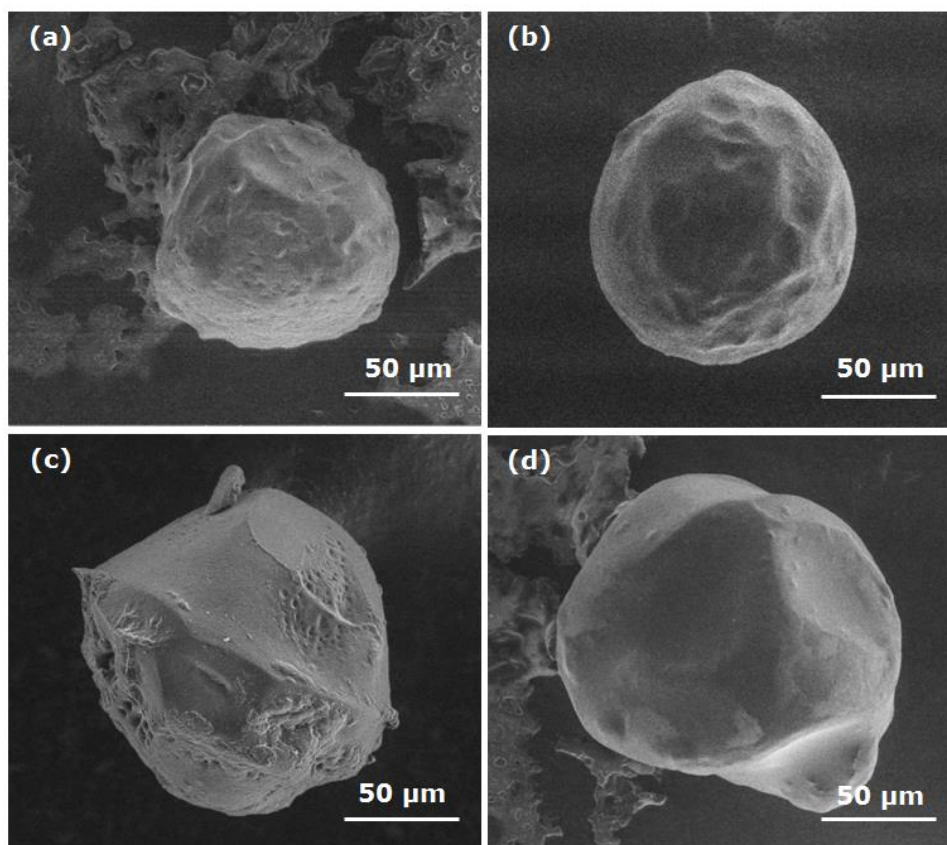
Figure 6.5 *SE micrographs of the poly(NIPAm-co-BMA) microspheres prepared using varying BMA comonomer content: (a) M1 (10 wt% BMA); (b) M2 (20 wt% BMA); (c) M3 (30 wt% BMA); and (d) M4 (40 wt% BMA)*

Additionally, it was found that the mean particle size (n = 100) of the copolymer increased slightly from 123 to 164 µm as the BMA content was increased up to 40 wt% (Table 6.4). With increasing amount of hydrophobic BMA, the number of the primary polymer particles formed during the homogeneous nucleation process reduced due to poor solubility of the BMA comonomer in water. As a result, the polymer particle size increased. Conversely, Ou *et al.* [226] reported that the particle size of polystyrene decreased upon the addition of hydrophilic vinyl acetate, being attributable to the increased concentration of hydrophobic comonomer in the aqueous phase, which subsequently led to an increase in the number of primary particles formed at the early stage of polymerisation. Similar findings were documented by Musyanovych *et al.* [227] and Dong *et al.* [228], from studies of the polymerisation of styrene with hydrophilic 2-aminoethyl methacrylate hydrochloride and acrylic acid, respectively. According to their findings, smaller polystyrene particles were obtained at

higher hydrophilic comonomer concentrations which promoted nuclei formation at the early stages of polymerisation.

Table 6.4 *Mean particle size of the poly(NIPAm-co-BMA) microspheres prepared using varying BMA comonomer content: M1 (10 wt% BMA); M2 (20 wt% BMA); M3 (30 wt% BMA); and M4 (40 wt% BMA)*

Sample code	Mean particle size (µm)
M1	123 ± 31
M2	124 ± 31
M3	148 ± 49
M4	164 ± 47

6.1.1.7 Protein Adsorption Determination

In order to appraise the amount of protein adsorbed as a function of BMA content, the microspheres were immersed in culture media for 24 h prior to the elemental analysis using EDX. The main focus for this part of study was to compare the amount of nitrogen (N) and sulphur (S) across the samples, as a function of BMA comonomer content. This is because the presence of N associated with the copolymers originates from proteins, being polypeptides formed from various amino acids ($-NH_3$), as depicted by Figure 6.6, whilst the presence of S is attributable to proteins containing thiol groups (S-H) or bound disulfides (S-S) [229].
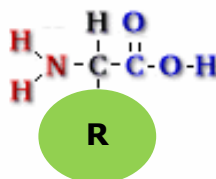
Figure 6.6 *Example of protein molecular structure*

Following soaking in culture media, N and S were detected by EDX in all four poly(NIPAm-*co*-BMA) microsphere sample sets, showing that the microspheres were covered by protein layer. Table 6.5 presents the elemental compositions of the poly(NIPAm-*co*-BMA) samples obtained from EDX analyses.

Table 6.5 *Elemental compositions of poly(NIPAm-co-BMA) samples*

Sample Code	Atomic %				N/C ratio	S/C ratio
	C	**O**	**N**	**S**		
M0	74.40	21.20	4.40	0	0.05914	0
M1	69.78	22.32	7.84	0.06	0.11230	0.00084
M2	68.34	21.76	9.82	0.08	0.14371	0.00112
M3	66.92	17.73	15.26	0.09	0.22806	0.00134
M4	63.89	26.78	9.26	0.07	0.14494	0.00110

In order to ascertain if there were any differences in amounts of N and S present in these samples, elemental ratios for N/C and S/C were determined since C is the most abundant element present in the copolymers [230]. Figure 6.7 presents the variation of N/C and S/C ratios as a function of BMA comonomer content.
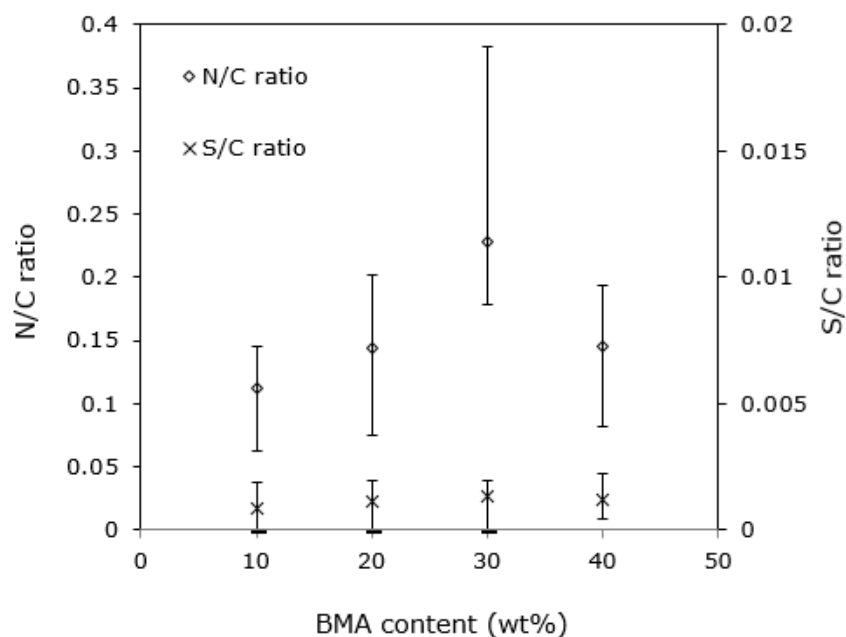
Figure 6.7 *Variation of N/C and S/C ratios as a function of BMA comonomer content*

The average ratios of N/C and S/C were computed from five measurements in each sample. In Figure 6.7, the lowest N/C ratio was found in Sample M1. As expected, the N/C ratio increased with increasing BMA content up to 30 wt%. This effect indicates that the amount of protein adsorbed onto the microsphere surface increased gradually with the addition of BMA content from 10 wt% to 30 wt%. This is in agreement with studies of Tengvall *et al.* [231] and Gessner *et al.* [232], that proteins were more firmly bound to hydrophobic surfaces containing CH_3 groups. Nevertheless, further addition of 40 wt% BMA comonomer resulted in ~ 36% drop of the N/C ratio. The decrease in N/C ratio suggests that relatively lower amount of protein adsorbed onto Sample M4 as compared to Sample M3. Similar trend was observed for S/C ratios of the samples. However, the change in S/C ratios was insignificant, presumably due to the low concentration of thiol groups (S-H) present in the proteins.

6.1.2 Cell Attachment

HEK cell seeding on the copolymer microspheres was performed to appraise cellular response, as a function of increasing amounts of BMA. The cultured cells were monitored periodically using optical microscopy. Cell attachment to the copolymer microspheres on Day 2 and Day 7 of the culturing process are compared in Figure 6.8. It was found that almost no cells attached to Samples M1 and M2, whilst only a few cells found on the surfaces of Sample M3 and M4 on Day 2 of culturing. However, significantly more cells were observed in all four samples on Day 7 of culturing. Maximal cell attachment was found for Sample M3, whilst minimal cell attachment was found for Sample M1.
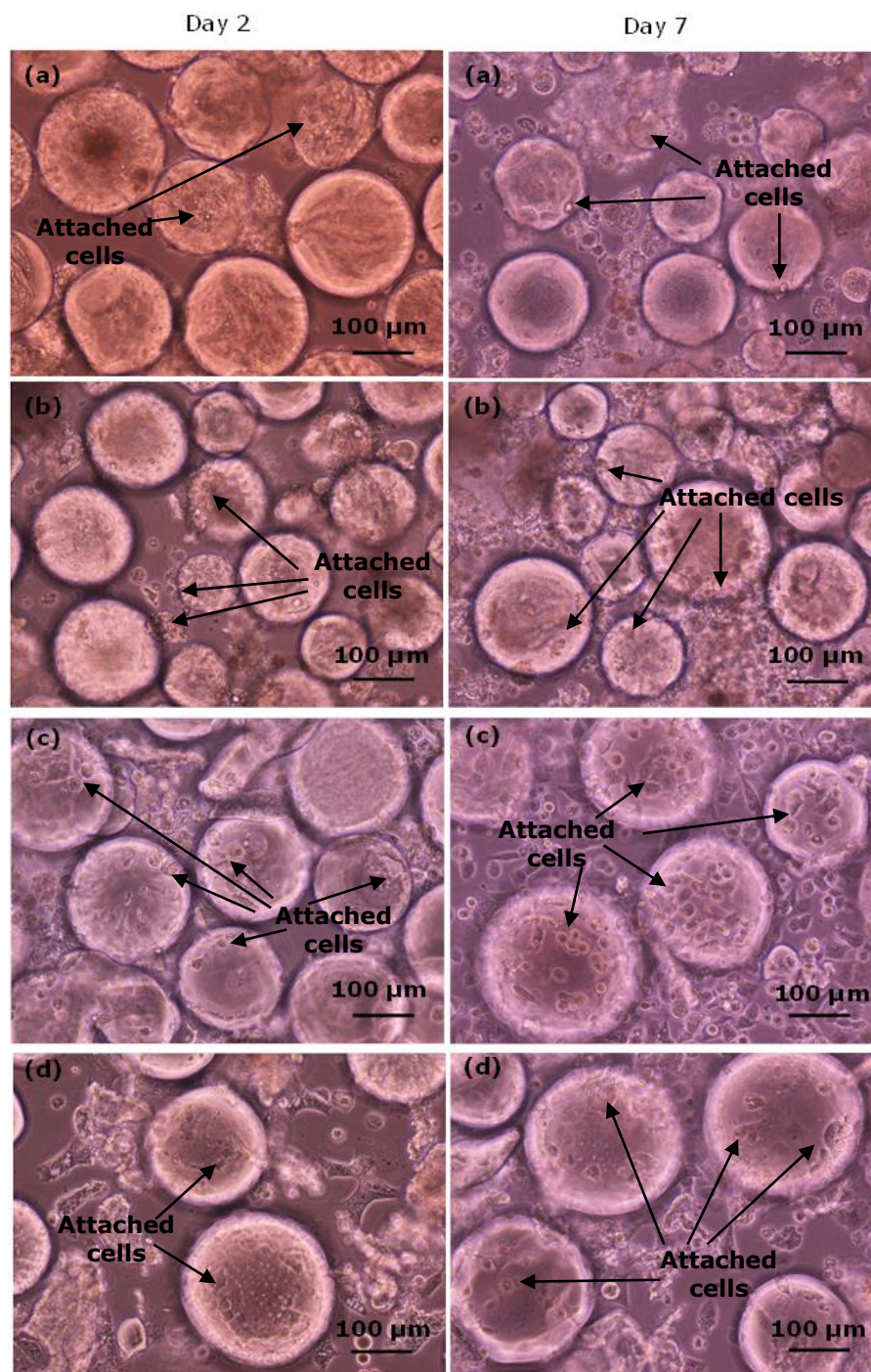
Figure 6.8 *Optical micrographs of HEK cell growth on polyNIPAm microspheres prepared using varying amounts of BMA comonomer: (a) M1 (10 wt% BMA); (b) M2 (20 wt% BMA); (c) M3 (30 wt% BMA); and (d) M4 (40 wt% BMA), on Day 2 and Day 7 of the culturing process, respectively*

To examine the cell attachment to the microspheres more carefully, SEM was employed. The SE micrographs of Figure 6.9 show the cell morphologies on the microspheres after cell fixing and drying processes, with attached cells being highlighted in red circles.
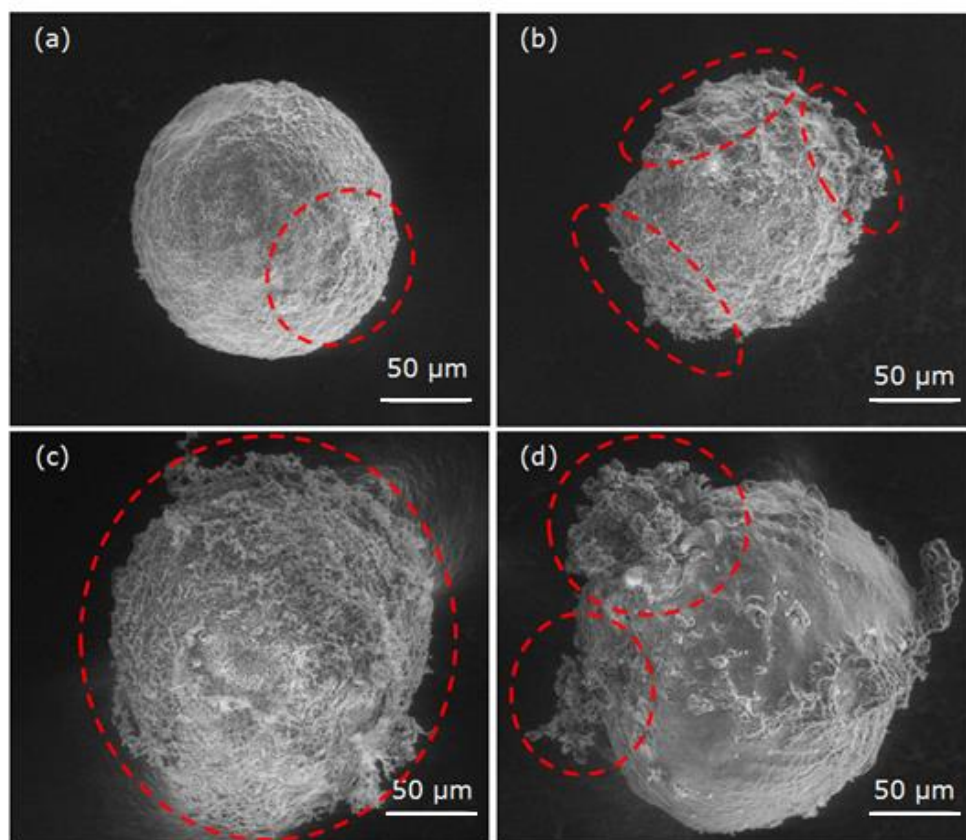
Figure 6.9 SE micrographs of HEK cells attached to poly(NIPAm-co-BMA) microspheres: (a) M1 (10 wt% BMA); (b) M2 (20 wt% BMA); (c) M3 (30 wt% BMA); and (d) M4 (40 wt% BMA), on Day 2 and Day 7 of the culturing process, respectively

It was found that Sample M1 exhibited minimal cell attachment, whilst Sample M3 exhibited maximal cell attachment, with entire microspheres being almost covered by cell layers. This was consistent with the optical microscopy observations shown in Figure 6.8. The number of cells attached to the microspheres increased significantly as the BMA comonomer content increased from 10 wt% to 30 wt%. This effect was attributed to increased surface hydrophobicity of the microspheres. As

mentioned previously, surface hydrophobicity of the microspheres increased with increasing BMA comonomer content due to the additional –CH_3 groups present in BMA. This is in agreement with the finding reported by Allen *et al.* (2003) [233], in which the addition of hydrophobic *N-ter-*butylacrylamide comonomer to a polyNIPAm film resulted in greater attachment and growth of human epithelial adenocarcinoma (HeLa) cells, attributed to the more hydrophobic surface as compared to the homopolymer film. According to Alsteens *et al.* [234], carbohydrates on cell surfaces bind to hydrophobic surfaces via hydrophobic interaction with protein molecules. A similar finding was reported by Dague *et al.* [235], stating that hydrophobic forces play an important role in cell attachment. The mechanism of cell attachment to hydrophobic and hydrophilic surfaces is depicted by Figure 6.10. The interaction between cells and substrate is mediated by extracellular proteins, which are responsible for the regulation of cell adhesion, propagation and growth [236]. It is established that protein molecules tend to adsorb to hydrophobic surface through hydrophobic interaction. Conversely, on hydrophilic surfaces, water molecules are competitive in interacting with hydrophilic surfaces via hydrogen bonding. As a result, protein adsorption to hydrophilic surface becomes hindered by adsorbed water molecules on the hydrophilic surface [237, 238]. Accordingly, cells in a biological system are more likely to adhere to substrates containing protein molecules.
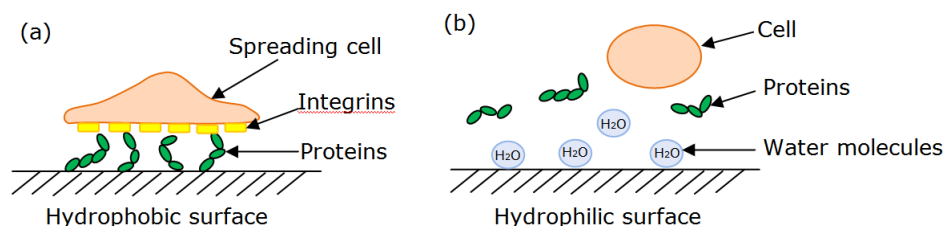
Figure 6.10 *Depiction of cell attachment to: (a) hydrophobic; and (b) hydrophilic surfaces*

Surprisingly, further increase of BMA content up to 40 wt% resulted in relatively poor cell attachment as compared to Sample M3 with 30 wt% BMA. This was probably because the surface of Sample M4 was too hydrophobic for the HEK cells to attach onto. According to Wei *et al.* [209], optimal fibroblast cell attachment occurs on surfaces with contact angles between 60° and 80°. This suggests that optimal contact angles vary with cell type. In the present study, it is concluded that Sample M3 exhibiting a contact angle of 103° showed the best attachment of HEK cells.

To study the effect of surface hydrophobicity on cell growth, the number of viable cells produced on each sample was counted for differing periods of the culturing process. HEK cell growth as a function of time is summarized in Figure 6.11. A monotonic increase in viable cell density with increasing culturing time was observed. When comparing the four samples, Sample M3 exhibited the greatest cell growth, followed by Samples M4, M2 and M1, being consistent with the direct observations of cell attachment to the microspheres, as shown in Figure 6.8.
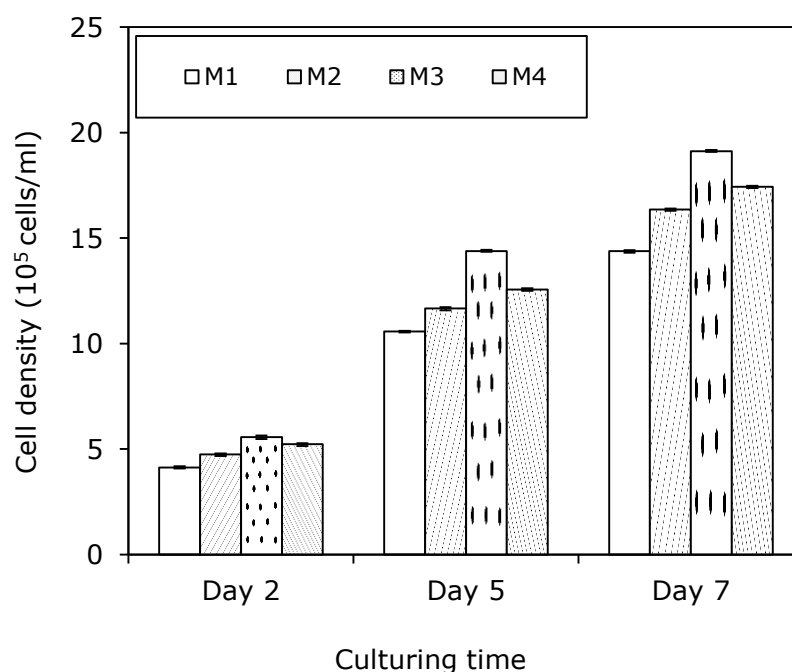
Figure 6.11 *HEK cell growth on poly(NIPAm-co-BMA) microspheres prepared using different amounts of BMA comonomer: (a) M1 (10 wt%); (b) M2 (20 wt%); (c) M3 (30 wt%); and (d) M4 (40 wt%), on Days 2, 5 and 7 of the culturing process, respectively*

6.1.3 Cell Detachment

To investigate the effect of hydrophobic comonomer content on cell detachment, temperature-induced detachment of the confluent cells was performed on Day 7 of culturing. Representative optical micrographs showing HEK cell detachment in each sample are presented in Figure 6.12. Upon lowering the incubation temperature to 20°C, the confluent cells changed spontaneously from elongated to a more rounded form, again an indicative of a cell detachment process. It was found that the starting time for initial detachment of HEK cells from the comonomer microspheres retarded with increasing hydrophobic BMA content. However, all four samples exhibited complete cell detachment at similar time frame, *i.e.* 2 h. The decreased initial detachment rate was attributed to the presence of additional hydrophobic molecules that acted to disturb the polyNIPAm chain continuities, whilst suppressing complete hydration of the polyNIPAm chains upon lowering the incubation temperature below the phase transition temperature. Consequently, a longer time was required to initiate the polyNIPAm chain hydration. According to Lynch *et al.* [222], both LCST and rehydration rate reduce as the hydrophobic comonomer content increases, resulting in a slower release of bovine endothelial cell sheets from poly(*N*-isopropylacrylamide) grafted TCPS dish [239]. In their study, an incubation time of 4 h at 20°C was required for complete detachment of all endothelial cells from the TCPS dish grafted with hydrophobic comonomer, because the hydrophobic molecules in the copolymer reduced copolymer hydrophilicity, in turn reducing surface hydration and hence cell lifting.
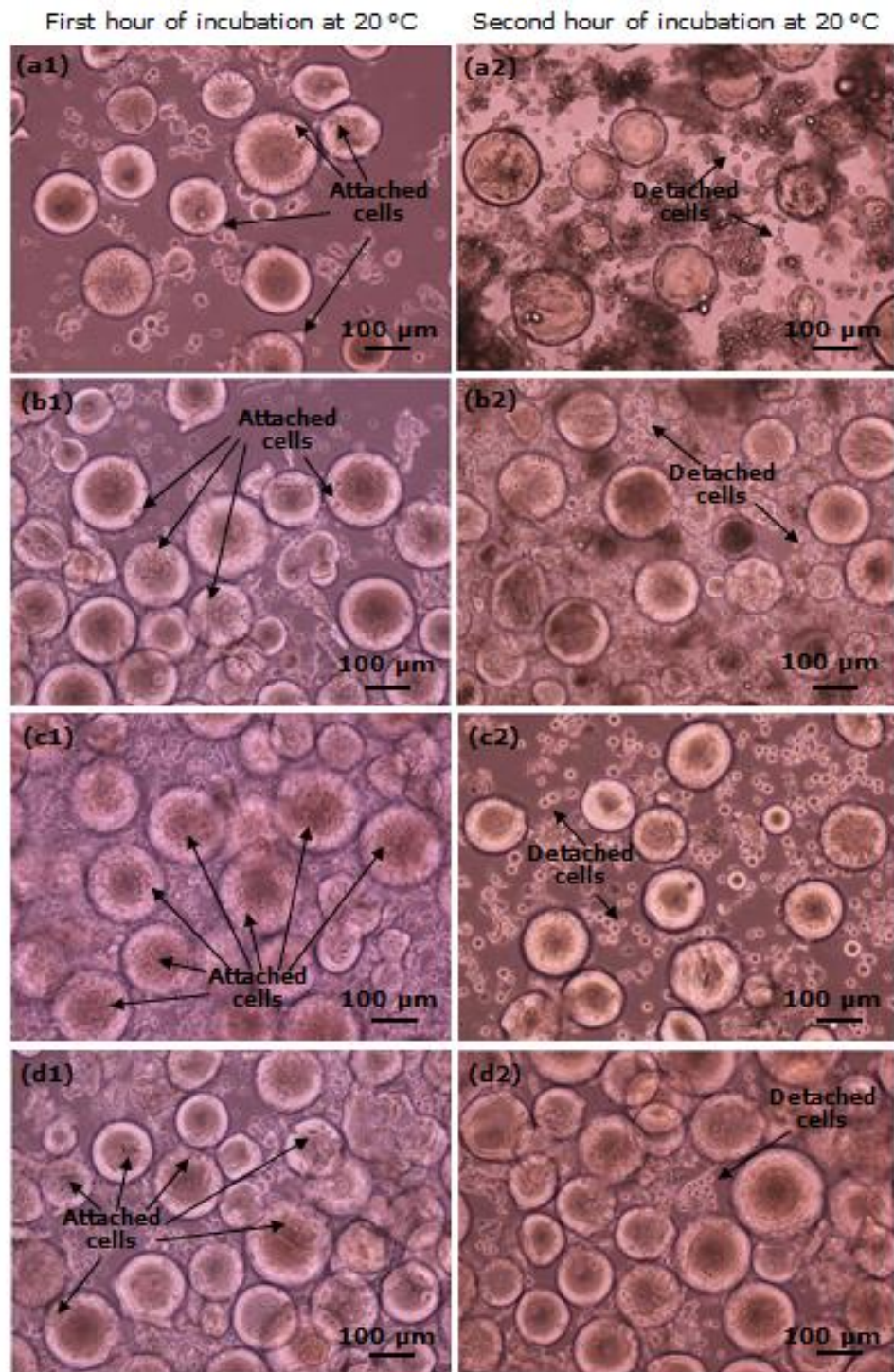
Figure 6.12 *Optical micrographs of detached HEK cells from poly(NIPAm-co-BMA) microspheres prepared using different amounts of BMA comonomer: (a) M1 (10 wt%); (b) M2 (20 wt%); (c) M3 (30 wt%); and (d) M4 (40 wt%), on Day 7 of culturing, after incubation at 20°C for 1 h and 2 h, respectively*

6.2 Summary

Copolymerisation of NIPAm with BMA was intended to functionalise the polyNIPAm surface with more CH_3 groups, with the aim of increasing polyNIPAm microsphere surface hydrophobicity, in order to promote better attachment and growth of HEK cells on the microspheres. The surface hydrophobicity of polyNIPAm microspheres was adjusted by the addition of BMA comonomer, and this study has demonstrated that surface hydrophobicity is an important determinant for cell attachment and growth. The interaction of cells with the microspheres correlated with protein adsorption onto the microspheres. Based on the cell culture data presented above, Sample M3 (with 30 wt% BMA comonomer) exhibited the optimal surface for HEK cell attachment and cell yield. Optimization of the processing parameters, *i.e.* stirring rate and cross-linker content, was performed, and the effect of each processing parameter on the properties of the polyNIPAm microspheres will be presented and discussed and in the following Chapter.

CHAPTER 7

OPTIMISATION OF PROCESSING PARAMETERS FOR THE SYNTHESIS OF POLYNIPAM MICROSPHERES

7.0 Introduction

To determine the optimal processing parameters for the synthesis of polyNIPAm microspheres, based on the highest cell yield, the effect of stirring rate and cross-linker content on the properties of the microspheres was investigated. It was established that the size of the microspheres varied with different stirring rates used in the polymer synthesis, whilst the compressive strength and modulus of the microspheres being adjustable by varying the cross-linker content. The objective of this part of the study was to appraise the effect of these processing parameters on the attachment and growth of human embryonic kidney (HEK) cells against the polyNIPAm microspheres. Eight sample sets of polyNIPAm microspheres were prepared via suspension polymerisation with varying stirring rate and cross-linker content at room temperature (25°C). The effects of stirring rate and cross-linker content on the physical and mechanical properties of the polyNIPAm microspheres were investigated using SEM and compression test. HEK cell seeding was performed on the polyNIPAm microspheres and the cellular response to the microspheres prepared using different stirring rates and cross-linker contents was monitored using optical microscopy. The cell growth in each sample was appraised using the Trypan blue exclusion method. The processing parameters used in the synthesis of the polyNIPAm microspheres are listed in Table 7.1.

Table 7.1 *Synthesis of polyNIPAm microspheres prepared using varying stirring rate and cross-linker content*

Sample code	Quantity in 10 ml ultrapure water (g)					Quantity in 100 ml cyclohexane (g)		Stirring rate (rpm)
	NIPAm	BMA	MBAm	APS	TEMED	Span 80®	CTAB	
R1	0.7	0.3	0.15	0.1	0.1	1.8	0.2	100
R2	0.7	0.3	0.15	0.1	0.1	1.8	0.2	200
R3	0.7	0.3	0.15	0.1	0.1	1.8	0.2	300
R4	0.7	0.3	0.15	0.1	0.1	1.8	0.2	400
C1	0.7	0.3	0.05	0.1	0.1	1.8	0.2	200
C2	0.7	0.3	0.10	0.1	0.1	1.8	0.2	200
C3	0.7	0.3	0.15	0.1	0.1	1.8	0.2	200
C4	0.7	0.3	0.20	0.1	0.1	1.8	0.2	200

It has been established that cell attachment and growth are dependent on microcarrier size [240]. According to Dike and Ingber [241], fibroblasts died rapidly when small microcarriers of diameter ~ 4 µm were used. In addition, the rigidity of the microcarrieris another determinant factor influencing cell adhesion and spreading (Pelham and Wang, 1997). Recently, Ohya *et al.* [242] reported that more endothelial cells adhered to polyNIPAm-gelatin hydrogels having higher modulus. Since stirring rate and cross-linker content affect the size and rigidity of polyNIPAm microspheres, respectively, the effect of these processing parameters on cell attachment and cell growth was appraised.

7.1 Results and Discussion

This section consists of two main parts. The effect of stirring rate on the microstructure of polyNIPAm microspheres is discussed first. The second part presents the effect of cross-linker content on the mechanical properties of the polyNIPAm microspheres. Cell trial data for each sample set is compared.

7.1.1 Effect of Stirring Rate

Four sample sets of polyNIPAm microspheres were prepared at stirring rate of 100, 200, 300 and 400 rpm, respectively. Adjusting the stirring rate was a simple way of controlling microsphere size. Morphologies of the microspheres were appraised using SEM. The mean particle size of the microspheres was compared and discussed. Cell trial was conducted to appraise the effect of particle size on cell attachment and growth.

7.1.1.1 Particle Size Measurement

To investigate the effect of stirring rate on polyNIPAm microspheres particle size, SEM was performed to observe the morphology of the prepared microspheres. Figure 7.1 presents the representative SE micrographs of the samples.
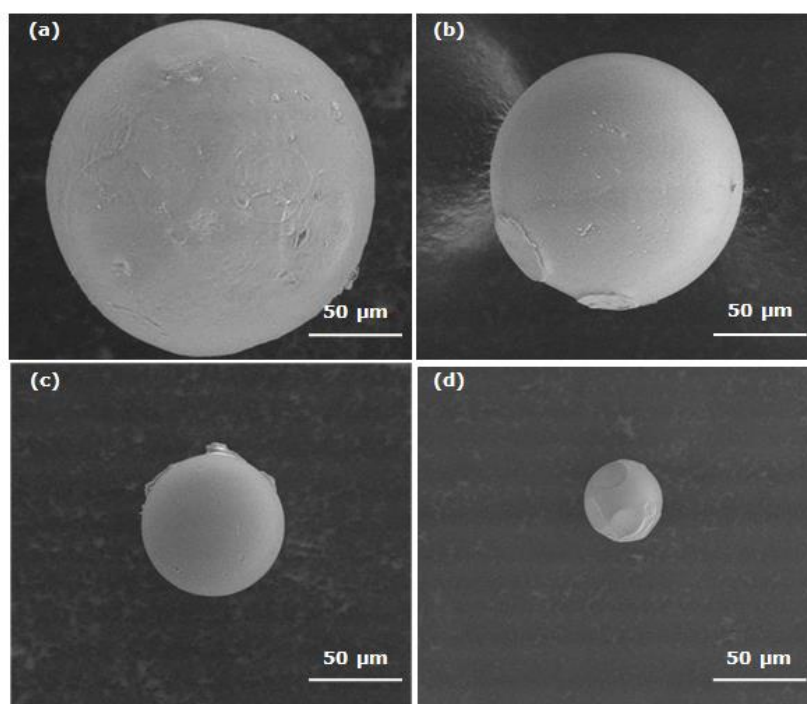
Figure 7.1 *SE micrographs of representative poly(NIPAm-co-BMA) microspheres prepared using different stirring rates: (a) R1 (100 rpm); (b) R2 (200 rpm); (c) R3 (300 rpm); and (d) R4 (400 rpm)*

Similar to previous sample sets, all four sets of microspheres exhibited round, smooth surfaces. It was clearly shown that the synthesized microspheres particle size changed with stirring rate. The mean particle size of the samples was calculated based on an average of 100 particles,

as tabulated in Table 7.2. There was a ~ 22 % reduction in size when the stirring rate was increased from 100 to 200 rpm. Further increase in stirring rate up to 400 rpm resulted in 80 % more reduction in the particle size compared to the sample prepared at 200 rpm. In immiscible liquid/liquid systems, stirring is performed to create a stable, homogeneous emulsion by breaking large liquid droplets into smaller droplets [243]. In this context, the energy input applied to the liquid/liquid systems play an important role in affecting the droplet size of the dispersed phase. During the stirring process, droplet break-up and coalescence occurs simultaneously (Figure 7.2). Droplet breakage is a phenomenon whereby a daughter droplet is separated into smaller droplets due to the shearing forces induced by the impeller, whilst droplet coalescence occurs when two or more droplets collide together [244].
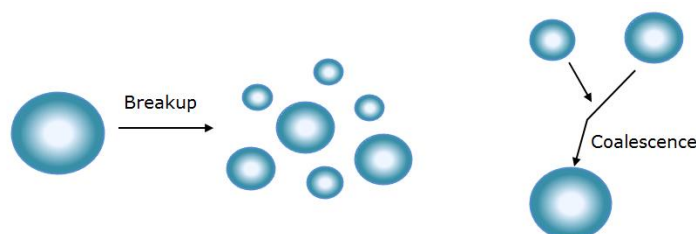
Figure 7.2 Depiction of the break-up and coalescence of droplets during stirring

It was observed that the Sauter mean diameter reduces gradually with increasing agitation. The decrease in particle size was attributed to an increase of the turbulent field, due to increased energy input to the suspension system, which caused the break-up of dispersed droplets into smaller size. This effect is in agreement with previous studies reported by Desnoyer *et al.* [137] and Torab-Mostaedi *et al.* [134] on the nickel chloride-tributyl phosphate and toluene-acetone-water systems, respectively. According to their findings, drop size is strongly dependent upon agitation speed, in which an increase of energy input leads to a rise in shear stress and the break-up of dispersed emulsion droplets. Consequently, the Sauter mean diameter decreased drastically with increasing agitation speed. Similar findings were documented by Harrison *et al.* [245], whereby the particle size of cadmium selenide microspheres reduced from > 50 to < 15 μm when the stirring rate was increased from 380 to 1100 rpm. Additionally, particle agglomerates were formed when a

stirring rate higher than 1100 rpm was used. The size distribution became narrower with increasing stirring rate.

Table 7.2 *Mean particle size of polyNIPAm microspheres prepared using different stirring rates: (a) R1 (100 rpm); (b) R2 (200 rpm); (c) R3 (300 rpm); and (d) R4 (400 rpm)*

Sample code	Mean particle size (µm)
R1	190 ± 59
R2	149 ± 54
R3	64 ± 16
R4	30 ± 11

To appraise the correlation between stirring rate and particle size, a plot of d_{32}/D against mean energy dissipation rate was constructed (Figure 7.3), based on the values in Table 7.3. As mentioned in Chapter 2, the Sauter mean diameter, d_{32}, defined as the ratio of the third and second moments of a drop size distribution, is used commonly in describing droplet size in two immiscible liquids system because it is directly related to the volume fraction of the dispersed phase.

Table 7.3 *Effect of specific energy dissipation rate on d_{32} for different stirring rates. ($N_p = 0.9$; $\rho_c = 779.0$ kg/m^3; D = 0.06 m; T = 25 °C)*

Stirring rate, N (rpm)	100	200	300	400
Angular speed, ω (rad/s)	10	21	31	42
Mean specific energy dissipation rate, $\bar{\varepsilon}_T$ (W/kg)	1	5	16	40
Experimental mean diameter, d_{32} (µm)	190 ± 59	149 ± 54	64 ± 16	30 ± 11

From Figure 7.3, it was found that d_{32}/D decreased exponentially with increasing $\bar{\varepsilon}_T$. Experimentally determined values of $\alpha = 0.469$, and $K_1 = 0.0042$ were obtained from Figure 7.3. By substituting these values into Equation 2.2, a correlation between specific energy dissipation rate and the Sauter mean diameter of the polyNIPAm secondary emulsion was obtained, *i.e.*:

$$d_{32}/D = 0.0042\,\bar{\varepsilon}_T{}^{-0.469} \qquad \text{...............} \quad (\text{Eq 7.1})$$

According to Hinze-Kolmogorov theory [129], in the inertia range of the turbulence field, only energies possessing eddies with size smaller than the drop diameter may cause drop breakage. Hence, the model leads to a decreasing power law of maximum stable drop diameter as a function of mean specific energy dissipation, with an exponent equal to -0.4 [246]. The experimental *a* value determined in the present study, *i.e.* -0.469, was close to this theoretical *a* value. In practice, the α value is dependent on mixer type, and hence related to the homogeneity of the flow field generated by the mixer. The higher the *a* value, the greater the homogeneity of the flow field [247]. For example, the experimental *a* value reported by Theron and Sauze was 0.36 for an SMX™ mixer and 0.64 for an SMV™ mixer, which indicates that the SMX™ mixer produces a more homogeneous flow field.

$$y = 0.0042x^{-0.469}$$
$$R^2 = 0.8237$$
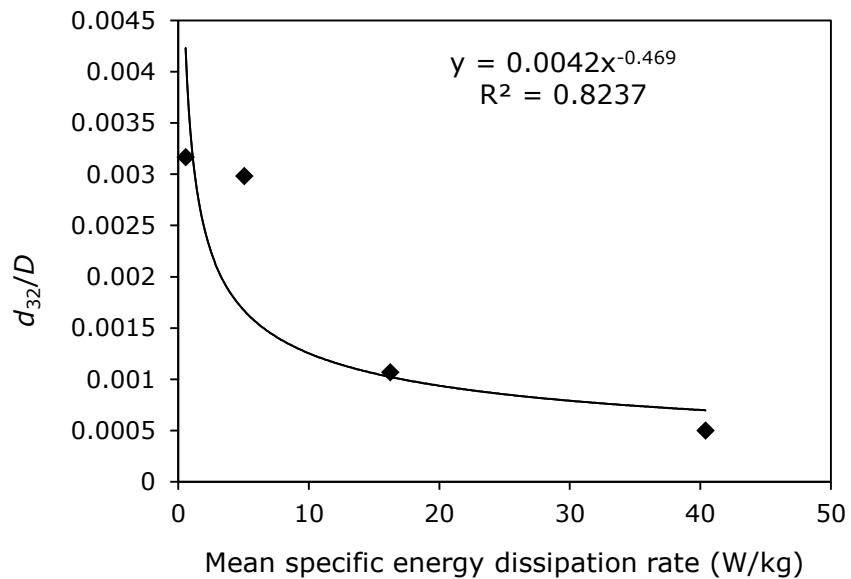
Figure 7.3 Plot of d_{32}/D versus $\bar{\varepsilon}_T$ ($N_p = 0.9$; $\rho_c = 779.0$ kg/m³; $D = 0.06$ m; $T = 25°C$)

7.1.1.2 Cell Attachment

To study the effect of particle size on HEK cell attachment and growth, the HEK cells were seeded on microspheres prepared using different stirring rates. The cellular response against the microspheres was monitored and compared using optical microscopy. Figure 7.4 shows optical micrographs of the cultured cells on Days 2 and 7 of the culturing process. The cells exhibited spherical morphology on Day 2, indicating that the cells were not ready to attach to the microspheres. In contrast, the morphology of the cells on Day 7 was elongated, showing that the cells were spreading and growing healthily with the microspheres. By way of comparison, Sample R2 exhibited the greatest number of attached cells, whilst Sample R4 showed the lowest number of attached cells. This confirms that cell attachment was affected by microcarrier size. Although smaller microcarriers offer higher surface to volume ratio, which facilitates higher cell density, microcarriers smaller than 5 µm do not provide sufficient space to support cell proliferation and growth [248].
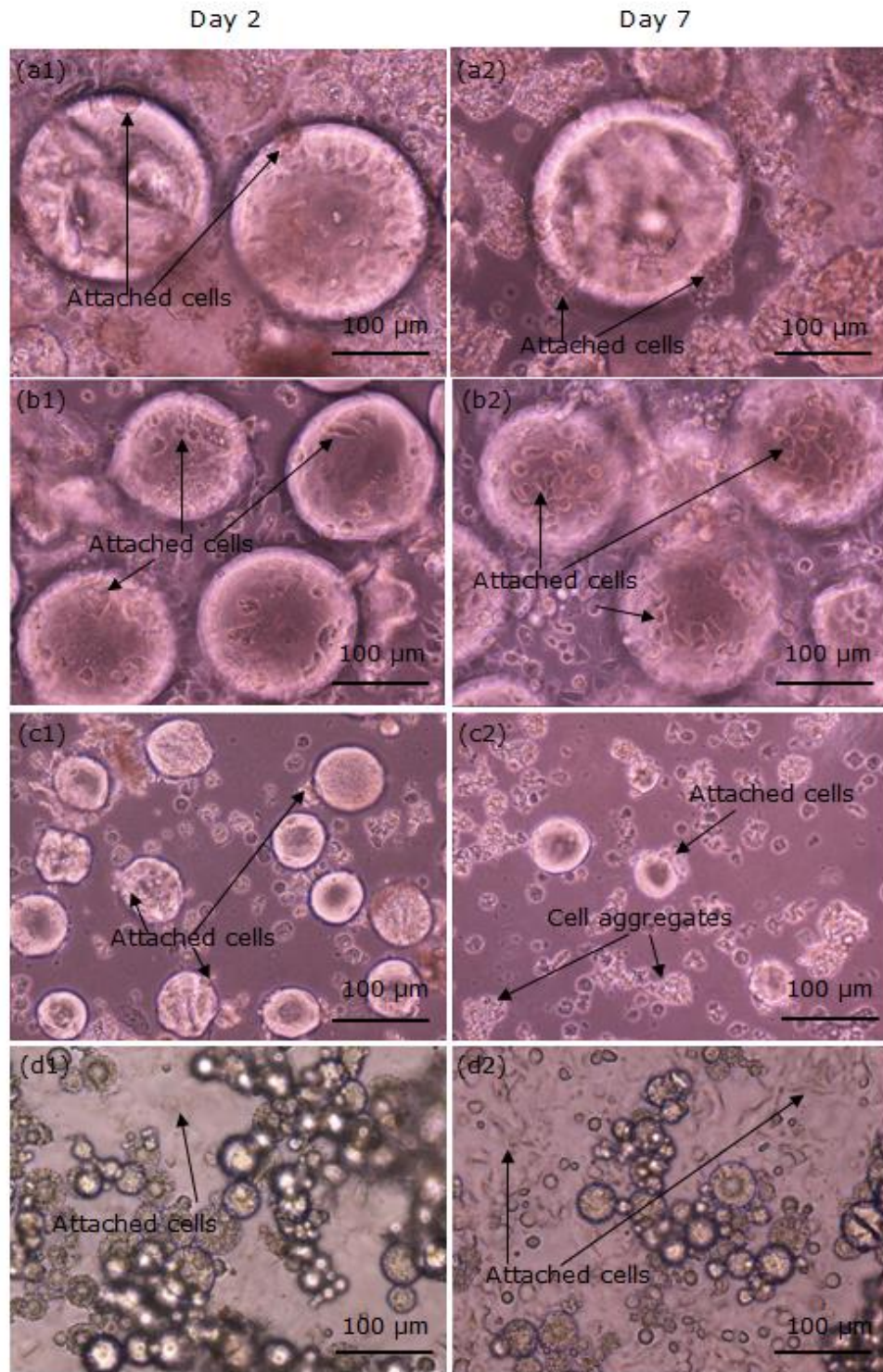
Figure 7.4 *Optical micrographs of HEK cell growth on polyNIPAm microspheres as a function of stirring rate: (a) R1 (100 rpm); (b) R2 (200 rpm); (c) R3 (300 rpm); and (d) R4 (400 rpm), on Day 2 and Day 7 of the culturing process, respectively*

149

The detailed morphologies of cells attached to the microspheres were examined using scanning electron microscopy. Representative SE micrographs are presented in Figure 7.5.
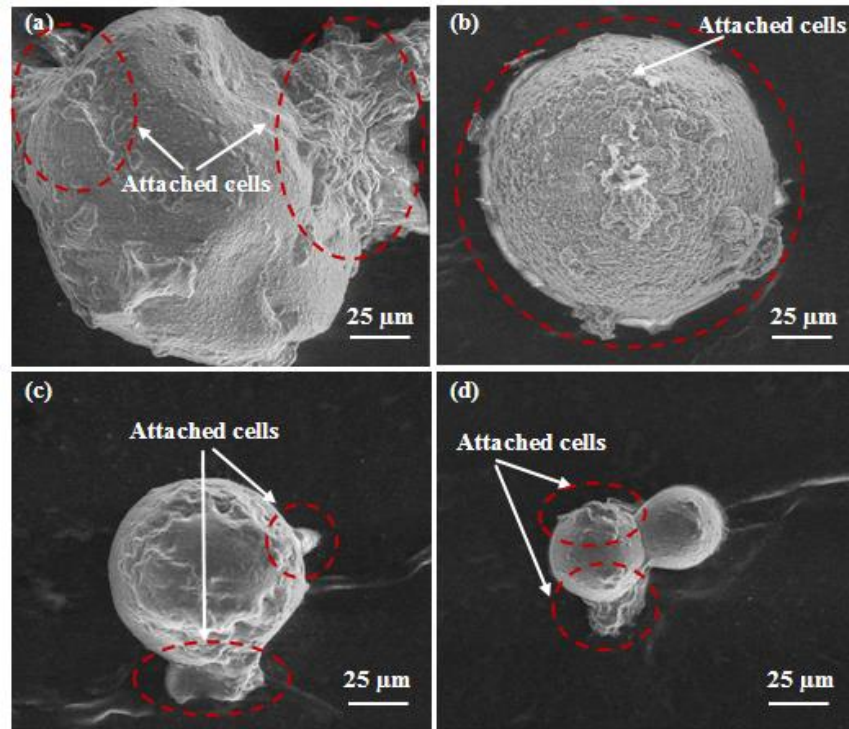
Figure 7.5 *SE micrographs of polyNIPAm microspheres with attached HEK cells: (a) R1 (100 rpm); (b) R2 (200 rpm); (c) R3 (300 rpm); and (d) R4 (400 rpm), on Day 7 of the culturing process*

More attached cells were observed for Sample R2 as compared to Sample R1, and poor cell attachment was found for Samples R3 and R4. This morphological observation was corroborated by the optical micrographs of Figure 7.5, confirming that cell attachment reduced as microcarrier size reduced.

To appraise cell growth for these four sets of samples having different particle sizes, cell counting was performed throughout the cell culturing process. Figure 7.7 presents a bar chart of cell growth as a function of culturing time. On Day 2 of cell culturing, Samples R1 and R3 exhibited similar cell yields of ~ 4 x 10^5 cells/ml. Although, by Day 5 of cell culturing, the viable cell density of Sample R1 was ~ 56 % greater than that of Sample R3.

On the other hand, Sample R2 exhibited the highest cell yield throughout the culturing process, from ~ 5 x 10^5 cells/ml on Day 2 to ~ 17 x 10^5 cells/ml on Day 7. Sample R4 exhibited the lowest cell yield with minimal increment, *i.e.* from 0.6 x 10^5 cells/ml on Day 2 to 1.1 x 10^5 cells/ml on Day 7. This cell trial result showed that Sample R4 did not support cell growth, attributable to its smaller carrier size compared to other samples. This size effect is consistent with the optical micrographs presented in Figure 7.4.
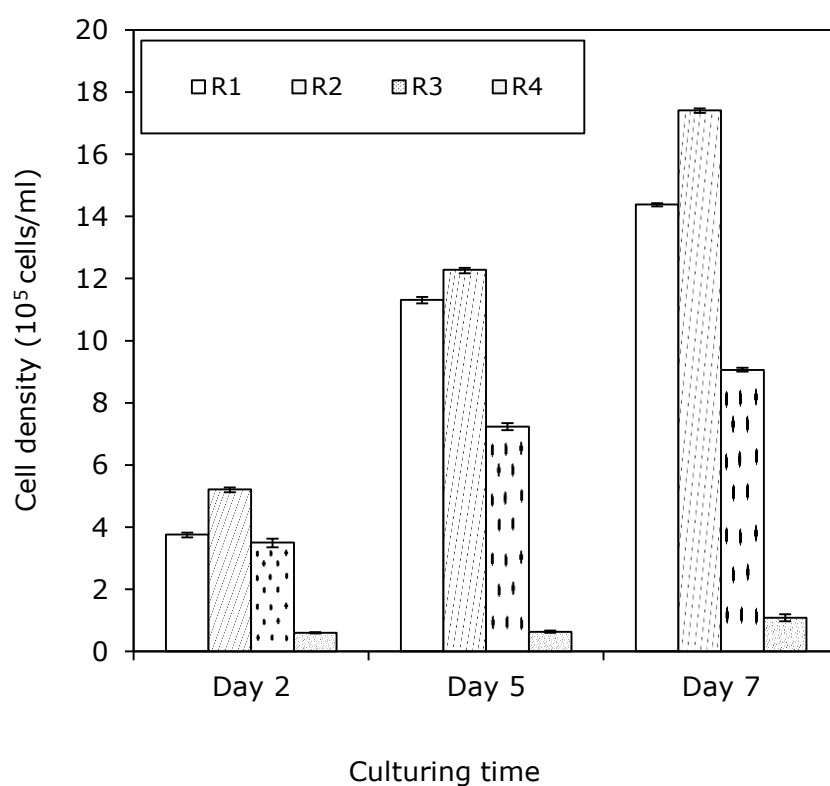
Figure 7.6 *HEK cell density on PNIPAm microspheres as a function of stirring rate: (a) R1 (100 rpm); (b) R2 (200 rpm); (c) R3 (300 rpm); and (d) R4 (400 rpm), on Days 2, 5 and 7 of the culturing process, respectively*

7.1.1.3 Cell Detachment

At the end of the culturing process, *i.e.* Day 7, the incubation temperature was reduced from 37 to 20°C to induce detachment of the confluent cells from the microspheres. Figure 7.7 shows the detached HEK cells, as observed using an inverted optical microscope. Similar to the previous results for cell detachment, the morphology of the confluent cells changed from elongated to spherical form spontaneously upon lowering the incubation temperature to 20°C. This change in cell morphology is attributed to the change in surface hydrophilicity of the microspheres with response to temperature, whereby the HEK cells were able to detach from the microsphere surfaces when the incubation temperature was reduced to 20°C.
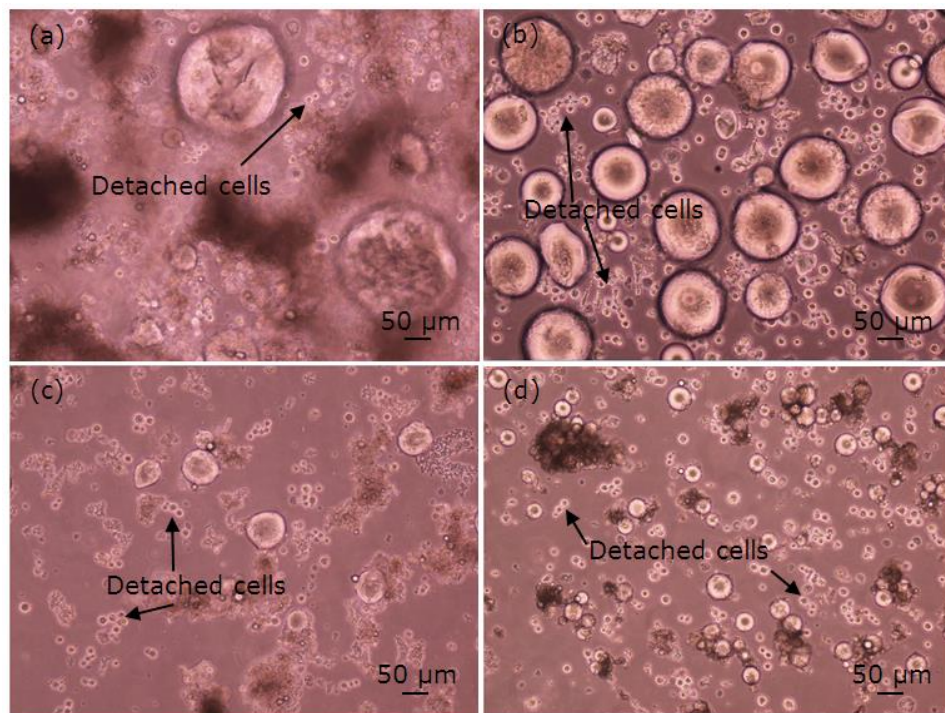
Figure 7.7 *Optical micrographs of detached HEK cells from the polyNIPAm microspheres as a function of stirring rate: (a) R1 (100 rpm); (b) R2 (200 rpm); (c) R3 (300 rpm); and (d) R4 (400 rpm), on Day 7 of culturing, after incubation at 20°C for 2 h*

7.1.2 Effect of Cross-linker Content

Cross-linking is a chemical process that promotes the formation of the 3-dimensional polymer structure. *N,N'*-methylene-bis-acrylamide (MBAm) was used as a cross-linker for the synthesis of polyNIPAm microspheres in the present study, owing to its capability of creating crosslinks between polyacrylamide chains. Four sample sets of polyNIPAm microspheres were prepared with different cross-linker contents, *i.e.* 5, 10, 15 and 20 wt%. The effects of cross-linker content on the microspheres particle size and mechanical properties were appraised using SEM and compressive test. Cell trial data for the four sample sets were compared and discussed.

7.1.2.1 Particle Size Measurement

The microstructures of the microspheres prepared using varying amounts of cross-linker are shown in Figure 7.8. It was found that the mean particle size reduced slightly from 154 ± 33 µm to 139 ± 39 µm when the cross-linker content was increased from 5 to 20 wt% (Table 7.4). This small reduction of particle size was attributed to the increased number of crosslinked polymer chains that restrict chain mobility [249]. This is in an agreement with studies reported by Khonakdar *et al.* [250] and Kojio *et al.* [251], regarding the effect of di-*tert* butyl cumyl peroxide and tolylene-2,4-diisocyanate cross-linker amounts on the properties of high-density polyethylene and polyurethane, respectively. According to their findings, the number of entangled chains increased with increasing cross-linker amount, leading to a decrease in free volume of the polymer.
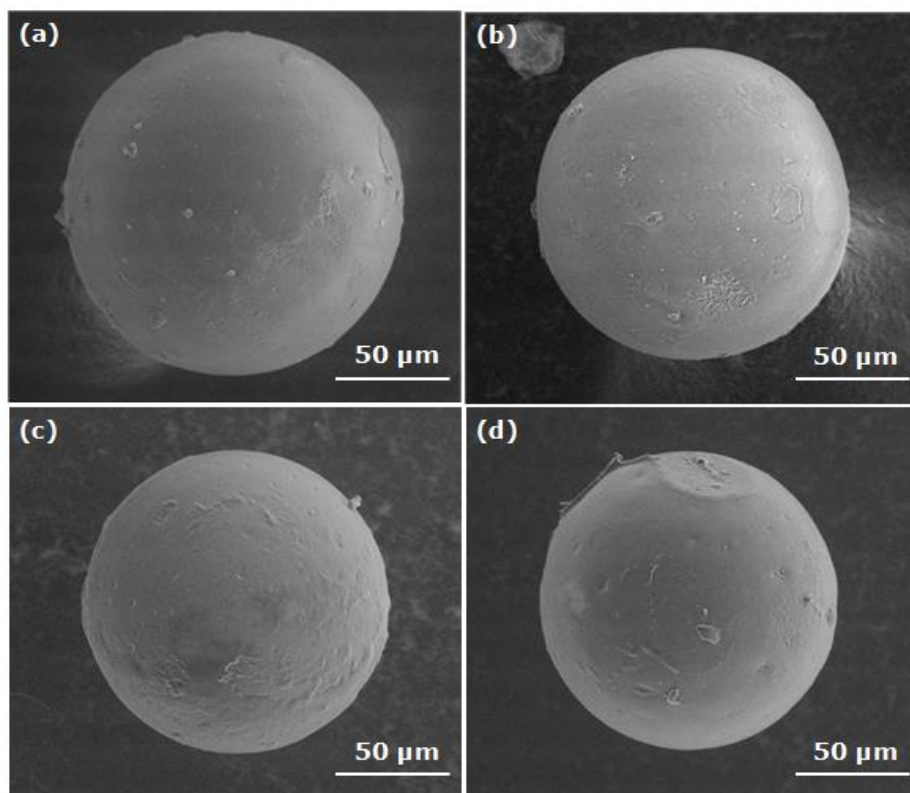
Figure 7.8 *SE micrographs of polyNIPAm microspheres as a function of cross-linker content: (a) C1 (5 wt% MBAm); (b) C2 (10 wt% MBAm); (c) C3 (15 wt% MBAm); and (d) C4 (20 wt% MBAm)*

Table 7.4 *Mean particle size of the polyNIPAm microspheres as a function of cross-linker content: (a) C1 (5 wt% MBAm); (b) C2 (10 wt% MBAm); (c) C3 (15 wt% MBAm); and (d) C4 (20 wt% MBAm)*

Sample code	Mean particle size (µm)
C1	154 ± 33
C2	148 ± 44
C3	140 ± 23
C4	139 ± 39

7.1.2.2 Compressive Strength and Modulus

Compression tests were performed to appraise the effect of cross-linker content on the mechanical properties of the poly(NIPAm) microspheres. Figure 7.10 illustrates the change in yield strength and Young's modulus of the microspheres as a function of cross-linker content.
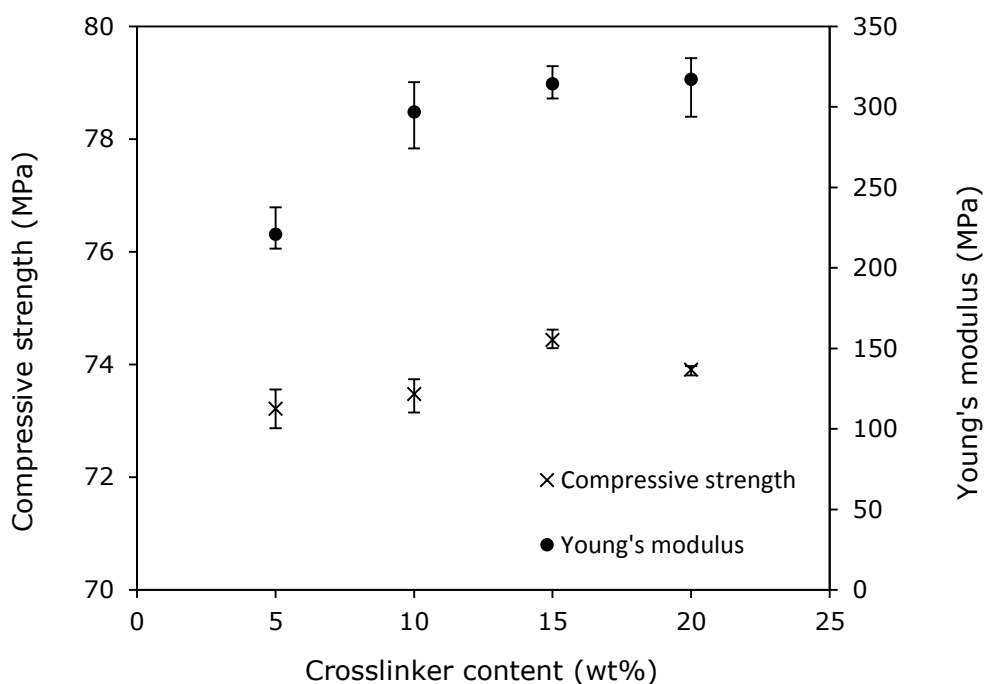
Figure 7.9 *Compressive strength and Young's modulus of the microspheres as a function of cross-linker content*

It was found that the Young's modulus of the polyNIPAm sample increased abruptly from ~ 221 ± 14 to ~ 297 ± 21 MPa when the cross-linker content was increased from 5 to 10 wt%. Only 6% increase of Young's modulus was found upon the addition of 15 wt% cross-linker compared to 10 wt%. At 20 wt% cross-linker, the Young's modulus was ~ 317 ± 20 MPa, which was ~ 1% higher than that of Sample C3. This trend shows that microsphere Young's modulus increases with increasing cross-linker content, being attributable to an increase in crosslinking density that reduced the flexibility of the polymer chains. Consequently, strain decreased with increased cross-linking of the polymer network. Since modulus is calculated from the slope of the linear portion of a stress

versus longitudinal strain curve, a decrease in strain leads to a rise in modulus [252]. This is in agreement with the study reported by Harmon *et al.* [253], whereby the modulus of poly(*N*-2-dimethylamino-ethyl-acrylamide) increased with an increase of 2-(dimethylmaleimido)-*N*-ethyl-acrylamide cross-linker. Furthermore, Hsieh *et al.* [254] reported that tensile modulus and strength increased with increasing MBAm cross-linker density.

Conversely, the compressive strength of Samples C1 and C2 were identical, *i.e.* ~ 73 ± 0.4 MPa. Further addition of 15 wt% cross-linker resulted in only a slight increase of compressive strength, *i.e.* ~ 1%. Sample C4 exhibited a compressive strength of ~74 ± 0.1 MPa, which was slightly lower than that of Sample C3. The increase in yield strength indicates that more stress would be required to break the highly crosslinked polymer chains in order to deform the material plastically [255]. With greater cross-linker content, the polymer chains become more compact and rigid, and thus exhibit greater ability to withstand higher stress from plastic deformation. A similar finding was reported by Seddiki and Aliouche [256], based on a study of a copolymer of polyNIPAm and acrylic acid. It was reported that copolymer mechanical strength increased proportionally with increasing MBAm cross-linker content.
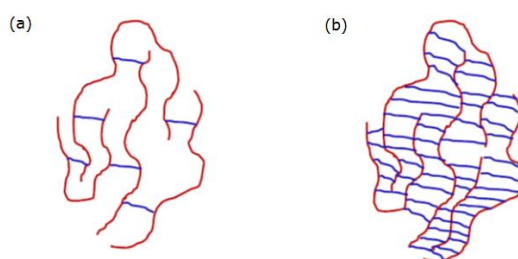
Figure 7.10 *Depiction of a polymer network with (a) low degree of cross-linking; and (b) high degree of cross-linking*

7.1.2.3 Cell Attachment

To study cellular response against microspheres containing different cross-linker contents, the culturing cells in the microsphere suspensions were monitored using optical microscopy. Figure 7.11 shows representative optical micrographs on Day 2 and Day 7 of the culturing process. All four samples exhibited poor cell attachment on Day 2 of culturing, with more cell attachment on Day 7, especially for Sample C3. Sample C1 showed relatively poor attachment of cells compared to the other samples, being attributable to the lower modulus of these microspheres with lower crosslinking density. According to Maroudas [257], fibroblasts exert mechanical stress on their growth surfaces. Hence, the growth surfaces must be rigid for cell spreading on the surfaces. Similar findings were reported by Wang *et al.* [258] and Marklein and Burdick [259], with the number of mouse MC3T3 cells attached to polypropylene fumarate/poly(ε-caprolactone) blend with the addition of 25% cross-linker, was 100% greater than that of uncross-linked sample. This was attributed to the increased tensile modulus from 166 ± 6 to 526 ± 12 MPa upon the addition of 25% cross-linker. A related study by Cai *et al.* (2012) [260] reported that the proliferation of neural progenitor cells at day 7 for [2-(methacryloyloxy)ethyl]-trimethylammonium chloride (MTAC) grafted polyethylene glycol diacrylate (PEGDA) with a shear modulus of 265 ± 12 kPa, was $\sim 50\%$ greater than that of PEGDA control sample with a shear modulus of 246 ± 7 kPa.
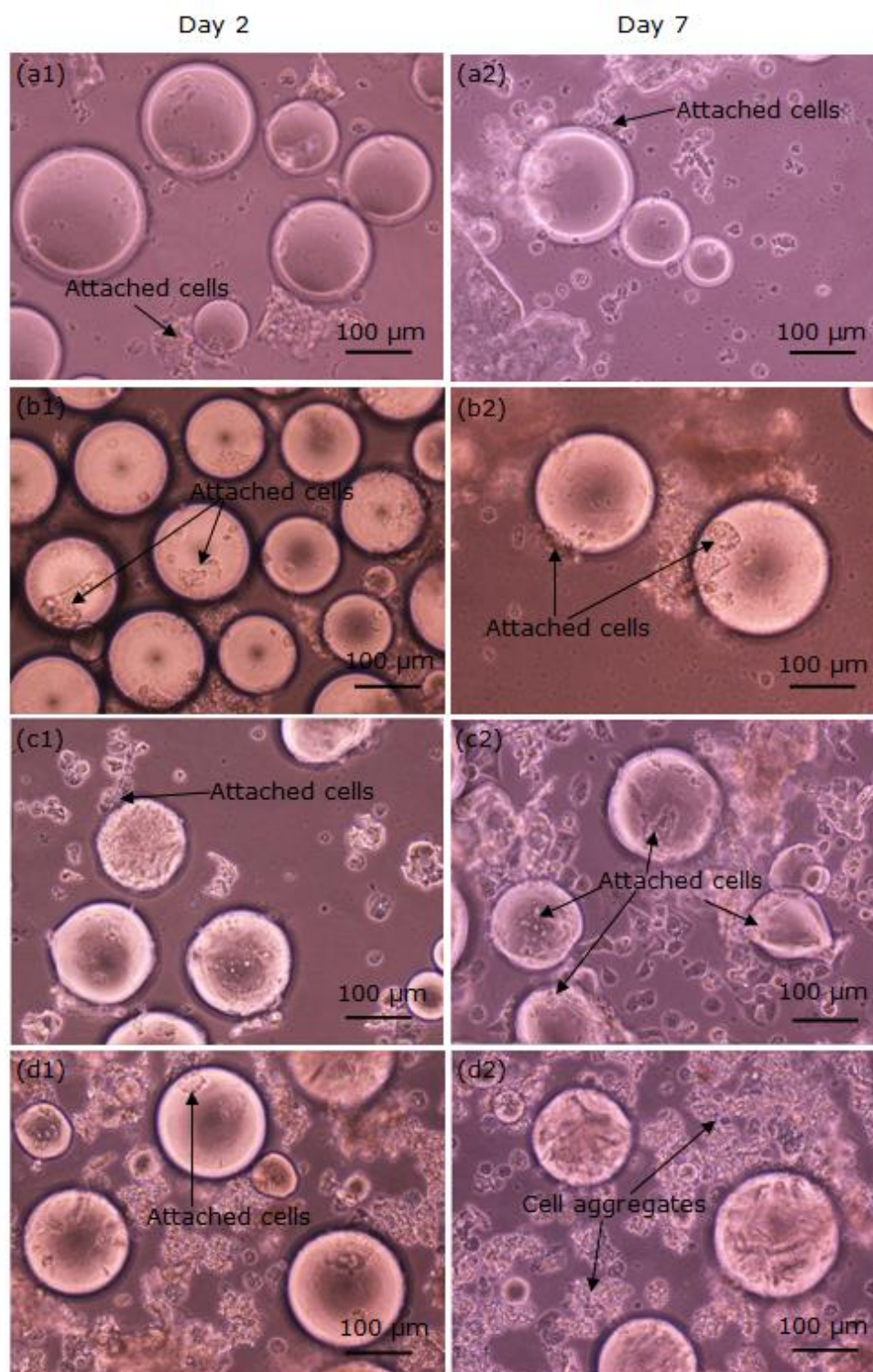
Figure 7.11 *Optical micrographs of HEK cell growth on polyNIPAm microspheres as a function of cross-linker content: (a) C1 (5 wt% MBAm); (b) C2 (10 wt% MBAm); (c) C3 (15 wt % MBAm); and (d) C4 (20 wt% MBAm), on Day 2 and Day 7 of the culturing process, respectively*

158

This cell trial data were corroborated by SE micrographs showing the morphologies of the cells and microspheres (Figure 7.12). Maximal cell attachment was found for Sample C3, where cells were observed to bridge the microspheres. This showed that the microspheres provided a good platform for cell spreading and growth. Similar cell bridging was observed for Sample C4. In contrast, Sample C1 exhibited minimal cell attachment, with only a few cells attached to the edges of the microspheres. In this case the cells would rather attach to the culture dish surface than to the microspheres. This data is consistent with the optical micrographs shown in Figure 7.11.
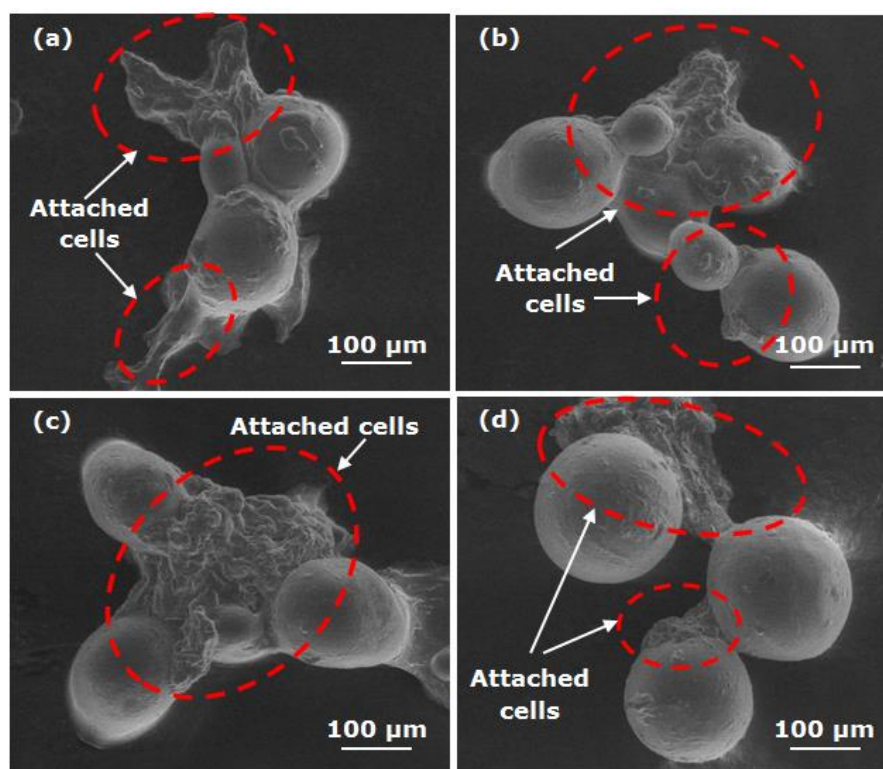
Figure 7.12 SE micrographs of polyNIPAm microspheres with attached HEK cells: (a) C1 (5 wt% MBAm); (b) C2 (10 wt% MBAm); (c) C3 (15 wt% MBAm); and (d) C4 (20 wt% MBAm), on Day 7 of the culturing process

To investigate the effect of cross-linker content on cell growth on the polyNIPAm microspheres, the viable cell density produced for each sample was counted at different time during the culturing process. Figure 7.13 summarises the HEK cell growth as a function of time. Overall, all the samples exhibited a positive cell growth throughout the cell culturing process. However, the increment in cell density varied considerably. Sample C1 exhibited the lowest cell yield, *i.e.* $< 5 \times 10^5$ cells/ml, whilst the highest cell yield was observed for Sample C3, *i.e.* $\sim 15 \times 10^5$ cells/ml, on Day 7 of the culturing process. Sample C4 showed the second highest cell yield, *i.e.* $\sim 14 \times 10^5$ cells/ml, followed by Sample C2 with a cell density of $\sim 6 \times 10^5$ cells/ml on Day 7 of the culturing process. This cell growth data supported the suggestion that the cell growth was dependent on the rigidity of the microspheres.
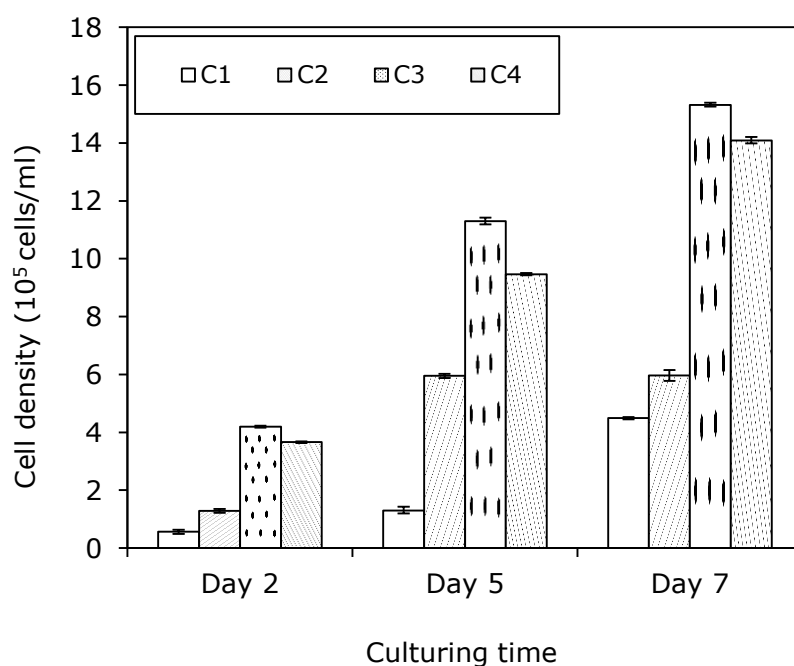
Figure 7.13 *HEK cell growth on polyNIPAm microspheres prepared using different cross-linker content: (a) C1 (5 wt% MBAm); (b) C2 (10 wt% MBAm); (c) C3 (15 wt% MBAm); and (d) C4 (20 wt% MBAm), on Days 2, 5 and 7 of the culturing process, respectively*

7.1.2.4 Cell Detachment

Similar to previous sample sets, cell detachment from the polyNIPAm microspheres was observed upon lowering the incubation temperature from 37 to 20°C for 2 h. Figure 7.14 shows the detached cells and polyNIPAm microspheres containing different amounts of cross-linker. This result showed that cross-linker content had no effect on the rate of cell detachment.
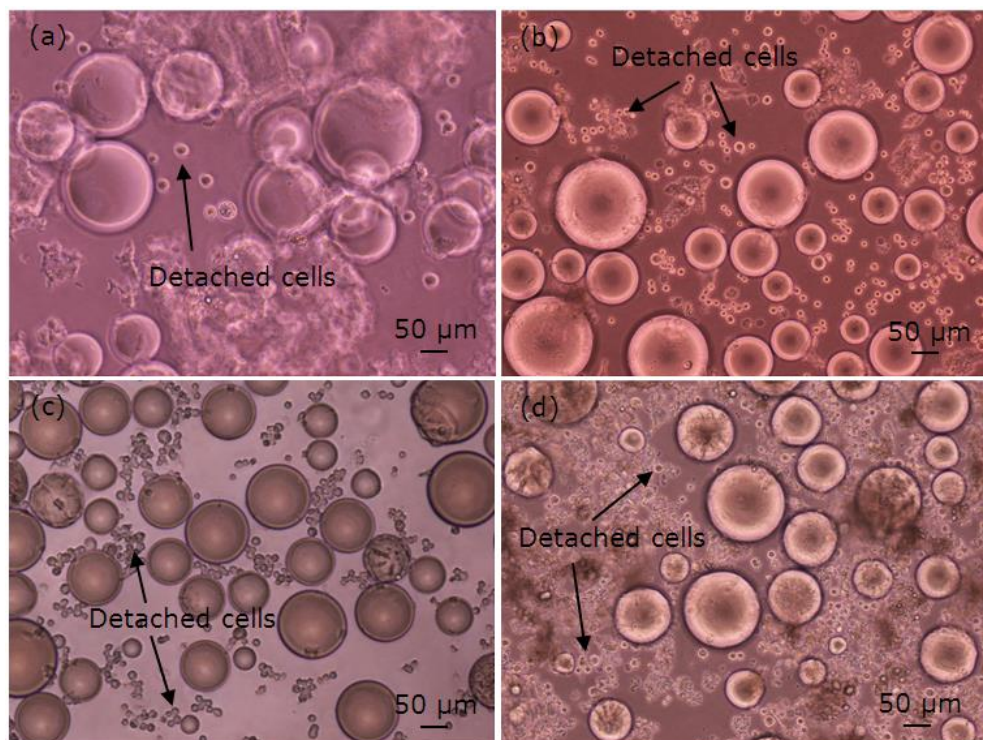
Figure 7.14 *Optical micrographs of detached HEK cells from the polyNIPAm microspheres as a function of cross-linker content: (a) C1 (5 wt% MBAm); (b) C2 (10 wt% MBAm); (c) C3 (15 wt% MBAm); and (d) C4 (20 wt% MBAm), on Day 7 of the culturing process*

7.2 Summary

The effects of the processing variables of stirring rate and cross-linker content, in the synthesis of the polyNIPAm microspheres, were investigated with a view to optimise cell yield, being related to the physical and mechanical properties of the microspheres. It was found that carrier particle size decreased with increasing stirring rate, whilst the microsphere compressive modulus increased with increasing cross-linker content. The correlation between particle size and stirring rate may be used to predict the size of the polyNIPAm microspheres. This study confirmed that HEK cell attachment and growth were dependent on particle size and the stiffness of the microspheres. Based on the cell culture data presented, Sample R2 (200 rpm) exhibited the highest cell yield of $\sim 1.7 \times 10^6$ cells/ml, which is comparable to the performance of the commercial microcarrier Cytodex ($> 1.0 \times 10^6$ cells/ml).

CHAPTER 8

OVERVIEW DISCUSSION

8.0 Introduction

In this Chapter, an overview of the development of a thermally responsive microcarrier for non-invasive cell harvesting is presented. The suitability of the suspension polymerisation technique and the effect of initiator type on the development of polyNIPAm microcarriers are discussed, with particular attention being given to the dependency of cell attachment on the surface chemistry of the polyNIPAm microcarriers. The effect of processing parameters on the size and mechanical properties of the polyNIPAm microcarriers is discussed. The effectiveness of polyNIPAm microcarriers on inducing cell detachment via temperature reduction is emphasised.

8.1 PolyNIPAm Microsphere Synthesis and the Effect of Initiator

It was found that initiator type played an important role in defining the physical properties and surface charge of the final polymer product. Suspension polymerisation, performed at 25°C in the presence of a redox initiator (APS/TEMED), produced polyNIPAm microspheres with a range diameters > 50 μm. This size range is considered suitable for microcarrier cell culturing. Conversely, relatively small microspheres, < 2 μm, were produced when a thermal initiator (AIBN) was used, with suspension polymerisation conducted at 70°C because AIBN only decomposes at temperature > 65°C to generate free radicals to initiate the polymerisation reaction. Hence, it is evident that polymerisation temperature has an effect on polymer particle size. High temperatures reversed the emulsion from O/W to W/O, leading to precipitation polymerisation whereby polymeric particles grow by capturing other monomers until a critical length was reached and became insoluble in the solvent [85]. However, the use of the neutral AIBN initiator produced a positively charged surface (~ 3 mV), whilst the APS/TEMED initiator resulted in a negatively charged surface (~ -29 mV), demonstrating that polyNIPAm microsphere surface charge is dependent on initiator type. This is in agreement with previous findings reported by Cheremisinoff [187] and van Berkel *et al.* [188].

163

Since microcarrier size must be greater than cell size (~ 10 µm) [182,183], the APS/TEMED redox initiator was clearly the better candidate for use in the synthesis of polyNIPAm microspheres.

8.2 Cell Attachment Dependency on the PolyNIPAm Microcarrier Surface Chemistry

The unmodified polyNIPAm microcarrier exhibited poor cell attachment, attributed to the negative surface charge of the microcarrier. Hence, a cationic surfactant (CTAB) was incorporated into the polyNIPAm microcarrier to modify the surface charge. The addition of 20 wt% of CTAB resulted in a positive surface charge (~ +8 mV), attributable to the cationic polar groups of the surfactant molecules adsorbed onto the microsphere's surface via electrostatic interaction [203]. This charge modified carrier exhibited better cell attachment and growth as compared to the unmodified polyNIPAm, being attributable to the negative charge of the cells [160]. This is consistent with previous findings documented by Lee *et al.* [185] and Schneider *et al.* [186], whereby more cell adhesion was promoted by positively charged culture substrates. However, the cell yield was found to be lower than that for commercial microcarriers. Hence, further modification of the polyNIPAm microcarrier was performed using a hydrophobic comonomer.

It was found that incorporation of the BMA comonomer increased the surface hydrophobicity of the polyNIPAm microcarriers, being attributable to the presence of the additional hydrophobic isopropyl ($-CH(CH_3)_2$) groups in the comonomer, facilitating more hydrophobic interactions whilst inhibiting hydrogen bonding with water molecules [171].

An increase in hydrophobic isopropyl ($-CH(CH_3)_2$) groups with increasing BMA comonomer content was confirmed by FTIR. Similar findings were reported by Bakhshi *et al.* [216] and Chen *et al.* [217]. In particular, a ~ 100% increase in cell yield was obtained for Sample M3 containing 30 wt% of BMA, as compared to the unmodified sample. This effect was attributed to the increased number of proteins adsorbed onto the hydrophobic surfaces, promoting more interaction between cells and the substrate. According to Tengvall *et al.* [231] and Gessner *et al.* [232],

hydrophobic surfaces promote protein adsorption and thus enhance cell adhesion onto the substrates.

The cell trial data showed that surface charge and the hydrophobicity of the polyNPAm microspheres had a significant influence on cell attachment and growth. Without the use of expensive RGD tripeptides, cell attachment and growth also can be improved by adjusting the surface hydrophobicity of polyNIPAm microcarrier. Overall, better cell attachment and growth were found for samples exhibiting positive surface charge and hydrophobic character.

8.3 Effect of Processing Parameters

The stirring speed applied to the suspension had a significant effect on size of the resultant polyNIPAm microspheres. An increase in stirring speed resulted in a decrease of microsphere size, with particle size reducing from ~ 190 to ~ 30 µm as the stirring speed increased from 100 to 400 rpm. This effect was attributed to an increase in shear forces that increased the frequency of droplet break-up [243]. Similar findings were reported by Desnoyer *et al.* [137] and Torab-Mostaedi *et al.* [134]. For example, minimal cell attachment was found for polyNIPAm samples prepared at 400 rpm, due to the relatively small microsphere size as compared to other samples. Again, this showed that particle size played an important role in affecting cell attachment [248].

Conversely, the addition of MBAm cross-linker resulted in a three-dimensional cross-linked polymer structure. To investigate the relationship between the cellular response and the mechanical property of the polyNIPAm microspheres, compression tests were performed using a Lloyd (LR50K) instrument. Since the individual microspheres were too small for compression testing, the microspheres were mechanically pressed into a pellet of diameter 13 mm and thickness 3 mm. It was found that the compressive strength and modulus of the polyNIPAm sample increased as the cross-linker content increased. This is consistent with previous studies conducted by Harmon *et al.* [261] and Hsieh *et al.* [254]. Sample containing 15 wt% cross-linker exhibited maximal cell attachment and growth, whilst minimal cell attachment and growth were found for samples prepared using 5 wt% cross-linker. This result demonstrated that cells

prefer to proliferate and grow on stiffer substrates. Similar improved cell attachment and growth were documented by Wang *et al.* [258] and Cai *et al.* [260].

In general, microcarriers must be sterilised at 121°C for 15 minutes prior to *in-vitro* cell culturing [24]. Based on the TGA thermal analysis data, all the polyNIPAm samples exhibited thermal decomposition at > 300°C, showing that these samples can be autoclaved at 121°C with no change in physical properties. Similar findings were reported by Shinde *et al.* [193] and Bauri *et al.* [194]. The high thermal stability of polyNIPAm showed that it is suitable for use as microcarrier for cell culturing.

8.4 Thermally-induced Cell Detachment

To appraise the effectiveness of cell harvestment from the polyNIPAm microspheres, without using destructive trypsin or scrapper, the incubation temperature of the confluent cells was lowered from 37 to 20°C for 2 h. The cells were monitored regularly using optical microscopy. In the first hour, there was not much change in terms of the cell morphology, *i.e.* with cells remaining elongated and spread on the microspheres. However, after incubating at 20°C for 2 h, the cells exhibited round shapes and were suspended in the culture media. This showed that cells could be harvested by simply reducing the incubation temperature. This was attributed to a change from dehydration to hydration of the polymer chains that facilitated cell detachment [212]. A previous study of Cooperstein and Canavan [213] also demonstrated the detachment of Madin-Darby canine kidney (MDCK) cells from tissue culture polystyrene (TCPS) dish grafted with polyNIPAm upon reducing the culturing temperature to 20°C. However, their product was a two-dimensional planar structure, whilst the polyNIPAm microcarriers synthesized in the present study are of three-dimensional structure, which offers greater surface-to-volume ratio for scaling-up of cell yields. In summary, these polyNIPAm microcarrieres enabled thermally-induced cell detachment without the use of trypsin, and thus preventing cell damage.

CHAPTER 9

CONCLUSIONS

9.0 Conclusions

In summary, the main objectives of the present study were achieved.

During the first initial stages of this research programme, a suitable initiator for the synthesis of polyNIPAm microspheres was identified. The key outcomes pertaining to this part of experiment are as follows:

- A polymerisation temperature of 70°C was required when using the thermal initiator AIBN which will only decompose at temperatures > 65°C to generate free radicals to initiate the polymerisation reaction.

- Only fine polyNIPAm microspheres with diameters < 2 µm were formed at 70°C.

- When a pair of redox initiators was used, polymerisation could be performed at room temperature (25°C), since free radicals were generated spontaneously when both APS and TEMED initiators were mixed together.

- Larger polyNIPAm microspheres of diameter of ~ 50 µm were produced at 25°C.

- The surface charge of the polyNIPAm microspheres was affected by initiator type. The polyNIPAm microspheres produced using the APS and TEMED redox initiators were more negatively charged, *i.e.* ~ - 29 mV, as compared to microspheres synthesised using the AIBN initiator.

- The attachment of HEK cells was influenced by the surface charge of the microspheres. There was no cell attachment to microspheres exhibiting negative surface charge of ~ -29 mV.

- The APS and TEMED initiators were selected for use in the synthesis of polyNIPAm microspheres as microsphere size must be greater than cell size for successful *in vitro* cell culture.

In the next stages of this research programme, the effect of surfactant composition on the surface charge of polyNIPAm microspheres was investigated. The key outcomes pertaining to this part of study are as follows:

- The surface charge of the polyNIPAm microsphere changed from negative (~ -29 mv) to positive (~ +8 mV) upon addition of 20 wt% CTAB cationic surfactant.

- Microspheres synthesised in the presence of 10 wt% CTAB cationic surfactant exhibited maximal cell attachment.

- The addition of CTAB had an effect on the surface hydrophobicity of the microspheres, which influenced the cellular response to the microspheres.

In order to further improve the surface hydrophobicity of the polyNIPAm microspheres, BMA was used to copolymerise polyNIPAm. The key outcomes pertaining to this stage of the study are as follows:

- The microspheres became more hydrophobic upon addition of the BMA comonomer.

- Protein adsorption was dependent on the surface hydrophobicity of the microspheres.

- The microspheres containing 30 wt% of BMA exhibited maximal cell attachment.

- All sample sets exhibited spontaneous cell detachment upon lowering the incubation temperature from 37 to 20°C.

During the final stages of this research programme, the effect of stirring rate and cross-linker content on the physical and mechanical properties of the microspheres was appraised. The key outcomes pertaining to this part of study are as follows:

- The mean size of the microsphere reduced from ~ 190 to ~ 30 μm when the stirring rate used during synthesis increased from 100 to 400 rpm.

- The compressive modulus of the microsphere increased from ~ 221 to ~ 317 MPa upon increase of the cross-linker from 5 to 20 wt%.

- The size and modulus of the microspheres affected HEK cell attachment and growth.

- The optimised processing conditions for the synthesis of polyNIPAm microspheres from the present study are summarised in Table 9.1:

Table 9.1 *Optimal processing conditions for the synthesis of polyNIPAm microsphere*

Processing conditions	Value
Stirring rate	200 rpm
Crosslinker content	15 wt%
Ratio of NIPAm to BMA	70/30
CTAB surfactant content	10 wt%

- The microspheres prepared from these optimised processing conditions exhibited a cell yield of ~ 1.7 x 10^6 cells/ml, which is comparable to the commercial microcarrier, Cytodex.

- Accordingly, it is concluded that polyNIPAm-*co*-BMA microspheres are promising microcarriers for non-invasive harvestment of cells.

9.1 Suggestions for Future Work

Thermoresponsive microcarriers offer better harvestment of confluent cells in anchorage-dependent cell cultures. In the present study, microspheres of desired size range and surface properties were developed. However, the production of polyNIPAm microspheres demonstrated in this study was only on laboratory-scale. Scaling-up of the production process is required for commercialisation. Hence, for future work it is proposed:

- The production of these microspheres must to be scaled-up in order to achieve high efficiency at low production cost. Hence, an automated system with large volume needs to be developed, to produce large numbers of microspheres per batch.

- A more efficient, ergonomical filtration system needs to be designed, for isolating and washing large quantities of the microspheres. This helps in reducing the number of tasks required during production.

- More detailed characterisation of the microspheres needs to be performed, to verify that the microspheres are indeed safe for use as microcarriers. For example, cytotoxicity tests using AlamarBlue^{TM} assay could be performed to appraise the metabolic activity of viable cells, confirming that the microspheres are non-cytotoxic to the cells.

- The cell membrane before and after harvestment needs to be appraised, using the lactate dehydrogenase (LDH) test, to assess if there is any cellular damage to the cells due to processing.

REFERENCES

1. Freshney, R.I., *Basic Principles of Cell Culture*, in *Culture of Cells for Tissue Engineering*. 2006, John Wiley & Sons, Inc. p. 1-22.

2. Uppangala, N. *Animal Cell Culture Media: Natural and Artificial*. 2010.

3. van Wezel, A.L., *Growth of cell-strains and primary cells on micro-carriers in homogeneous culture.* Nature, 1967. **216**(5110): p. 64-65.

4. Wong, K., *Overview of Microcarrier Culture*, in *Cellular Bioprocess Technology* 2004, Minneapolis: University of Minnesota. p. 1-8.

5. Canavan, H.E., Cheng, X., Graham, D.J., Ratner, B.D., and Castner, D.G., *Cell sheet detachment affects the extracellular matrix: A surface science study comparing thermal liftoff, enzymatic, and mechanical methods.* Journal of Biomedical Materials Research Part A, 2005. **75A**(1): p. 1-13.

6. Gil, E.S. and Hudson, S.M., *Stimuli-responsive polymers and their bioconjugates.* Progress in polymer science, 2004. **29**(12): p. 1173-1222.

7. Hirokawa, Y. and Tanaka, T., *Volume phase transition in a nonionic gel.* The Journal of Chemical Physics, 1984. **81**(12): p. 6379-6380.

8. Nakayama, M., Okano, T., and Winnik, F.M., *Poly(N-isopropylacrylamide)-based Smart Surfaces for Cell Sheet Tissue Engineering.* Material Matters, 2010. **5**(3): p. 56.

9. Schmidt, S., Zeiser, M., Hellweg, T., Duschl, C., Fery, A., and Möhwald, H., *Adhesion and Mechanical Properties of PNIPAM Microgel Films and Their Potential Use as Switchable Cell Culture Substrates.* Advanced Functional Materials, 2010. **20**(19): p. 3235-3243.

10. Cooperstein, M.A. and Canavan, H.E., *Assessment of cytotoxicity of (N-isopropyl acrylamide) and Poly(N-isopropyl acrylamide)-coated surfaces.* Biointerphases, 2013. **8**: p. 19-30.

11. Okano, T., Yamada, N., Okuhara, M., Sakai, H., and Sakurai, Y., *Mechanism of cell detachment from temperature-modulated, hydrophilic-hydrophobic polymer surfaces.* Biomaterials, 1995. **16**(4): p. 297-303.

12. Forestell, S.P., Kalogerakis, N., Behie, L.A., and Gerson, D.F., *Development of the optimal inoculation conditions for microcarrier cultures.* Biotechnology and Bioengineering, 1992. **39**(3): p. 305-313.

13. Shi, X., Sun, L., Jiang, J., Zhang, X., Ding, W., and Gan, Z., *Biodegradable Polymeric Microcarriers with Controllable Porous Structure for Tissue Engineering.* Macromolecular Bioscience, 2009. **9**(12): p. 1211-1218.

14. Yu, Q., Qin, Z., Li, J., and Zhu, S., *Diffusion-controlled atom transfer radical polymerization with crosslinking.* Polymer Engineering & Science, 2008. **48**(7): p. 1254-1260.

15. Fernandez-Nieves, A., Wyss, H., Mattsson, J., and Weitz, D.A., *Microgel Suspensions: Fundamentals and Applications*. 2011: Wiley.

16. Van Hemert, P., Kilburn, D.G., and Van Wezel, A.L., *Homogeneous cultivation of animal cells for the production of virus and virus products.* Biotechnology and Bioengineering, 1969. **11**(5): p. 875-885.

17.   Wang, Y. and Ouyang, F., *Bead-to-bead transfer of Vero cells in microcarrier culture.* Cytotechnology, 1999. **31**(3): p. 221-224.

18.   Healthcare, G. and Biosciences, A., *Microcarrier Cell Culture: Principles and Methods*. 2005: GE Healthcare/Amersham Biosciences.

19.   Griffiths, B., Thornton, B., and McEntee, I., *Production of Herpes viruses in microcarrier cultures of human diploid and primary chick fibroblast cells.* European Journal of Cell Biology, 1980. **22**: p. 606.

20.   Crespi, C.L. and Thilly, W.G., *Continuous cell propagation using low-charge microcarriers.* Biotechnology and Bioengineering, 1981. **23**(5): p. 983-993.

21.   Olivier, L.A. and Truskey, G.A., *A numerical analysis of forces exerted by laminar flow on spreading cells in a parallel plate flow chamber assay.* Biotechnology and Bioengineering, 1993. **42**(8): p. 963-973.

22.   Hughes, R.C., Pena, S.D.J., Clark, J., and Dourmashkin, R.R., *Molecular requirements for the adhesion and spreading of hamster fibroblasts.* Experimental Cell Research, 1979. **121**(2): p. 307-314.

23.   Grinnell, F. and Feld, M.K., *Spreading of human fibroblasts in serum-free medium: inhibition by dithiothreitol and the effect of cold insoluble globulin (plasma fibronectin).* J. Cell. Physiol. , 1980. **104**: p. 321–334

24.   Griffiths, J.B., *Advances in immobilization technology*, in *Animal Cell Biotechnology*, R.E. Spier and J.B. Griffiths, Editors. 1990, Academic Press Inc.: London. p. 149-166.

25.   Ng, Y.C., Berry, J.M., and Butler, M., *Optimization of physical parameters for cell attachment and growth on macroporous microcarriers.* Biotechnology and Bioengineering, 1996. **50**(6): p. 627-635.

26.   Zhang, S., Handa-Corrigan, A., and Spier, R.E., *A comparison of oxygenation methods fro high-density perfusion culture of animal cells.* Biotechnology and Bioengineering, 1993. **41**(7): p. 685-692.

27.   Spier, R.E. and Whiteside, J.P., *The production of foot-and-mouth disease virus from BHK 21 C 13 cells grown on the surface of DEAE sephadex A50 beads.* Biotechnology and Bioengineering, 1976. **18**(5): p. 659-667.

28.   Mered, B., Albrecht, P., Hopps, H.E., Petricciani, J.C., and Salk, J., *Monkey kidney cell growth optimization and poliovirus propagation in microcarrier culture.* Developments in biological standardization, 1981. **47**: p. 41-53.

29.   Levine, D.W., Wang, D.I.C., and Thilly, W.G., *Optimization of growth surface parameters in microcarrier cell culture.* Biotechnology and Bioengineering, 1979. **21**(5): p. 821-845.

30.   Manousos, M., Ahmed, M., Torchio, C., Wolff, J., Shibley, G., Stephens, R., and Mayyasi, S., *Feasibility studies of oncornavirus production in microcarrier cultures.* In Vitro, 1980. **16**(6): p. 507-515.

31.   Windig, W., Haverkamp, J., and van Wezel, A.L., *Control on the absenceof DEAE-polysaccharides in DEAE-Sphadex-purified poliovirus suspensions by pyrolysis mass spectrometry.* Dev. Biol. Standard, 1981. **47**: p. 160-177.

32.   Gebb, C., Clark, J.M., and Hirtenstein, M.D., Dev. Bio. Standard, 1982. **50**: p. 93-102.

33.   Konigsberg, I.R., *[45] Skeletal myoblasts in culture*, in *Methods in Enzymology*. 1979, Academic Press. p. 511-527.

34. John, H.A. and Lawson, H., *The effect of different collagen types used as substrata on myogenesis in tissue culture.* Cell Biology International Reports, 1980. **4**(9): p. 841-850.

35. Rawlings, N.D. and Barrett, A.J., *[2] Families of serine peptidases*, in *Methods in Enzymology*. 1994, Academic Press. p. 19-61.

36. Jeong, B. and Gutowska, A., *Lessons from nature: stimuli-responsive polymers and their biomedical applications.* Trends in Biotechnology, 2002. **20**(7): p. 305-311.

37. Shirakawa, M., Yamatoya, K., and Nishinari, K., *Tailoring of xyloglucan properties using an enzyme.* Food Hydrocolloids, 1998. **12**(1): p. 25-28.

38. Philips, G.O. and Williams, P.A., *Handbook of Hydrocolloids*. 2009, UK: Woodhead Publishing.

39. Bhalekar, M., Sonawane, S., and Shimpi, S., *Synthesis and characterization of a cysteine xyloglucan conjugate as mucoadhesive polymer.* Brazilian Journal of Pharmaceutical Sciences, 2013. **49**: p. 285-292.

40. Bromberg, L.E. and Ron, E.S., *Temperature-responsive gels and thermogelling polymer matrices for protein and peptide delivery.* Advanced Drug Delivery Reviews, 1998. **31**(3): p. 197-221.

41. Qiu, Y. and Park, K., *Environment-sensitive hydrogels for drug delivery.* Advanced Drug Delivery Reviews, 2001. **53**(3): p. 321-339.

42. Schmolka, I.R., *Artificial skin I. Preparation and properties of pluronic F-127 gels for treatment of burns.* Journal of Biomedical Materials Research, 1972. **6**(6): p. 571-582.

43. Cao, N., Cheng, D., Zou, S., Ai, H., Gao, J., and Shuai, X., *The synergistic effect of hierarchical assemblies of siRNA and chemotherapeutic drugs co-delivered into hepatic cancer cells.* Biomaterials, 2011. **32**(8): p. 2222-2232.

44. Li, L., Shan, H., Yue, C.Y., Lam, Y.C., Tam, K.C., and Hu, X., *Thermally Induced Association and Dissociation of Methylcellulose in Aqueous Solutions.* Langmuir, 2002. **18**(20): p. 7291-7298.

45. Takahashi, M., Shimazaki, M., and Yamamoto, J., *Thermoreversible gelation and phase separation in aqueous methyl cellulose solutions.* Journal of Polymer Science Part B: Polymer Physics, 2001. **39**(1): p. 91-100.

46. Schild, H.G., *Poly(N-isopropylacrylamide): experiment, theory and application.* Progress in Polymer Science, 1992. **17**(2): p. 163-249.

47. Graziano, G., *On the temperature-induced coil to globule transition of poly-N-isopropylacrylamide in dilute aqueous solutions.* International Journal of Biological Macromolecules, 2000. **27**(1): p. 89-97.

48. Baysal, B.M. and Karasz, F.E., *Coil-Globule Collapse in Flexible Macromolecules.* Macromolecular Theory and Simulations, 2003. **12**(9): p. 627-646.

49. Zhang, X.-Z., Zhuo, R.-X., Cui, J.-Z., and Zhang, J.-T., *A novel thermo-responsive drug delivery system with positive controlled release.* International Journal of Pharmaceutics, 2002. **235**(1–2): p. 43-50.

50. Kopeček, J., *Smart and genetically engineered biomaterials and drug delivery systems.* European Journal of Pharmaceutical Sciences, 2003. **20**(1): p. 1-16.

51. Malonne, H., Eeckman, F., Fontaine, D., Otto, A., De Vos, L., Moës, A., Fontaine, J., and Amighi, K., *Preparation of poly (N-isopropylacrylamide) copolymers and preliminary assessment of their acute and subacute toxicity in mice.* European journal of pharmaceutics and biopharmaceutics, 2005. **61**(3): p. 188-194.

52. Vernon, B., Kim, S.W., and Bae, Y.H., *Thermoreversible copolymer gels for extracellular matrix4.* Journal of Biomedical Materials Research, 2000. **51**(1): p. 69-79.

53. Yamato, M., Utsumi, M., Kushida, A., Konno, C., Kikuchi, A., and Okano, T., *Thermo-responsive culture dishes allow the intact harvest of multilayered keratinocyte sheets without dispase by reducing temperature.* Tissue engineering, 2001. **7**(4): p. 473-480.

54. Kim, D.-H., Kim, J.-H., Seo, J.-H., Lee, J.-W., Lim, S.-Y., Lee, H.-J., and Byun, M.-W., *Polymerization of SDS–PAGE gel by gamma irradiation and its use for characterization by electrophoresis of a protein.* Radiation Physics and Chemistry, 2005. **74**(5): p. 395-398.

55. Murata, H., Koepsel, R.R., Matyjaszewski, K., and Russell, A.J., *Permanent, non-leaching antibacterial surfaces—2: How high density cationic surfaces kill bacterial cells.* Biomaterials, 2007. **28**(32): p. 4870-4879.

56. Ista, L.K., Mendez, S., Pérez-Luna, V.H., and López, G.P., *Synthesis of Poly(N-isopropylacrylamide) on Initiator-Modified Self-Assembled Monolayers.* Langmuir, 2001. **17**(9): p. 2552-2555.

57. Fathi, M., Entezami, A., Ebrahimi, A., and Safa, K., *Synthesis of thermosensitive nanohydrogels by crosslinker free method based on N-isopropylacrylamide: Applicable in the naltrexone sustained release.* Macromolecular Research, 2013. **21**(1): p. 17-26.

58. Jung, N., Kim, S.M., Kang, D.H., Chung, D.Y., Kang, Y.S., Chung, Y.-H., Choi, Y.W., Pang, C., Suh, K.-Y., and Sung, Y.-E., *High-Performance Hybrid Catalyst with Selectively Functionalized Carbon by Temperature-Directed Switchable Polymer.* Chemistry of Materials, 2013. **25**(9): p. 1526-1532.

59. Campbell, S.B., Patenaude, M., and Hoare, T., *Injectable Superparamagnets: Highly Elastic and Degradable Poly(N-isopropylacrylamide)–Superparamagnetic Iron Oxide Nanoparticle (SPION) Composite Hydrogels.* Biomacromolecules, 2013. **14**(3): p. 644-653.

60. Trzebicka, B., Robak, B., Trzcinska, R., Szweda, D., Suder, P., Silberring, J., and Dworak, A., *Thermosensitive PNIPAM-peptide conjugate – Synthesis and aggregation.* European Polymer Journal, 2013. **49**(2): p. 499-509.

61. Ren, L., Huang, S., Zhang, C., Wang, R., Tjiu, W., and Liu, T., *Functionalization of graphene and grafting of temperature-responsive surfaces from graphene by ATRP "on water".* Journal of Nanoparticle Research, 2012. **14**(6): p. 1-9.

62. Klein Gunnewiek, M., Di Luca, A., Sui, X., van Blitterswijk, C.A., Moroni, L., and Vancso, G.J., *Controlled Surface Initiated Polymerization of N-Isopropylacrylamide from Polycaprolactone Substrates for Regulating Cell Attachment and Detachment.* Israel Journal of Chemistry, 2012. **52**(3-4): p. 339-346.

63. Patenaude, M. and Hoare, T., *Injectable, Mixed Natural-Synthetic Polymer Hydrogels with Modular Properties.* Biomacromolecules, 2012. **13**(2): p. 369-378.

64. Kleinen, J., Klee, A., and Richtering, W., *Influence of Architecture on the Interaction of Negatively Charged Multisensitive Poly(N-isopropylacrylamide)-co-Methacrylic Acid Microgels with Oppositely Charged Polyelectrolyte: Absorption vs Adsorption.* Langmuir, 2010. **26**(13): p. 11258-11265.

65. Tang, Z., Akiyama, Y., Yamato, M., and Okano, T., *Comb-type grafted poly(N-isopropylacrylamide) gel modified surfaces for rapid detachment of cell sheet.* Biomaterials, 2010. **31**(29): p. 7435-7443.

66. Jiang, X., Zhang, G., Narain, R., and Liu, S., *Covalently stabilized temperature and pH responsive four-layer nanoparticles fabricated from surface 'clickable' shell cross-linked micelles.* Soft Matter, 2009. **5**(7): p. 1530-1538.

67. Mizutani, A., Kikuchi, A., Yamato, M., Kanazawa, H., and Okano, T., *Preparation of thermoresponsive polymer brush surfaces and their interaction with cells.* Biomaterials, 2008. **29**(13): p. 2073-2081.

68. Singh, N. and Lyon, L.A., *Au Nanoparticle Templated Synthesis of pNIPAm Nanogels.* Chemistry of Materials, 2007. **19**(4): p. 719-726.

69. Lokuge, I., Wang, X., and Bohn, P.W., *Temperature-Controlled Flow Switching in Nanocapillary Array Membranes Mediated by Poly(N-isopropylacrylamide) Polymer Brushes Grafted by Atom Transfer Radical Polymerization†.* Langmuir, 2007. **23**(1): p. 305-311.

70. Cheng, N., Liu, W., Cao, Z., Ji, W., Liang, D., Guo, G., and Zhang, J., *A study of thermoresponsive poly(N-isopropylacrylamide)/polyarginine bioconjugate non-viral transgene vectors.* Biomaterials, 2006. **27**(28): p. 4984-4992.

71. Karg, M., Pastoriza-Santos, I., Liz-Marzán, L.M., and Hellweg, T., *A Versatile Approach for the Preparation of Thermosensitive PNIPAM Core–Shell Microgels with Nanoparticle Cores.* ChemPhysChem, 2006. **7**(11): p. 2298-2301.

72. Suzuki, D. and Kawaguchi, H., *Modification of Gold Nanoparticle Composite Nanostructures Using Thermosensitive Core−Shell Particles as a Template.* Langmuir, 2005. **21**(18): p. 8175-8179.

73. Wang, Y.-P., Yuan, K., Li, Q.-L., Wang, L.-P., Gu, S.-J., and Pei, X.-W., *Preparation and characterization of poly(N-isopropylacrylamide) films on a modified glass surface via surface initiated redox polymerization.* Materials Letters, 2005. **59**(14–15): p. 1736-1740.

74. Kwon, I.K. and Matsuda, T., *Photo-iniferter-based thermoresponsive block copolymers composed of poly(ethylene glycol) and poly(N-isopropylacrylamide) and chondrocyte immobilization.* Biomaterials, 2006. **27**(7): p. 986-995.

75. Cunliffe, D., de las Heras Alarcón, C., Peters, V., Smith, J.R., and Alexander, C., *Thermoresponsive Surface-Grafted Poly(N−isopropylacrylamide) Copolymers: Effect of Phase Transitions on Protein and Bacterial Attachment.* Langmuir, 2003. **19**(7): p. 2888-2899.

76. Takeoka, Y. and Watanabe, M., *Template Synthesis and Optical Properties of Chameleonic Poly(N-isopropylacrylamide) Gels Using Closest-Packed Self-Assembled Colloidal Silica Crystals.* Advanced Materials, 2003. **15**(3): p. 199-201.

77. Shan, J., Nuopponen, M., Jiang, H., Kauppinen, E., and Tenhu, H., *Preparation of Poly(N-isopropylacrylamide)-Monolayer-Protected Gold Clusters: Synthesis Methods, Core Size, and Thickness of Monolayer.* Macromolecules, 2003. **36**(12): p. 4526-4533.

78. Zhang, J. and Peppas, N.A., *Synthesis and Characterization of pH- and Temperature-Sensitive Poly(methacrylic acid)/Poly(N-isopropylacrylamide) Interpenetrating Polymeric Networks.* Macromolecules, 2000. **33**(1): p. 102-107.

79. Kwon, O.H., Kikuchi, A., Yamato, M., Sakurai, Y., and Okano, T., *Rapid cell sheet detachment from Poly(N-isopropylacrylamide)-grafted porous cell culture membranes.* Journal of Biomedical Materials Research, 2000. **50**(1): p. 82-89.

80. Stile, R.A., Burghardt, W.R., and Healy, K.E., *Synthesis and Characterization of Injectable Poly(N-isopropylacrylamide)-Based Hydrogels That Support Tissue Formation in Vitro.* Macromolecules, 1999. **32**(22): p. 7370-7379.

81. Brazel, C.S. and Peppas, N.A., *Synthesis and Characterization of Thermo- and Chemomechanically Responsive Poly(N-isopropylacrylamide-co-methacrylic acid) Hydrogels.* Macromolecules, 1995. **28**(24): p. 8016-8020.

82. Wu, X.S., Hoffman, A.S., and Yager, P., *Synthesis and characterization of thermally reversible macroporous poly(N-isopropylacrylamide) hydrogels.* Journal of Polymer Science Part A: Polymer Chemistry, 1992. **30**(10): p. 2121-2129.

83. Cowie, J.M.G. and Arrigh, V., *Polymers: Chemistry and physics of modern materials*. 1998, Boca Raton: CRC Press.

84. Romack, T.J., Maury, E.E., and DeSimone, J.M., *Precipitation Polymerization of Acrylic Acid in Supercritical Carbon Dioxide.* Macromolecules, 1995. **28**(4): p. 912-915.

85. Sosnowski, S., Gadzinowski, M., and Slomkowski, S., *Poly(l,l-lactide) Microspheres by Ring-Opening Polymerization.* Macromolecules, 1996. **29**(13): p. 4556-4564.

86. Nomura, M., Tobita, H., and Suzuki, K., *Emulsion Polymerization: Kinetic and Mechanistic Aspects*, in *Polymer Particles*, M. Okubo, Editor. 2005, Springer Berlin Heidelberg. p. 1-128.

87. Lee, D.-H., Kim, J.-W., and Suh, K.-D., *Monodisperse micron-sized polymethylmethacrylate particles having a crosslinked network structure.* Journal of Materials Science, 2000. **35**: p. 6181-6188.

88. Jönsson, B., Lindman, B., Holmberg, K., and Kronberg, B., *Surfactants and Polymers in Aqueous Solution*. 2000: Wiley.

89. Troy, D.B., Remington, J.P., and Beringer, P., *Remington: The Science and Practice of Pharmacy*. 2006: Lippincott Williams & Wilkins.

90. Wang, W. and Kwak, J.C.T., *Adsorption at the alumina–water interface from mixed surfactant solutions.* Colloids and Surfaces A: Physicochemical and Engineering Aspects, 1999. **156**(1–3): p. 95-110.

91. Rosen, M.J. and Kunjappu, J.T., *Surfactants and Interfacial Phenomena*. 2012: Wiley.

92. Housecroft, C.E. and Sharpe, A.G., *Inorganic Chemistry*. 2005: Pearson Prentice Hall.

93. Davies, J.T., *Surface Active Agents*, in *Proc. 2nd Int. Congr.* 1957, Butterworths: London. p. 426.

94. Xiao, L., Xu, G., Zhang, Z., Wang, Y., and Li, G., *Adsorption of sodium oleate at the interface of oil sand/aqueous solution.* Colloids and Surfaces A: Physicochemical and Engineering Aspects, 2003. **224**(1–3): p. 199-206.

95. Fuerstenau, D.W., *Equilibrium and Nonequilibrium Phenomena Associated with the Adsorption of Ionic Surfactants at Solid–Water Interfaces.* Journal of Colloid and Interface Science, 2002. **256**(1): p. 79-90.

96.   Penfold, J., Staples, E.J., Tucker, I., Thompson, L.J., and Thomas, R.K., *The structure and composition of mixed cationic and non-ionic surfactant layers adsorbed at the hydrophilic silicon surface.* Physica B: Condensed Matter, 1998. **248**(1–4): p. 223-228.

97.   Peck, A.S. and Wadsworth, M.E. *Infrared studies of the effect of fluoride, sulfate and chloride on chemisorption of oleate on fluoride and barite*. in *Proceedings of 7th International Mineral Processing Congress*. 1965. New York: Gordon and Breach Science Publishers.

98.   Somasundaran, P., Fu, E., and Xu, Q., *Coadsorption of Anionic and Nonionic Surfactant Mixtures at the Alumina-Water Interface.* Langmuir 1992. **8**: p. 1065-1069.

99.   Xu, Q., Vasudevan, T.V., and Somasundaran, P., *Adsorption of anionic—nonionic and cationic—nonionic surfactant mixtures on kaolinite.* Journal of Colloid and Interface Science, 1991. **142**(2): p. 528-534.

100.   Zhang, M., Desai, T., and Ferrari, M., *Proteins and cells on PEG immobilized silicon surfaces.* Biomaterials, 1998. **19**(10): p. 953-960.

101.   Wang, Y.-C., Peterson, S.E., and Loring, J.F., *Protein post-translational modifications and regulation of pluripotency in human stem cells.* Cell Res, 2014. **24**(2): p. 143-160.

102.   Aveyard, R. and Haydon, D.A., *An Introduction to the Principles of Surface Chemistry*. 1973: Cambridge University Press.

103.   Harasym, T.O., Tardi, P., Longman, S.A., Ansell, S.M., Bally, M.B., Cullis, P.R., and Choi, L.S.L., *Poly(ethylene glycol)-Modified Phospholipids Prevent Aggregation during Covalent Conjugation of Proteins to Liposomes.* Bioconjugate Chemistry, 1995. **6**(2): p. 187-194.

104.   Bollag, D.M., Rozycki, M.D., and Edelstein, S.J., *Protein Methods*. 1996.

105.   Jeon, S.I., Lee, J.H., Andrade, J.D., and De Gennes, P.G., *Protein—surface interactions in the presence of polyethylene oxide.* Journal of Colloid and Interface Science, 1991. **142**(1): p. 149-158.

106.   Zalipsky, S., *Functionalized Poly(ethylene glycols) for Preparation of Biologically Relevant Conjugates.* Bioconjugate Chemistry, 1995. **6**(2): p. 150-165.

107.   Lan, Z., Kurata, W.E., Martyn, K.D., Jin, C., and Lau, A.F., *Novel Rab GAP-like Protein, CIP85, Interacts with Connexin43 and Induces Its Degradation†.* Biochemistry, 2005. **44**(7): p. 2385-2396.

108.   Sawhney, A.S. and Hubbell, J.A., *Poly(ethylene oxide)-graft-poly(L-lysine) copolymers to enhance the biocompatibility of poly(L-lysine)-alginate microcapsule membranes.* Biomaterials, 1992. **13**(12): p. 863-870.

109.   Vogler, E.A., *Water and the acute biological response to surfaces.* Journal of Biomaterials Science, Polymer Edition, 1999. **10**(10): p. 1015-1045.

110.   Cha, P., Krishnan, A., Fiore, V.F., and Vogler, E.A., *Interfacial Energetics of Protein Adsorption from Aqueous Buffer to Surfaces with Varying Hydrophilicity.* Langmuir, 2008. **24**(6): p. 2553-2563.

111.   Chen, H., Yuan, L., Song, W., Wu, Z., and Li, D., *Biocompatible polymer materials: Role of protein–surface interactions.* Progress in Polymer Science, 2008. **33**(11): p. 1059-1087.

112.   Pirone, D. and Chen, C., *Strategies for Engineering the Adhesive Microenvironment.* Journal of Mammary Gland Biology and Neoplasia, 2004. **9**(4): p. 405-417.

113. Ruoslahti, E., *RGD and other recognition sequences for integrins.* Annual Review of Cell and Developmental Biology, 1996. **12**: p. 697–715.

114. Yamaki, K., Harada, I., Goto, M., Cho, C.-S., and Akaike, T., *Regulation of cellular morphology using temperature-responsive hydrogel for integrin-mediated mechanical force stimulation.* Biomaterials, 2009. **30**(7): p. 1421-1427.

115. Bodin, A., Ahrenstedt, L., Fink, H., Brumer, H., Risberg, B., and Gatenholm, P., *Modification of Nanocellulose with a Xyloglucan– RGD Conjugate Enhances Adhesion and Proliferation of Endothelial Cells: Implications for Tissue Engineering.* Biomacromolecules, 2007. **8**(12): p. 3697-3704.

116. Stabenfeldt, S.E., García, A.J., and LaPlaca, M.C., *Thermoreversible laminin-functionalized hydrogel for neural tissue engineering.* Journal of Biomedical Materials Research Part A, 2006. **77A**(4): p. 718-725.

117. Park, K.-H., Na, K., and Chung, H.-M., *Enhancement of the adhesion of fibroblasts by peptide containing an Arg-Gly-Asp sequence with poly(ethylene glycol) into a thermo-reversible hydrogel as a synthetic extracellular matrix.* Biotechnology Letters, 2005. **27**(4): p. 227-231.

118. Higuchi, A., Yamamoto, T., Sugiyama, K., Hayashi, S., Tak, T.M., and Nakagawa, T., *Temperature-Dependent Cell Detachment on Pluronic Gels.* Biomacromolecules, 2005. **6**(2): p. 691-696.

119. Biltresse, S., Attolini, M., and Marchand-Brynaert, J., *Cell adhesive PET membranes by surface grafting of RGD peptidomimetics.* Biomaterials, 2005. **26**(22): p. 4576-4587.

120. Ebara, M., Yamato, M., Aoyagi, T., Kikuchi, A., Sakai, K., and Okano, T., *Temperature-Responsive Cell Culture Surfaces Enable "On−Off" Affinity Control between Cell Integrins and RGDS Ligands.* Biomacromolecules, 2004. **5**(2): p. 505-510.

121. Liu, J.C., Heilshorn, S.C., and Tirrell, D.A., *Comparative Cell Response to Artificial Extracellular Matrix Proteins Containing the RGD and CS5 Cell-Binding Domains.* Biomacromolecules, 2004. **5**(2): p. 497-504.

122. Kim, M.R., Jeong, J.H., and Park, T.G., *Swelling Induced Detachment of Chondrocytes Using RGD-Modified Poly(N-isopropylacrylamide) Hydrogel Beads.* Biotechnology Progress, 2002. **18**(3): p. 495-500.

123. Stile, R.A. and Healy, K.E., *Thermo-Responsive Peptide-Modified Hydrogels for Tissue Regeneration.* Biomacromolecules, 2001. **2**(1): p. 185-194.

124. Yamaoka, T., Hotta, Y., Kobayashi, K., and Kimura, Y., *Synthesis and properties of malic acid-containing functional polymers.* International Journal of Biological Macromolecules, 1999. **25**(1–3): p. 265-271.

125. Drotleff, S., Lungwitz, U., Breunig, M., Dennis, A., Blunk, T., Tessmar, J., and Göpferich, A., *Biomimetic polymers in pharmaceutical and biomedical sciences.* European Journal of Pharmaceutics and Biopharmaceutics, 2004. **58**(2): p. 385-407.

126. Hersel, U., Dahmen, C., and Kessler, H., *RGD modified polymers: biomaterials for stimulated cell adhesion and beyond.* Biomaterials, 2003. **24**(24): p. 4385-4415.

127. Espejo Guardiola, R., *Influence of the dispersed phase fraction on drop sizes in liquid/liquid systems*, 2008, The University of Vienna Austria.

128. Liao, Y. and Lucas, D., *A literature review of theoretical models for drop and bubble breakup in turbulent dispersions.* Chemical Engineering Science, 2009. **64**(15): p. 3389-3406.

129. Kolmogorov, A.N., *On the disintegration of drops in a turbulent flow.* Dokl. Akad. Nauk SSSR, 1949. **66**: p. 825-828.

130. Moinard-Chécot, D., Chevalier, Y., Briançon, S., Beney, L., and Fessi, H., *Mechanism of nanocapsules formation by the emulsion–diffusion process.* Journal of Colloid and Interface Science, 2008. **317**(2): p. 458-468.

131. Zhou, G. and Kresta, S.M., *Correlation of mean drop size and minimum drop size with the turbulence energy dissipation and the flow in an agitated tank.* Chemical Engineering Science, 1998. **53**(11): p. 2063-2079.

132. Leng, D.E. and Calabrese, R.V., *Immiscible Liquid–Liquid Systems*, in *Handbook of Industrial Mixing*. 2004, John Wiley & Sons, Inc. p. 639-753.

133. Pacek, A., Man, C., and Nienow, A., *On the Sauter mean diameter and size distributions in turbulent liquid/liquid dispersions in a stirred vessel.* Chemical Engineering Science, 1998. **53**(11): p. 2005-2011.

134. Torab-Mostaedi, M., Safdari, J., and Asadollahzaded, M., *Mean Drop Size and Drop Size Distribution in a Hanson Mixer-Settler Extraction Column.* Iranian Journal of Chemical Engineering, 2012. **9**(2): p. 54-65.

135. Sechremeli, D., Stampouli, A., and Stamatoudis, M., *Comparison of mean drop sizes and drop size distributions in agitated liquid–liquid dispersions produced by disk and open type impellers.* Chemical Engineering Journal, 2006. **117**(2): p. 117-122.

136. Giapos, A., Pachatouridis, C., and Stamatoudis, M., *Effect of the Number of Impeller Blades on the Drop Sizes in Agitated Dispersions.* Chemical Engineering Research and Design, 2005. **83**(12): p. 1425-1430.

137. Desnoyer, C., Masbernat, O., and Gourdon, C., *Experimental study of drop size distributions at high phase ratio in liquid–liquid dispersions.* Chemical Engineering Science, 2003. **58**(7): p. 1353-1363.

138. Quadros, P.A. and Baptista, C.M.S.G., *Effective interfacial area in agitated liquid–liquid continuous reactors.* Chemical Engineering Science, 2003. **58**(17): p. 3935-3945.

139. Lemenand, T., Della Valle, D., Zellouf, Y., and Peerhossaini, H., *Droplets formation in turbulent mixing of two immiscible fluids in a new type of static mixer.* International Journal of Multiphase Flow, 2003. **29**(5): p. 813-840.

140. Ruiz, M.C., Lermanda, P., and Padilla, R., *Drop size distribution in a batch mixer under breakage conditions.* Hydrometallurgy, 2002. **63**(1): p. 65-74.

141. Ma, J.L. and Zhang, X.H., *Preparation of Polystyrene Microspheres by Suspension Polymerization.* Advanced Materials Research, 2011. **233-235**: p. 2215-2218.

142. Tamura, A., Kobayashi, J., Yamato, M., and Okano, T., *Temperature-responsive poly(N-isopropylacrylamide)-grafted microcarriers for large-scale non-invasive harvest of anchorage-dependent cells.* Biomaterials, 2012. **33**(15): p. 3803-3812.

143. Arashiro, E.Y. and Demarquette, N.R., *Use of the pendant drop method to measure interfacial tension between molten polymers.* Materials Research, 1999. **2**: p. 23-32.

144. Heftmann, E., *Chromatography: Fundamentals and applications of chromatography and related differential migration methods - Part A: Fundamentals and techniques*. 2004: Elsevier Science.
145. Smith, B.C., *Infrared Spectral Interpretation: A Systematic Approach*. 1998, Hoboken: Taylor & Francis.
146. Braun, R.D., *Introduction to instrumental analysis*. 1987: McGraw-Hill Ryerson, Limited.
147. Cazes, J., *Analytical Instrumentation Handbook, Third Edition*. 2004: CRC Press.
148. Reimer, L., *Scanning Electron Microscopy: Physics of Image Formation and Microanalysis*. 1998: Springer.
149. Slayter, E.M. and Slayter, H.S., *Light and Electron Microscopy*. 1992: Cambridge University Press.
150. Goldstein, J., Newbury, D.E., Echlin, P., Joy, D.C., Romig, A.D., Lyman, C.E., Fiori, C., and Lifshin, E., *Scanning Electron Microscopy and X-Ray Microanalysis: A Text for Biologists, Materials Scientists, and Geologists*. 2012, New York: Springer US.
151. Khursheed, A., *Scanning Electron Microscope Optics and Spectrometers*. 2011: World Scientific.
152. Braet, F., De Zanger, R., and Wisse, E., *Drying cells for SEM, AFM and TEM by hexamethyldisilazane: a study on hepatic endothelial cells.* Journal of Microscopy, 1997. **186**(Pt 1): p. 84-87.
153. Brundle, C.R., Evans, C.A., and Wilson, S., *Encyclopedia of Materials Characterization: Surfaces, Interfaces, Thin Films*. 1992: Butterworth-Heinemann.
154. Bell, D. and Garratt-Reed, A., *Energy Dispersive X-ray Analysis in the Electron Microscope*. 2003: Taylor & Francis.
155. Wiklund, M., Brismar, H., and Onfelt, B., *Acoustofluidics 18: Microscopy for acoustofluidic micro-devices.* Lab on a Chip, 2012. **12**(18): p. 3221-3234.
156. Murphy, D.B. and Davidson, M.W., *Fundamentals of Light Microscopy*, in *Fundamentals of Light Microscopy and Electronic Imaging*. 2012, John Wiley & Sons, Inc. p. 1-19.
157. Lemasters, J.J., Chacon, E., Zahrebelski, G., Reece, J.M., and Nieminen, A.-L., *12 - LASER SCANNING CONFOCAL MICROSCOPY OF LIVING CELLS*, in *Optical Microscopy*, B. Herman and J.J. Lemasters, Editors. 1993, Academic Press: San Diego. p. 339-354.
158. Shaked, N.T., Zalevsky, Z., and Satterwhite, L.L., *Biomedical Optical Phase Microscopy and Nanoscopy*. 2012: Elsevier Science.
159. Dukhin, A.S., Goetz, P.J., and Travers, B., *Use of Ultrasound for Characterizing Dairy Products.* Journal of Dairy Science, 2005. **88**(4): p. 1320-1334.
160. Ishikawa, J., Tsuji, H., Sato, H., and Gotoh, Y., *Ion implantation of negative ions for cell growth manipulation and nervous system repair.* Surface and Coatings Technology, 2007. **201**(19–20): p. 8083-8090.
161. Hatakeyama, T. and Quinn, F.X., *Thermal analysis: fundamentals and applications to polymer science*. 1999: Wiley.
162. Chartoff, R.P. and Sircar, A.K., *Thermal Analysis of Polymers*, in *Encyclopedia of Polymer Science and Technology*. 2002, John Wiley & Sons, Inc.
163. Gabbott, P., *A Practical Introduction to Differential Scanning Calorimetry*, in *Principles and Applications of Thermal Analysis*. 2008, Blackwell Publishing Ltd: Singapore. p. 1-50.
164. Brown, M.E., *Introduction to Thermal Analysis: Techniques and Applications*. 2001: Springer Netherlands.

165. Menczel, J.D. and Prime, R.B., *Thermal Analysis of Polymers: Fundamentals and Applications*. 2014, New Jersey: John Wiley & Son.

166. Louis, K. and Siegel, A., *Cell Viability Analysis Using Trypan Blue: Manual and Automated Methods*, in *Mammalian Cell Viability*, M.J. Stoddart, Editor. 2011, Humana Press. p. 7-12.

167. Brandriss, S. and Margel, S., *Synthesis and characterization of self-assembled hydrophobic monolayer coatings on silica colloids.* Langmuir, 1993. **9**(5): p. 1232-1240.

168. Gilcreest, V.P., Carroll, W.M., Rochev, Y.A., Blute, I., Dawson, K.A., and Gorelov, A.V., *Thermoresponsive Poly(N-isopropylacrylamide) Copolymers: Contact Angles and Surface Energies of Polymer Films.* Langmuir, 2004. **20**(23): p. 10138-10145.

169. Sun, B., Lin, Y., and Wu, P., *Structure Analysis of Poly(N-isopropylacrylamide) Using Near-Infrared Spectroscopy and Generalized Two-Dimensional Correlation Infrared Spectroscopy.* Applied Spectroscopy, 2007. **61**(7): p. 765-771.

170. Yi, G., Huang, Y., Xiong, F., Liao, B., Yang, J., and Chen, X., *Preparation and swelling behaviors of rapid responsive semi-IPN NaCMC/PNIPAm hydrogels.* Journal of Wuhan University of Technology-Mater. Sci. Ed., 2011. **26**(6): p. 1073-1078.

171. Zhang, J., Jiang, X., Zhang, Y., Li, Y., and Liu, S., *Facile Fabrication of Reversible Core Cross-Linked Micelles Possessing Thermosensitive Swellability.* Macromolecules, 2007. **40**(25): p. 9125-9132.

172. Costa, R.O.R. and Freitas, R.F.S., *Phase behavior of poly(N-isopropylacrylamide) in binary aqueous solutions.* Polymer, 2002. **43**(22): p. 5879-5885.

173. Qiu, J., Charleux, B., and Matyjaszewski, K., *Controlled/living radical polymerization in aqueous media: homogeneous and heterogeneous systems.* Progress in Polymer Science, 2001. **26**(10): p. 2083-2134.

174. Walter, D., *Primary Particles – Agglomerates – Aggregates*, in *Nanomaterials*. 2013, Wiley-VCH Verlag GmbH & Co. KGaA. p. 9-24.

175. Israelachvili, J.N., *3 - Strong Intermolecular Forces: Covalent and Coulomb Interactions*, in *Intermolecular and Surface Forces (Third Edition)*, J.N. Israelachvili, Editor. 2011, Academic Press: San Diego. p. 53-70.

176. Leong, Y.W., Abu Bakar, M.B., Ishak, Z.A.M., Ariffin, A., and Pukanszky, B., *Comparison of the mechanical properties and interfacial interactions between talc, kaolin, and calcium carbonate filled polypropylene composites.* Journal of Applied Polymer Science, 2004. **91**(5): p. 3315-3326.

177. Mandzy, N., Grulke, E., and Druffel, T., *Breakage of TiO2 agglomerates in electrostatically stabilized aqueous dispersions.* Powder Technology, 2005. **160**(2): p. 121-126.

178. Schick, M.J., *Nonionic Surfactants: Physical Chemistry*. 1987: Taylor & Francis.

179. Fitch, R.M., *Chapter 2 - Emulsion Polymerization*, in *Polymer Colloids*, R.M. Fitch, Editor. 1997, Academic Press: London. p. 6-47.

180. Heuts, J.P.A., *Theory of Radical Reactions*, in *Handbook of Radical Polymerization*, K. Matyjaszewski and T.P. Davis, Editors. 2003, John Wiley & Sons, Inc.: New York. p. 1-76.

181. Soltani, N., Saion, E., Hussein, M., Erfani, M., Rezaee, K., and Bahmanrokh, G., *Phase Controlled Monodispersed CdS Nanocrystals Synthesized in Polymer Solution Using Microwave Irradiation.* Journal of Inorganic and Organometallic Polymers and Materials, 2012. **22**(4): p. 830-836.

182. Senuma, Y., Franceschin, S., Hilborn, J.G., Tissières, P., Bisson, I., and Frey, P., *Bioresorbable microspheres by spinning disk atomization as injectable cell carrier: from preparation to in vitro evaluation.* Biomaterials, 2000. **21**(11): p. 1135-1144.

183. Chen, A.K.-L., Chen, X., Choo, A.B.H., Reuveny, S., and Oh, S.K.W., *Critical microcarrier properties affecting the expansion of undifferentiated human embryonic stem cells.* Stem Cell Research, 2011. **7**(2): p. 97-111.

184. Re, F., Zanetti, A., Sironi, M., Polentarutti, N., Lanfrancone, L., Dejana, E., and Colotta, F., *Inhibition of anchorage-dependent cell spreading triggers apoptosis in cultured human endothelial cells.* The Journal of Cell Biology, 1994. **127**(2): p. 537-546.

185. Lee, J.H., Jung, H.W., Kang, I.-K., and Lee, H.B., *Cell behaviour on polymer surfaces with different functional groups.* Biomaterials, 1994. **15**(9): p. 705-711.

186. Schneider, G.B., English, A., Abraham, M., Zaharias, R., Stanford, C., and Keller, J., *The effect of hydrogel charge density on cell attachment.* Biomaterials, 2004. **25**(15): p. 3023-3028.

187. Cheremisinoff, P., *Handbook of Engineering Polymeric Materials*. 1997: Taylor & Francis.

188. van Berkel, K.Y., Russell, G.T., and Gilbert, R.G., *Entry in Emulsion Polymerization: Effects of Initiator and Particle Surface Charge.* Macromolecules, 2003. **36**(11): p. 3921-3931.

189. Shi, Q. and Jackowski, G., *One-dimensional polyacrylamide gel electrophoresis.* Gel electrophoresis of proteins: A practical approach, 3rd ed. Oxford University Press, Oxford, 1998: p. 1-52.

190. Su, X., Shuai, Y., Guo, Z., and Feng, Y., *Functionalization of Multi-Walled Carbon Nanotubes with Thermo-Responsive Azide-Terminated Poly(N-isopropylacrylamide) via Click Reactions.* Molecules, 2013. **18**(4): p. 4599.

191. Ivanova, E.D., Dimitrov, I., V., Georgieva, V.G., and Turmanova, S.C., *Non-Isothermal Degradation Kinetics of Hybrid Copolymers Containing Thermosensitive and Polypeptide Blocks.* Open Journal of Polymer Chemistry, 2012. **2**: p. 91-98.

192. Yang, D., Zhang, X., Wang, C., Tang, Y., Li, J., and Hu, J., *Preparation of water-soluble multi-walled carbon nanotubes by Ce(IV)-induced redox radical polymerization.* Progress in Natural Science, 2009. **19**(8): p. 991-996.

193. Shinde, V.S., Girme, M.R., and Pawar, V.U., *Thermoresponsive polystyrene-b-poly(N-isopropylacrylamide) copolymers by atom transfer radical polymerization.* Indian Journal of Chemistry, 2011. **50A**: p. 781-787.

194. Bauri, K., Roy, S., Arora, S., Dey, R., Goswami, A., Madras, G., and De, P., *Thermal degradation kinetics of thermoresponsive poly(N-isopropylacrylamide-co-N,N-dimethylacrylamide) copolymers prepared via RAFT polymerization.* Journal of Thermal Analysis and Calorimetry, 2013. **111**(1): p. 753-761.

195. Bae, Y.H., Okano, T., and Kim, S.W., *Temperature dependence of swelling of crosslinked poly(N,N'-alkyl substituted acrylamides) in water.* Journal of Polymer Science Part B: Polymer Physics, 1990. **28**(6): p. 923-936.

196. Mendes, P.M., *Stimuli-responsive surfaces for bio-applications.* Chemical Society Reviews, 2008. **37**(11): p. 2512-2529.

197. Feil, H., Bae, Y.H., Feijen, J., and Kim, S.W., *Effect of comonomer hydrophilicity and ionization on the lower critical solution temperature of N-isopropylacrylamide copolymers.* Macromolecules, 1993. **26**(10): p. 2496-2500.

198. Yoshida, R., Sakai, K., Okano, T., and Sakurai, Y., *Modulating the phase transition temperature and thermosensitivity in N-isopropylacrylamide copolymer gels.* Journal of Biomaterials Science, Polymer Edition, 1994. **6**(6): p. 585-598.

199. Haba, Y., Kojima, C., Harada, A., and Kono, K., *Comparison of Thermosensitive Properties of Poly(amidoamine) Dendrimers with Peripheral N-Isopropylamide Groups and Linear Polymers with the Same Groups.* Angewandte Chemie International Edition, 2007. **46**(1-2): p. 234-237.

200. Purushotham, S. and Ramanujan, R.V., *Thermoresponsive magnetic composite nanomaterials for multimodal cancer therapy.* Acta Biomaterialia, 2010. **6**(2): p. 502-510.

201. Sjoblom, J., *Emulsions and Emulsion Stability: Surfactant Science Series/61*. 2005: CRC Press.

202. Shahin, M., Hady, S.A., Hammad, M., and Mortada, N., *Development of stable O/W emulsions of three different oils.* International Journal of Pharmaceutical Studies and Research (IJPSR), 2011. **II**(II): p. 45-51.

203. Desai, T.R. and Dixit, S.G., *Interaction and Viscous Properties of Aqueous Solutions of Mixed Cationic and Nonionic Surfactants.* Journal of Colloid and Interface Science, 1996. **177**(2): p. 471-477.

204. Lim, Z.-Z.J., Li, J.-E.J., Ng, C.-T., Yung, L.-Y.L., and Bay, B.-H., *Gold nanoparticles in cancer therapy.* Acta Pharmacologica Sinica, 2011. **32**(8): p. 983-990.

205. Chun, K.W., Yoo, H.S., Yoon, J.J., and Park, T.G., *Biodegradable PLGA Microcarriers for Injectable Delivery of Chondrocytes: Effect of Surface Modification on Cell Attachment and Function.* Biotechnology Progress, 2004. **20**(6): p. 1797-1801.

206. Poncin-Epaillard, F., Vrlinic, T., Debarnot, D., Mozetic, M., Coudreuse, A., Legeay, G., El Moualij, B., and Zorzi, W., *Surface Treatment of Polymeric Materials Controlling the Adhesion of Biomolecules.* Journal of Functional Biomaterials, 2012. **3**(3): p. 528-543.

207. Yuan, Y. and Lee, T.R., *Contact Angle and Wetting Properties*, in *Surface Science Techniques*, G. Bracco and B. Holst, Editors. 2013, Springer Berlin Heidelberg. p. 3-34.

208. Binks, B.P., Desforges, A., and Duff, D.G., *Synergistic Stabilization of Emulsions by a Mixture of Surface-Active Nanoparticles and Surfactant.* Langmuir, 2007. **23**(3): p. 1098-1106.

209. Wei, J., Igarashi, T., Okumori, N., Igarashi, T., Maetani, T., Liu, B., and Yoshinari, M., *Influence of surface wettability on competitive protein adsorption and initial attachment of osteoblasts.* Biomedical Materials, 2009. **4**(4): p. 045002.

210. Nasser, A.A. and El-Moghaz, *Factors effects the Growth of Chinese Hamster Ovary (CHO) cell on Microcarriers Culture.* Advances in Bioresearch, 2010. **11**: p. 182-188.

211. Schild, H.G. and Tirrell, D.A., *Microcalorimetric detection of lower critical solution temperatures in aqueous polymer solutions.* The Journal of Physical Chemistry, 1990. **94**(10): p. 4352-4356.

212. Yagi, Y., Inomata, H., and Saito, S., *Solubility Parameter of an N-Isopropylacrylamide Gel.* Macromolecules, 1992. **25**: p. 2997-2998.
213. Cooperstein, M.A. and Canavan, H.E., *Biological Cell Detachment from Poly(N-isopropyl acrylamide) and Its Applications.* Langmuir, 2010. **26**(11): p. 7695-7707.
214. Liu, S.-Q., Yang, Y.-Y., Liu, X.-M., and Tong, Y.-W., *Preparation and Characterization of Temperature-Sensitive Poly(N-isopropylacrylamide)-b-poly(d,l-lactide) Microspheres for Protein Delivery.* Biomacromolecules, 2003. **4**(6): p. 1784-1793.
215. Akiva, U. and Margel, S., *Surface-modified hemispherical polystyrene/polybutyl methacrylate composite particles.* Journal of Colloid and Interface Science, 2005. **288**(1): p. 61-70.
216. Bakhshi, H., Zohuriaan-Mehr, M.J., Bouhendi, H., and Kabiri, K., *Spectral and chemical determination of copolymer composition of poly (butyl acrylate-co-glycidyl methacrylate) from emulsion polymerization.* Polymer Testing, 2009. **28**(7): p. 730-736.
217. Chen, Y., Mastalerz, M., and Schimmelmann, A., *Heterogeneity of shale documented by micro-FTIR and image analysis.* Journal of Microscopy, 2014. **256**(3): p. 177-189.
218. Trivedi, J., Bhatt, T., and Trivedi, H., *Synthesis and characterization of poly(butyl methacrylate) grafted sodium salt of partially carboxymethylated guar gum.* Cellulose Chemistry and Technology, 2014. **48**(5-6): p. 503-514.
219. Özlem, S. and Hacaloglu, J., *Thermal degradation of poly(n-butyl methacrylate), poly(n-butyl acrylate) and poly(t-butyl acrylate).* Journal of Analytical and Applied Pyrolysis, 2013. **104**: p. 161-169.
220. Choi, Y. and Chung, I., *Poly(n-butyl acrylate-co-methyl methacrylate) and poly(n-butyl acrylate-co-styrene)/ silicate nanocomposites prepared by emulsion polymerization.* Macromolecular Research, 2003. **11**(6): p. 425-430.
221. Chung, J.E., Yokoyama, M., Aoyagi, T., Sakurai, Y., and Okano, T., *Effect of molecular architecture of hydrophobically modified poly(N-isopropylacrylamide) on the formation of thermoresponsive core-shell micellar drug carriers.* Journal of Controlled Release, 1998. **53**(1–3): p. 119-130.
222. Lynch, I., Blute, I.A., Zhmud, B., MacArtain, P., Tosetto, M., Allen, L.T., Byrne, H.J., Farrell, G.F., Keenan, A.K., Gallagher, W.M., and Dawson, K.A., *Correlation of the Adhesive Properties of Cells to N-Isopropylacrylamide/N-tert-Butylacrylamide Copolymer Surfaces with Changes in Surface Structure Using Contact Angle Measurements, Molecular Simulations, and Raman Spectroscopy.* Chemistry of Materials, 2005. **17**(15): p. 3889-3898.
223. Zobrist, C., Sobocinski, J., Lyskawa, J., Fournier, D., Miri, V., Traisnel, M., Jimenez, M., and Woisel, P., *Functionalization of Titanium Surfaces with Polymer Brushes Prepared from a Biomimetic RAFT Agent.* Macromolecules, 2011. **44**(15): p. 5883-5892.
224. Horák, D., Švec, F., and Fréchet, J.M.J., *Preparation and control of surface properties of monodisperse micrometer size beads by dispersion copolymerization of styrene and butyl methacrylate in polar media.* Journal of Polymer Science Part A: Polymer Chemistry, 1995. **33**(14): p. 2329-2338.
225. Mujumdar, A.S. and Devahastin, S., *Mujumdar's Practical Guide to Industrial Drying.* 2000: Exergex Corporation.

226. Ou, J.-L., Yang, J.-K., and Chen, H., *Styrene/potassium persulfate/water systems: effects of hydrophilic comonomers and solvent additives on the nucleation mechanism and the particle size.* European Polymer Journal, 2001. **37**(4): p. 789-799.

227. Musyanovych, A., Rossmanith, R., Tontsch, C., and Landfester, K., *Effect of Hydrophilic Comonomer and Surfactant Type on the Colloidal Stability and Size Distribution of Carboxyl- and Amino-Functionalized Polystyrene Particles Prepared by Miniemulsion Polymerization.* Langmuir, 2007. **23**(10): p. 5367-5376.

228. Dong, H., Lee, S.-Y., and Yi, G.-R., *Controlling the size and surface morphology of carboxylated polystyrene latex particles by ammonium hydroxide in emulsifier-free polymerization.* Macromolecular Research, 2009. **17**(6): p. 397-402.

229. Habicht, W., Behrens, S., Wu, J., Unger, E., and Dinjus, E., *Characterization of metal decorated protein templates by scanning electron/scanning force microscopy and microanalysis.* Surface and Interface Analysis, 2004. **36**(8): p. 720-723.

230. Rabiller-Baudry, M., Gouttefangeas, F., Le Lannic, J., and Rabiller, P., *Coupling of SEM-EDX and FTIR-ATR to (quantitatively) investigate organic fouling on porous organic composite membranes*, in *Current Microscopy Contributions to Advances in Science and Technology* 2012. p. 1066-1076.

231. Tengvall, P., Lundström, I., and Liedberg, B., *Protein adsorption studies on model organic surfaces: an ellipsometric and infrared spectroscopic approach.* Biomaterials, 1998. **19**(4–5): p. 407-422.

232. Gessner, A., Waicz, R., Lieske, A., Paulke, B.R., Mäder, K., and Müller, R.H., *Nanoparticles with decreasing surface hydrophobicities: influence on plasma protein adsorption.* International Journal of Pharmaceutics, 2000. **196**(2): p. 245-249.

233. Allen, L.T., Fox, E.J.P., Blute, I., Kelly, Z.D., Rochev, Y., Keenan, A.K., Dawson, K.A., and Gallagher, W.M., *Interaction of soft condensed materials with living cells: Phenotype/transcriptome correlations for the hydrophobic effect.* Proceedings of the National Academy of Sciences, 2003. **100**(11): p. 6331-6336.

234. Alsteens, D., Van Dijck, P., Lipke, P.N., and Dufrêne, Y.F., *Quantifying the Forces Driving Cell–Cell Adhesion in a Fungal Pathogen.* Langmuir, 2013. **29**(44): p. 13473-13480.

235. Dague, E., Alsteens, D., Latgé, J.-P., Verbelen, C., Raze, D., Baulard, A.R., and Dufrêne, Y.F., *Chemical Force Microscopy of Single Live Cells.* Nano Letters, 2007. **7**(10): p. 3026-3030.

236. Bidanset, D.J., LeBaron, R., Rosenberg, L., Murphy-Ullrich, J.E., and Hook, M., *Regulation of cell substrate adhesion: effects of small galactosaminoglycan-containing proteoglycans.* The Journal of Cell Biology, 1992. **118**(6): p. 1523-1531.

237. Rochev, Y., Golubeva, T., Gorelov, A., Allen, L., Gallagher, W.M., Selezneva, I., Gavrilyuk, B., and Dawson, K., *Surface modification for controlled cell growth on copolymers of N-isopropylacrylamide*, in *Trends in Colloid and Interface Science XV*, P. Koutsoukos, Editor. 2001, Springer Berlin Heidelberg. p. 153-156.

238. Collier, T.O., Anderson, J.M., Kikuchi, A., and Okano, T., *Adhesion behavior of monocytes, macrophages, and foreign body giant cells on poly (N-isopropylacrylamide) temperature-responsive surfaces.* Journal of Biomedical Materials Research, 2002. **59**(1): p. 136-143.

239. Tsuda, Y., Kikuchi, A., Yamato, M., Sakurai, Y., Umezu, M., and Okano, T., *Control of cell adhesion and detachment using temperature and thermoresponsive copolymer grafted culture surfaces.* Journal of Biomedical Materials Research Part A, 2004. **69A**(1): p. 70-78.

240. Chen, C.S., Mrksich, M., Huang, S., Whitesides, G.M., and Ingber, D.E., *Geometric Control of Cell Life and Death.* Science, 1997. **276**(5317): p. 1425-1428.

241. Dike, L.E. and Ingber, D.E., *Integrin-dependent induction of early growth response genes in capillary endothelial cells.* Journal of cell science, 1996. **109**(12): p. 2855-2863.

242. Ohya, S., Kidoaki, S., and Matsuda, T., *Poly(N-isopropylacrylamide) (PNIPAM)-grafted gelatin hydrogel surfaces: interrelationship between microscopic structure and mechanical property of surface regions and cell adhesiveness.* Biomaterials, 2005. **26**(16): p. 3105-3111.

243. Chen, G. and Tao, D., *An experimental study of stability of oil–water emulsion.* Fuel Processing Technology, 2005. **86**(5): p. 499-508.

244. Lobry, E., Theron, F., Gourdon, C., Le Sauze, N., Xuereb, C., and Lasuye, T., *Turbulent liquid–liquid dispersion in SMV static mixer at high dispersed phase concentration.* Chemical Engineering Science, 2011. **66**(23): p. 5762-5774.

245. Harrison, R.G., Washburn, A.L., Pickett, A.T., and Call, D.M., *Assembly of CdSe nanoparticles into microspheres by a liquid droplet emulsion process.* Journal of Materials Chemistry, 2008. **18**(31): p. 3718-3722.

246. Hinze, J.O., *Fundamentals of the hydrodynamic mechanism of splitting in dispersion processes.* AIChE J., 1955. **1**: p. 289-295.

247. Theron, F. and Sauze, N.L., *Comparison between three static mixers for emulsification in turbulent flow.* International Journal of Multiphase Flow, 2011. **37**(5): p. 488-500.

248. Pelham, R.J. and Wang, Y.-l., *Cell locomotion and focal adhesions are regulated by substrate flexibility.* Proceedings of the National Academy of Sciences, 1997. **94**(25): p. 13661-13665.

249. Baker, D.A., Bellare, A., and Pruitt, L., *The effects of degree of crosslinking on the fatigue crack initiation and propagation resistance of orthopedic-grade polyethylene.* Journal of Biomedical Materials Research Part A, 2003. **66A**(1): p. 146-154.

250. Khonakdar, H.A., Morshedian, J., Wagenknecht, U., and Jafari, S.H., *An investigation of chemical crosslinking effect on properties of high-density polyethylene.* Polymer, 2003. **44**(15): p. 4301-4309.

251. Kojio, K., Furukawa, M., Matsumura, S., Motokucho, S., Osajima, T., and Yoshinaga, K., *The effect of cross-linking density and dangling chains on surface molecular mobility of network polyurethanes.* Polymer Chemistry, 2012. **3**(8): p. 2287-2292.

252. Rees, D., *Basic Engineering Plasticity: An Introduction with Engineering and Manufacturing Applications*. 2012: Elsevier Science.

253. Harmon, M.E., Kuckling, D., Pareek, P., and Frank, C.W., *Photo-Cross-Linkable PNIPAAm Copolymers. 4. Effects of Copolymerization and Cross-Linking on the Volume-Phase Transition in Constrained Hydrogel Layers.* Langmuir, 2003. **19**(26): p. 10947-10956.

254. Hsieh, T.-T., Hisieh, K.-H., Simin, G.P., Tiu, C., and Hsu, H.-P., *Effect of Crosslinking Density on the Physical Properties of Interpenetrating Polymer Networks of Polyurethane and 2-Hydroxyethyl Methacrylate-terminated Polyurethane.* Journal of Polymer Research, 1998. **5**(3): p. 153-162.
255. Krupa, I. and Luyt, A.S., *Mechanical properties of uncrosslinked and crosslinked linear low-density polyethylene/wax blends.* Journal of Applied Polymer Science, 2001. **81**(4): p. 973-980.
256. Seddiki, N. and Aliouche, D., *Synthesis, rheological behavior and swelling properties of copolymer hydrogels based on poly(N-isopropylacrylamide) with hydrophilic monomers.* Bulletin of the Chemical Society ofEnthiopia, 2013. **27**(3): p. 447-457.
257. Maroudas, N.G., *Chemical and Mechanical Requirements for Fibroblast Adhesion.* Nature, 1973. **244**(5415): p. 353-354.
258. Wang, K., Cai, L., Hao, F., Xu, X., Cui, M., and Wang, S., *Distinct Cell Responses to Substrates Consisting of Poly(ε-caprolactone) and Poly(propylene fumarate) in the Presence or Absence of Cross-Links.* Biomacromolecules, 2010. **11**(10): p. 2748-2759.
259. Marklein, R.A. and Burdick, J.A., *Spatially controlled hydrogel mechanics to modulate stem cell interactions.* Soft Matter, 2010. **6**(1): p. 136-143.
260. Cai, L., Lu, J., Sheen, V., and Wang, S., *Promoting Nerve Cell Functions on Hydrogels Grafted with Poly(l-lysine).* Biomacromolecules, 2012. **13**(2): p. 342-349.
261. Harmon, M.E., Kuckling, D., and Frank, C.W., *Photo-Cross-Linkable PNIPAAm Copolymers. 5. Mechanical Properties of Hydrogel Layers.* Langmuir, 2003. **19**(26): p. 10660-10665.